Flow Analysis for Energy Efficiency in Data Centers: Experimental & Numerical Study

Author

Kamran Nazir

2010-NUST-MsPhD-Mech-05

Supervisor

Imran Akhtar, PhD

DEPARTMENT OF MECHANICAL ENGINEERING

COLLEGE OF ELECTRICAL & MECHANICAL ENGINEERING

NATIONAL UNIVERSITY OF SCIENCES AND TECHNOLOGY

ISLAMABAD

August, 2013

Flow Analysis for Energy Efficiency in Data Centers: Experimental & Numerical Study

Author

Kamran Nazir

2010-NUST-MsPhD-Mech-05

A thesis submitted in partial fulfillment of the requirements for the degree of

M.Sc. Mechanical Engineering

Thesis Supervisor:

Imran Akhtar, PhD

Thesis Supervisor Signature:_____

DEPARTMENT OF MECHANICAL ENGINEERING

COLLEGE OF ELECTRICAL & MECHANICAL ENGINEERING

NATIONAL UNIVERSITY OF SCIENCES AND TECHNOLOGY, ISLAMABAD

August, 2013

Declaration

I certify that research work titled "Flow Analysis for Energy Efficiency in Data Centers: Experimental & Numerical Study" is my own work. The work has not been presented elsewhere for assessment. Where material has been used from other sources it has been properly acknowledged / referred.

Kamran Nazir

2010-NUST-MsPhD-Mech05

Copyright Statement

Acknowledgements

I am thankful to you, my Creator Allah Subhana-watala that you guide me throughout this work at every step and for every new thought which you setup in my mind to improve it. Indeed I could have done nothing without your priceless help and guidance, not even I breathe without your intention let alone other endeavors. Whosoever helped me, weather my parents or any other individual was your will, so indeed none be worthy of praise other than you and you be worthy of all praise and thanks and rest is just a formality.

I am profusely thankful to my beloved parents who raised me when I was not capable of walk and continue to support me throughout in every department of my life.

I would also like to pay special thanks to my supervisor Dr. Imran Akhtar for his tremendous support and cooperation. Each time I got stuck in something, he comes up with the solution. Without his help I wouldn't have been able to complete my thesis. I appreciate his patience and his guidance for the whole thesis. Special Thanks to Dr Naveed Durrani for his help throughout my thesis.

Thanks to Dr. HassanAftab, Dr. Aamir Shafi and Mr. Saif Ullah Khalid for being on my thesis committee. Dr. Aamir Shafi helped a lot in obtaining experimental valued in SEECS HPC Lab. Mr Usman also helped a lot in conducting experiments at RCMS Data Center.

Special thanks to my brother, Saqib Nazir for helping me in writing the thesis report. Thanks to Mr Haseeb Choudhary for helping me in preparation of experimental equipment and in taking experimental data. I am also thankful to Imran Aziz, M. Nadeem Azam and Nabeel ur Rehman for their support and cooperation. Finally, I would like to express my gratitude to all the individuals who have rendered valuable assistance to my study.

Dedicated to my exceptional parents and adored siblings whose tremendous support and cooperation led me to this wonderful accomplishment.

Flow Analysis for Energy Efficiency in Data Centers: Experimental & Numerical Study

Kamran Nazir

Abstract

One of the major reasons for high energy consumption in data centers is due to less focus (e.g., intermixing of hot and cold air, creation of stagnation points in cold-aisle etc) on the proper flow of air inside the data center. To enhance energy efficiency and improve air flow movement in data center requires well verified CFD model. The research in this field conducted so far majorly emphasis on thermal behavior of a data center. Thermal study verifies the temperature distribution in a data center, but it does not authentically assures the airflow patterns inside the data center which play important role in energy efficiency of a data center. This thesis summarizes effects of aisle configurations on energy efficiency of a data center. Experimental data of point velocity and temperature distribution in a real data center is obtained. CFD analysis of the data center is then performed and results are compared with the experimental data. In order to analyze the effect of hot and cold aisle configuration effect on energy efficiency of a data center, a numerical study for two even numbered rows of racks data center is performed. Based on results obtained, we conclude that for any even numbered rows of racks data center, configuration with one more cold aisle than number of hot aisles gives energy efficiency in the data center.

Table of Contents

Table of Figures

List of Tables

Chapter 1

Introduction

Adequate supply of cheap energy is the basic necessity of today. Energy effects the economic as well as industrial growth of any country. With the passage of time, challenge to provide electricity has become a prominent issue. Energy crisis in Pakistan is one of the severe challenges the country is facing today. Shortage of electricity and gas has badly affected the economy and overall living in Pakistan. On the other hand, requirement of Information technology equipment is on increasing trend. One way to meet the energy requirement of that equipment is to produce more energy. Resources of fossil fuels are decreasing and becoming more costly day by day. This fast depletion has brought the world in the grip of energy crisis. Therefore, energy efficiency is the cheapest and quickest way to cope with that crisis.

1.1 Energy Consumption in Buildings:

Figure 1.1 shows the distribution of energy consumption by each sector. It is found that domestic buildings are the largest contributors of energy consumption [1]. They share almost 46% of total energy consumption. Overall, building consumes almost 54% of total energy while industries have only about 27% shares [2]. Figure 1.2 shows that heating and cooling are the major contributors in energy consumption for both commercial and residential buildings. Almost half of the total energy consumed in any building is shared by heating and cooling issues [3].

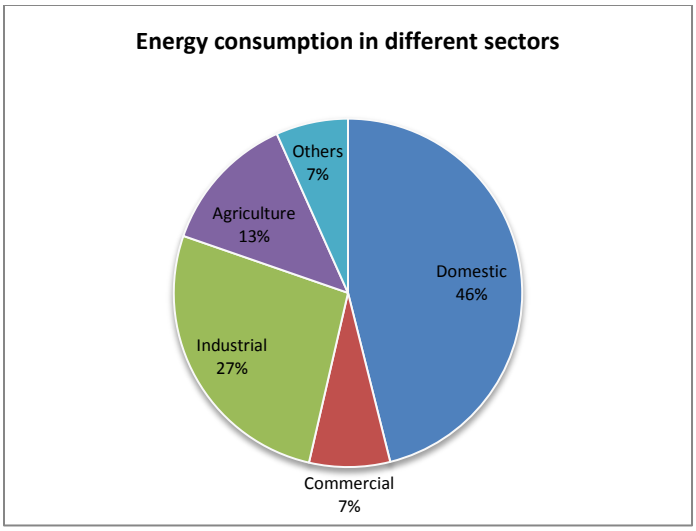

Figure 1.1: Sector Wise Energy Consumption

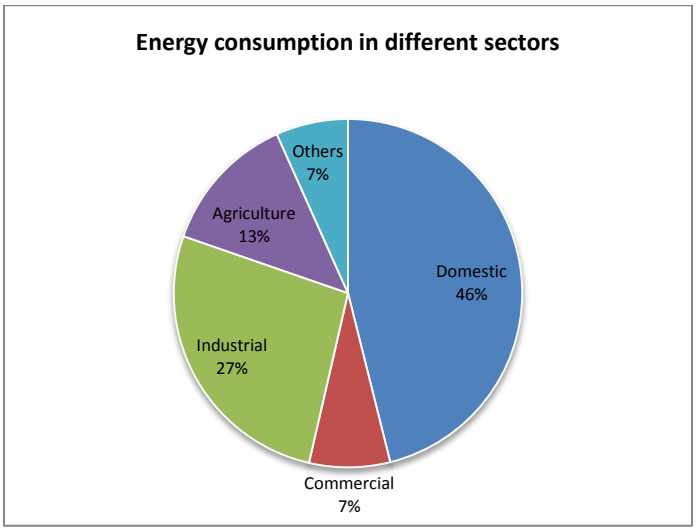

Figure 1.2: Building Energy Consumption

Energy Shortfall in Pakistan

Pakistan has witnessed the most severe energy crisis in recent times. On an average, there is about 4000 MW energy supply-demand gap. At present, this gap is filled by scheduled load-shedding. This results in 6 to 8 hours of power outage in cities, while these cuts are much more prolonged in rural areas[4]. Pakistan is among the leading countries in inefficient use of energy. Most of Pakistani industries suffer from high energy consumption according to international

norms. According to a report in 2006, the intensity of Total Primary energy supply is about twice of the world's average [5]. Similarly, Pakistan consumes more energy in buildings than other countries. This trend is shown in Figure 1.3 [6].

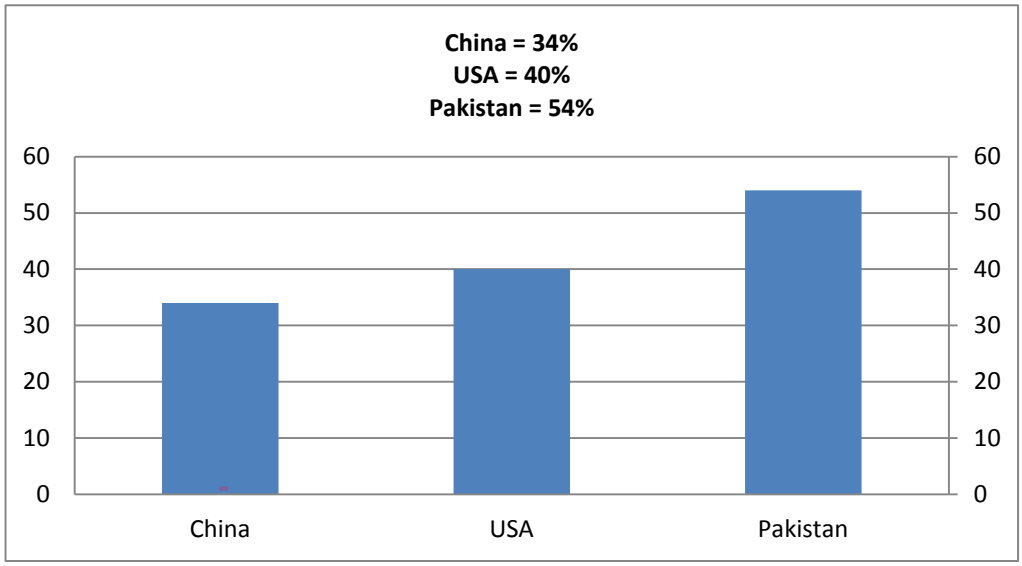

Figure 1.3: Energy Consumption in Buildings

1.2 Data Centers

Data center is a facility that house computer systems and related equipment to perform storage operation, manage and process data and exchange data and information. These computer servers are collectively called as "IT Equipment". This equipment is utilized by many end users including internet service providers, banks, stock exchanges, corporations, educational institutions, government installations, and research laboratories. In addition to this IT Equipment, data center also contain power conversion equipment (UPS) and environmental control equipment (HVAC systems) to maintain operating conditions.

A data center comprises of following components as shown in Figure 1.4

a. Computer Room Air Conditioning (CRAC) units
b. Server Racks
c. Perforated Tiles

CRAC units are used to maintain appropriate temperature and humidity inside the data center. A single CRAC unit contains multiple heat exchangers, which accept heat energy generated by IT

equipment, cool it and throw it back into the data center environment. Capacities for CRAC units are typically measured in tons. Server racks are the cabinets used to place computer servers. Front and back side of racks are perforated surfaces so that chilled air is pulled through the front of rack and hot air is exhausted through back. Standard dimensions of a rack are height = 2m, width = 0.6m and depth = 1m. Chilled air comes into the room through perforated tiles. Standard size of tile is Length = 0.61m and Height = 0.61m. Perforated tiles are placed in cold aisle, aligned with the intake of the rack. Percentage open area of tiles may be varied to air flow in the data center.

Figure 1.4: Basic components of a data center

Air Flow Distribution in a Data Center:

Figure 1.5 represents the schematic of air flow distribution in a data center. Initially, cool air from CRAC units introduced to the area which is below floor. This is called below plenum area. This cold air then moves to area above floor from perforated tiles located at floor. This makes the cold air gathered above the perforated tiles and we call this region as cold aisle. Air from cold aisle is then sucked by the fans of servers located inside racks. This air becomes hot while passing over the servers and comes out from back of racks. Therefore, rack back region is called hot aisle. The hot air is then sucked by CRAC units where it loses its heat and whole process is repeated.

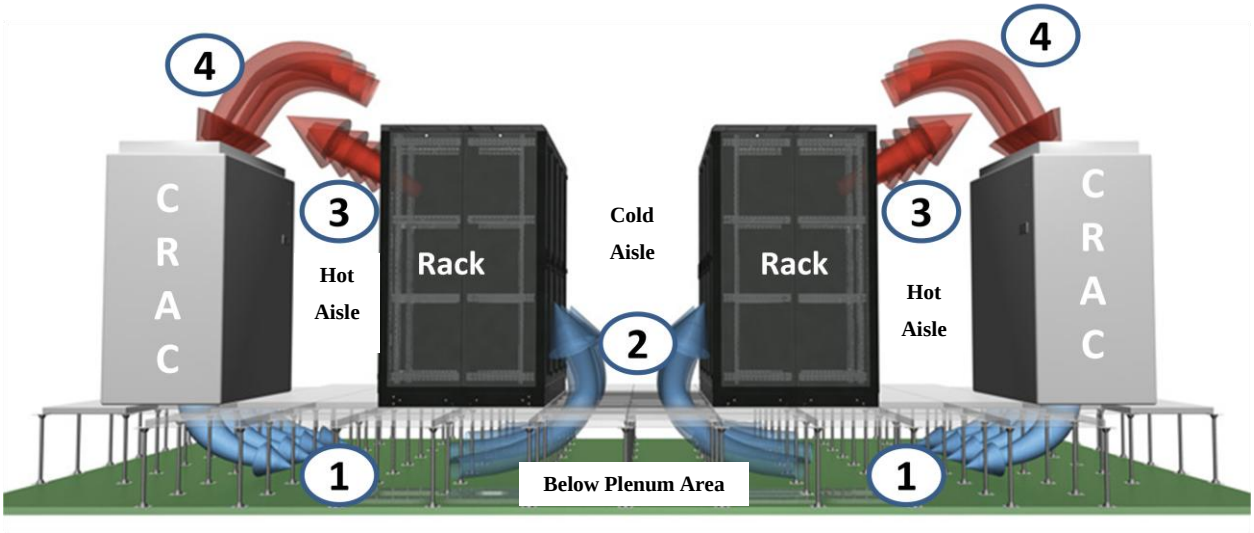

Figure 1.5: Air flow distribution of a typical data center

There are two different ways of supplying air into the data center. First method represents conventional way of supplying air into raised floor data center. Schematic of air movement in this configuration is explained above.

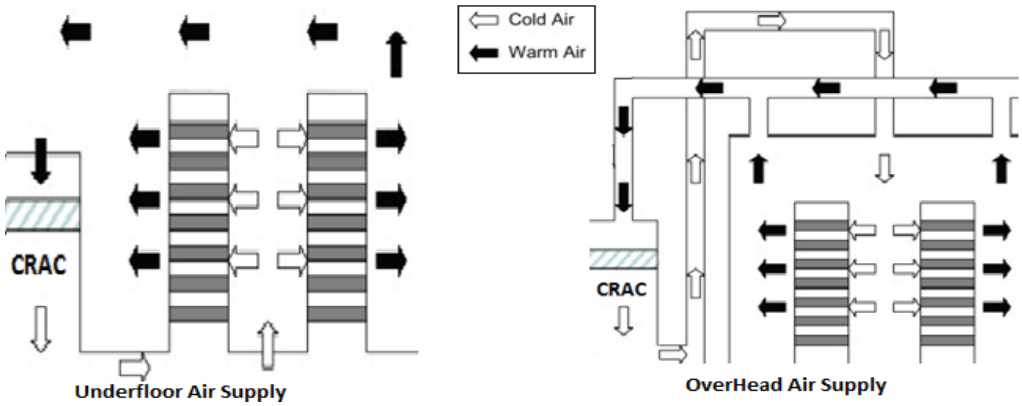

Figure 1.6: Different layouts of Air Supply into Data Center

Second method is overhead air supply configuration in which air is brought into room through diffusers located at roof above cold-aisle. After passing through racks, hot air then exits the room through vents on the wall. Eventually, heat is removed by passing hot air from heat exchangers and cold air is again supplied to diffusers.

Energy Consumption by Data Center:

The Environmental Protection Agency (EPA) report suggests that as US economy shifts from paper to digital data, importance of data centers which are basically used for containing and processing digital data increases. Data centers are used in various fields including financial services, universities, media and government institutions. Their use increases as more industries look into it like internet communication, global commerce, online banking, electronic records etc.

EPA forecasts that data center annual electrical use will increase from 61.4 billion kWh / year in 2006, accounting for 1.5 percent of current national electricity use, to 107 billion kWh / year in 2011 at the current efficiency trend.

The Energy usage by data centers as compared to other economic sectors is rising much faster. Figure 1.7 shows the energy consumption by different sectors in past and it also projected future data [7]. If this trend continues according to Figure 1.7, i.e., Data center energy usage doubled every five years, this will demand urgent improvement in the design of Data centers infrastructure for energy efficiency.

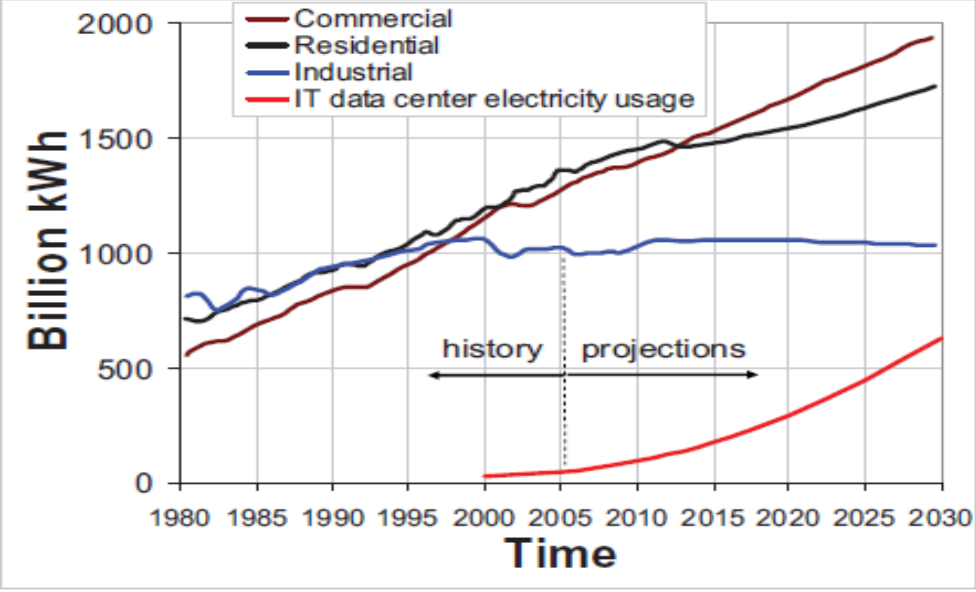

Figure 1.7: Past & Projected data for US delivered electricity consumption by different sectors

Figure 1.8 shows overall energy consumption by data center equipment. According to figure, IT equipment and HVAC system share 70-80 % of total electricity consumed by data center [8].

Energy consumed by IT equipment cannot be reduced as servers need to run for proper working. HVAC energy consumption can be reduced by improving the infrastructure design of data center.

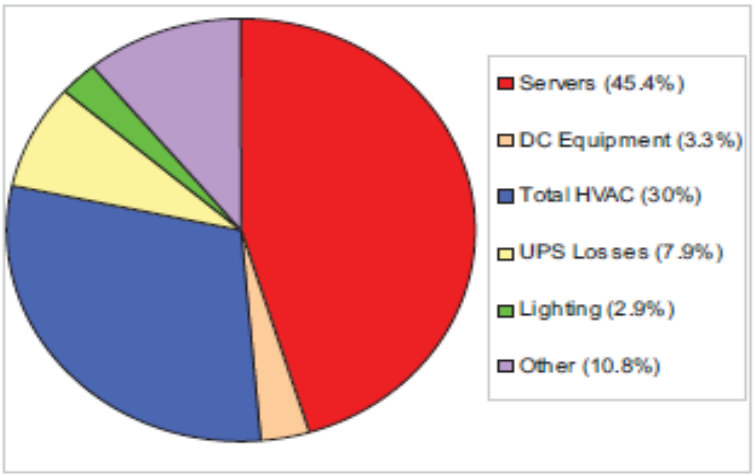

Figure 1.8: Energy Consumption by DC Equipment

Breakdown of HVAC energy consumption is shown in Figure 1.9. From figure it is found that Refrigeration chiller plants and CRAC units are mainly contributors of HVAC energy consumption. Chiller Plants consume about half while data center air conditioning units (CRAC's) uses one third of HVAC energy [8].

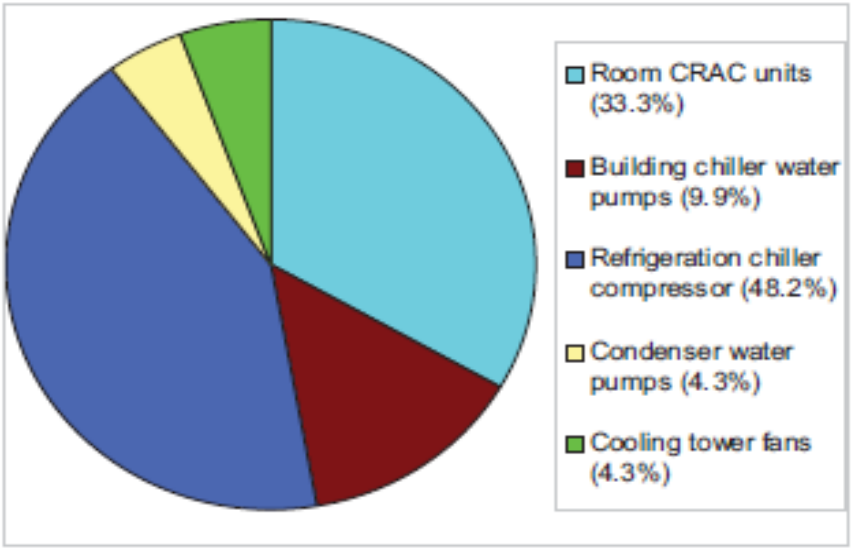

Figure 1.9: HVAC Equipment Energy Breakdown

1.3 **Literature Review:**

CFD models are used to estimate airflow patterns and distribution of temperature inside the data center. By controlling Temperature, humidity and amount of air to be entered or leaving the building, energy requirement for cooling and heating can be greatly reduced. CFD study can help us to understand the flow physics inside the buildings which will lead us to improve the building designs for proper heating and ventilation.

CFD results are questionable unless they are validated against experimental data inside the data center. The research done so far in this field can be divided into two broad categories. That is the studies based upon above plenum area and secondly the studies based upon below plenum area. All the studies for below plenum area mainly focus on analyzing and controlling air flow rates through perforated tiles. On the other hand, above plenum studies are performed for analysis of thermal and flow distribution inside data centers. In this thesis, we are focusing on experimental numerical validation of above plenum area only.

Below Plenum Studies:

Schmidt et al [9] studied the affect of plenum height and tile open area on flow distribution through tiles. They found that uniform flow through tiles can be achieved either by using variable open area of tiles or by deeper plenum depths. Karki et al. [10] also studied the flow rates and pressure distribution through perforated tiles. They assumed that pressure above the tiles is uniform. This reduces the computational domain of above plenum area. The model is then applied to physical data center and it is found that predicted flow rates shows in well agreement with measured values. The model is independent of plenum height as compared to Schmidt [9] model which can be only used for 0.284 m high. Numerical study of flow distribution through perforated tiles in raised floor data centers was performed by Kang et al [11]. They investigate the effect of percentage open area of tiles on flow rate distribution through perforated tiles. It is found that resistance to flow increases as percentage open area of the tile decreases, and at 60% open area, tile resistance was significantly diminished and effects of flow inertia start becoming important.

Schmidt et al [12] studied experimentally the air flow rates through perforated tiles for various floor layouts. This will explain the dependence of air flow rates on perforated tile and CRAC locations. It also explains the effect of flow discharge directions from CRAC on air flow patterns

in plenum area. They then performed numerical study and found that numerical and experimental results are in good agreement. It also explains the effect of flow discharge directions from CRAC on air flow patterns in raised floor.

Kailash et al. [13] studied different techniques used for controlling airflow distribution in raised floor data center. These techniques involve changing the plenum height, open area of perforated tiles, variable open area of tiles throughout floor and installing solid or perforated thin partitions in the plenum. Study showed that by using deeper plenum heights or by using variable open area of tiles, uniform airflow distribution can be achieved. Also, using thin partitions will greatly help to control airflow distribution throughout the data center.

Patel et al. [14] studied the affect of asymmetry in data centers on inlet air temperatures. They studied two cases, one with uniform distance between all rows of racks (Symmetric Case) and the other with a little difference in distance between two rows of racks (Perturbed case). They found that even a minor asymmetry can cause significant changes in rack inlet air temperatures as compared to symmetric case.

Karki et al. [15] performs the under floor study and propose a CFD model for finding flow rates through perforated tiles. He then applied the model to a real world data center and obtained data of velocity and pressure distribution is discussed. He found that flow rates of CFD model are in good agreement with the experimental data.

Bhopte et al. [16] studied the effect of under floor blockages on tile flow rates and rack inlet air temperatures. They analyzed the effects of both parallel and perpendicular blockages with sizes of blocked region ranging from 25% to 100% at constant increment rate of 25%. They found that parallel blockages have less adverse effects as compared to perpendicular blockages. They devised the regions for both parallel and perpendicular cases where by placing these blockages, gives minimum effect on flow rates through tiles.

Above Plenum Studies:

Tiles are modeled as fully open velocity inlet source. This model ensures the mass flux conservation, but momentum flux is not satisfied in this model. In [17] Abdelmaksoud et al studied that modeling tile as open source is good for 50% or larger perforation. But for CFD of tiles with low perforation, this method does not predict temperature profiles accurately. He performed experimental and numerical study on several tile models and found that intermixing

of inlet jet and room air is best predicted by modeling tiles as multiple openings. Kumar et al. [18] studied the affect of tile open area on airflow distribution at perforated tile surface, rack inlet, cold aisle center and cold aisle top. They find that by reducing the open area of the tile to 56%, rack get 25% less intake as compared to the intake for fully open tile (100% open area). They also analyzed that due to air entrainment created at the center of the cold aisle, 65% of the air discharged from tile escapes from the top. It also causes reverse flow at rack inlet surface near to perforated tile. Abdelmaksoud et al. [19] showed three ways of modeling of perforated tiles to conserve both mass and momentum near tiles and rack rear area. They showed that modeling tile as a multiple opening surface or as a momentum source gives better results as compared to single opening surface. They also highlight the importance of including buoyancy effect for flows with Archimedes number of order one or higher. Fakhim et al. [20] discussed the affect of different angles of air coming out perforated tile. They showed that air coming perpendicular to tile (90 degree angle) will serve best, as it counters the affect of hot air recirculation at the top of the rack.

The most important component of data center is rack, typically a 2-m-tall enclosure, which contains various servers, data storage and networking equipment placed vertically. The density of racks increased with time resulting in increase of watts/ft^2, as shown in Table 1.1.

Table 1.1: Data is based on 5,000-square-foot room power distribution units in the same space [21]

Year	Rack Density	Watts Per Square Foot
2004	15 kilowatts (kW)	250
2006	22.5 kW	375
Current	30 kW	500

Zhang et al. [22] numerically investigates three different models of rack (from black box model to detailed representation of server and rack) to predict temperature distribution in the data center test cell. The results from all three models do not differ substantially. So, it is concluded that rack detail did not affect results greatly.

Kumar et al. [23] studied the effect of server load variation on the air flow distribution in the cold aisle. They found that cold air was best utilized when all the servers have same air flow rate. It was also shown that modeling of servers as a cluster lead to better air flow management as compared to individual servers. Ghosh et al [24] performed the experimental and numerical

study to investigate the results of server heat load on temperatures in the data center. Temperature contours are examined for variable number of servers in the test rack (N = 42, 32, 22 and 12). Where N represents number of servers and N=42 represent maximum load case. It is found that location of server affect fan speed and power consumption. i.e., placing the server at highest location improves energy efficiency.

Bedekar et al. [25] did numerical study to investigate the effect of CRAC location for three different flow rates from CRAC (6000cfm, 8000cfm and 10,000 cfm). Study showed that at 6000 and 8000 cfm, temperature was high at the top of rack due to recirculation of hot air. This can be overcome by placing CRAC near to rack.

Gang Tan et al. [26] perform the experimental-numerical validation of a data center to devise an expansion plan in the existing data center. After numerical validation of existing data center, they performed CFD simulation to study the effects of two expansion projects. One project is to add two 10KW racks and other involves the addition of entire row of rack. They found that each rack in added row should be below 9KW for the rack inlet temperature to be within ASHARE standards. They also propose percentage open area of tiles for different density racks in added row.

Above discussion shows that much less literature is available on experimental-numerical validation of data centers. Most papers published in this regard concentrate on the studies of thermal behavior of data center. [27] Discuss the validation of temperature and velocity profiles, but there are some limitations about this paper. One, the paper describes the study of Non Conventional cooling system which is not the focus of the present study. Second, although the paper takes into account the measurement of velocity data, but it is not the primary index for comparison of numerical experimental study.

In 2010, M. D. Lloyd [28] studied a small data center. He performed experimental as well as numerical study for the validation of thermal and velocity profiles in the data center. He separates the region around two racks in the data center located at MIT Laboratory for nuclear science. He use hot wire anemometer to obtain velocities at the surface of tiles and in cold aisles. He also obtains average inlet and outlet temperatures of both racks. He then performs numerical study and found that results show agreement with the experimental data. Although this study include validation of velocity profiles which is not the comparison parameter before, but the domain of this study is such that it does not represent real data center. Racks are packed such that

there is no free space around racks. Therefore recirculation of air from hot to cold aisle is not possible in this configuration. This can also be cleared from the fact that his average inlet temperature of rack is 284K which is equal to room inlet temperature. While in real data centers, this will vary up to 4K.

1.4 Scope of the work

Objectives

The objectives of the thesis are as follows

a. Reduce the energy consumption in a data center at Research Center of Modeling & Simulation, NUST.

b. Suggest configuration of servers to enhance heat transfer to lower electricity cost.

Contribution

The purpose of this thesis is to study the flow patterns and thermal behavior of a data center located at Research Center for Modeling and Simulation (RCMS), NUST. For energy efficiency of the existing setup, different configurations are analyzed and results are compared to obtain a better configuration. A generic study is also performed in this thesis for even numbered rows of racks data center and different configurations of Hot/Cold Aisle are analyzed. Based on results obtained, a configuration is proposed for efficient heat transfer across servers. This stud will help in the expansion project of RCMS data center.

The Approach

This work was done in four phases as shown in Figure 1.10. In first phase, cooling strategies used in different data centers were studied. There are many articles with focus on different configurations of above and below plenum data centers. Some of these papers were discussed in literature review section of chapter 1. Also governing equations and methodology was studied in this phase. That was discussed in chapter 2.

Some of above mentioned strategies were studied in more detail and being validated by performing numerical study in second phase. These studies and validation results were summarized in chapter 3. In phase three, experimental tests were conducted on a real data center

to analyze the flow patterns and thermal behavior inside the data center. Numerical study was then performed on same data center and results were compared with the experimental data.

During the last phase (Phase four), Hot/Cold aisle configuration effect on thermal behavior of data centers is performed. Numerical study was performed on two even numbered rows of racks data centers and results are compared with each other to decide which configuration provides higher transfer across racks. These results were summarized in chapter 6. The conclusion drawn from above mentioned work was then presented in chapter 7. Future recommendations were also presented in same chapter

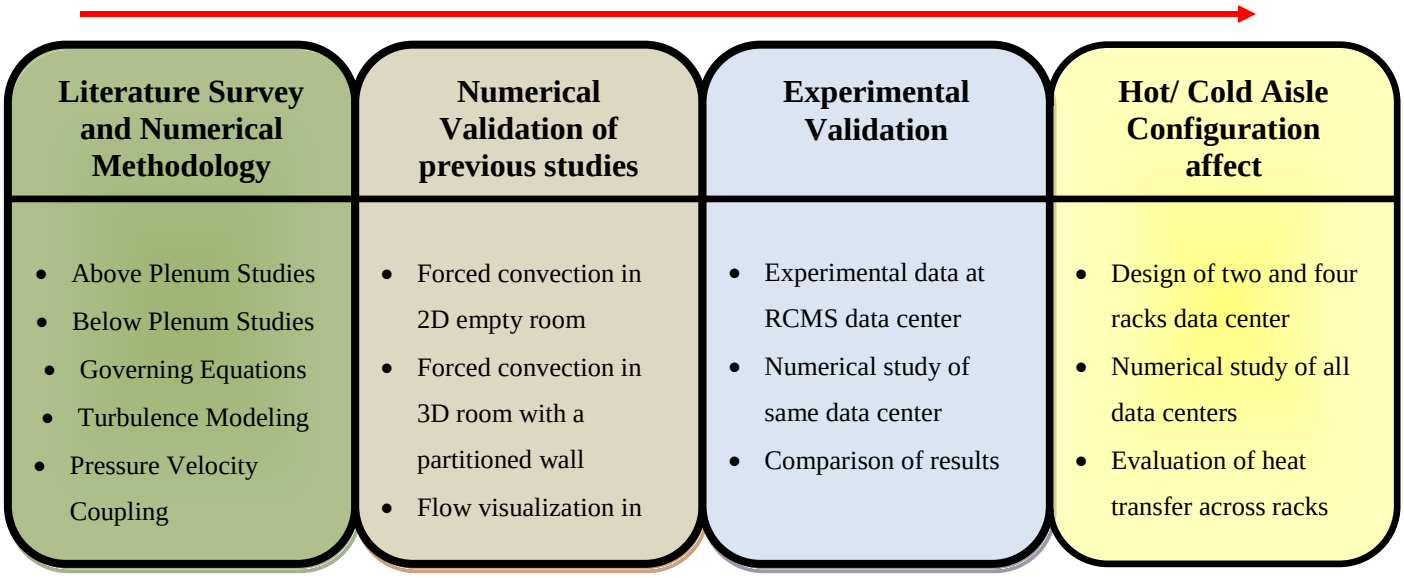

Figure 1.10: Schematic Diagram of Dissertation

Chapter 2

Numerical Methodology

The solution methods in Fluent are based on CFD models. CFD deals with numerical solution of fluid flow, heat transfer and other similar phenomena like radiation. The objective of CFD in this thesis is to obtain computer based predictions of the airflow and heat transfer process occurring within and around electronics equipment e.g., racks, servers, tiles etc.

2.1 Sequence of Solution

We used ANSYS FLUENT 13 **[**29**]** as CFD software to simulate fluid problems. FLUENT uses Finite Volume Method to solve governing equations described below. There are three steps to solve any problem; Pre Processing Step, Processing Step, and Post Processing Step

2.1.1 Pre Processing Step

In this step, geometry and mesh of the problem domain is generated. We use GAMBIT software [30] for this purpose. Firstly, geometry is produced by making surfaces (Rack inlet and outlet, Tiles, Room Walls etc) and then these surfaces are joined together to make volumes Racks, Servers, Room etc). Steps involved in meshing phase are

1. Edge Mesh: Firstly, all the edges are meshed as required. Non Uniform Mesh is applied for regions near the walls and near boundary condition areas.
2. Face Mesh: After edge mesh, all faces are selected and meshed accordingly.
3. Volume Mesh: All volumes are selected individually and meshed as required.

After generating mesh, all solid and fluid zones are identified. In present study, faces represent solid regions (i.e., walls, velocity inlet region etc) and volumes contain fluids.

2.1.2 Processing Step:

Once the mesh is generated, it is imported to FLUENT to solve for domain. Figure 2.1 shows the steps in this phase

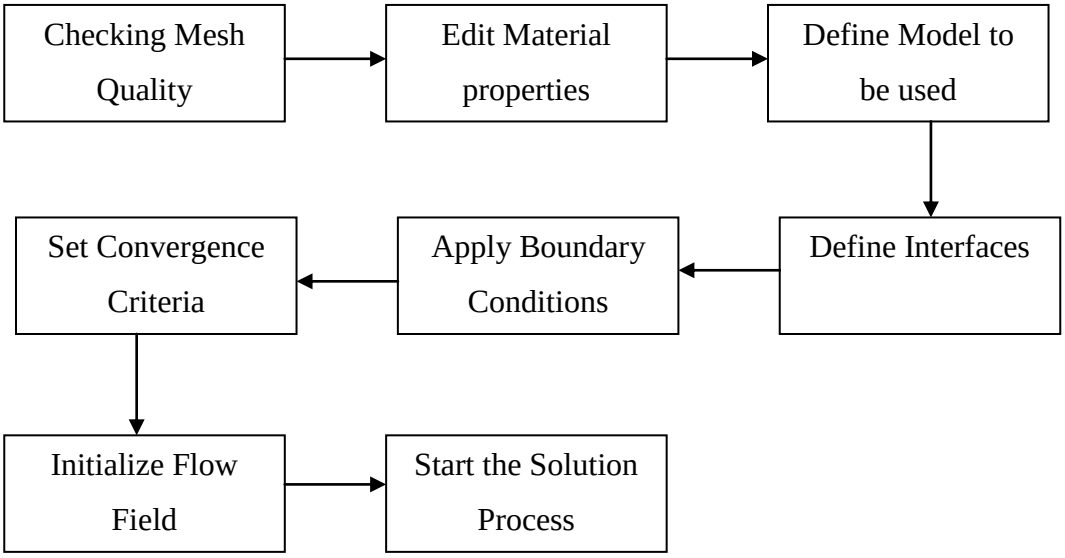

Figure 2.1: Processing Step undertaken in FLUENT for solution

2.1.3 Post Processing Step:

Once the solution process is complete, case and data file is stored. This is then imported to TECPLOT software [31] to view contours, streamline, velocity vectors etc of parameters like velocity magnitude, temperature, x velocity etc. Plots of a specific parameter at different sets of points can also be obtained to compare data with previous studies or experimental data.

2.2 Governing Equations:

The numerical solution of fluid flow and heat transfer phenomena involves solution of some coupled, non-linear partial differential equations known as Navier Stokes Equations. Field Variables involved in these governing equations are u, v, w, T and P. Where u, v and w are velocity components in x, y and z direction respectively. T is temperature and P is pressure. All these variables are function of space dimensions x, y, z and time t. The differential equations satisfied by these variables are known as conservation equations. For example, u, v and w satisfy momentum equation in all three coordinates. Temperature satisfies the conservation of energy

principal. Pressure did not satisfy any equation itself, but it is derived from continuity equation which represents the differential form of conservation of mass.

Navier Stoke's Equations:

We assume that our flow is incompressible under steady state situation. Navier Stokes equations under our assumption are reduced to following equations. These are governing equations for our model.

Continuity Equation:

$$\frac{\partial(v_i)}{\partial x_i} = 0$$

Momentum Equation:

$$\rho \frac{\partial(v_j v_i)}{\partial x_j} = \frac{\partial \tau_{ij}}{\partial x_j} - \frac{\partial p}{\partial x_i}$$

Energy Equation:

$$\rho \frac{\partial(v_j E)}{\partial x_j} = \frac{\partial}{\partial x_j}\left(K \frac{\partial T}{\partial x_j}\right) + \frac{\partial}{\partial x_j}(\tau_{ij} v_i)$$

Where, according to Stoke's hypothesis, for Newtonian Fluids

$$\tau_{ij} = \mu \left[\left(\frac{\partial v_i}{\partial x_j} + \frac{\partial v_j}{\partial x_i}\right) - \frac{2}{3}\frac{\partial v_k}{\partial x_k}\right]$$

And i, j = 1, 2, 3 and v represent Cartesian velocity components.

P = Pressure, T= Temperature, ρ = Density, K = Thermal Conductivity, μ = Viscosity

There are five equations and six unknowns (ρ, P, u, v, w, T). For Compressible flows, the mass conservation becomes a transport equation for density. An additional equation in the form of ideal gas law becomes transport equation for pressure. In incompressible flows, density variation does not link to pressure. Continuity equation becomes constraint on velocity field. Pressure appears as a source term in momentum equation. There is no separate equation for pressure. Therefore continuity equation combined with momentum equation to give equation for pressure, known as Pressure – Velocity coupling.

2.3 **Turbulence Modeling:**

Majority of flow inside the data center is turbulent. Reynolds numbers, even for conservative estimates of velocities, are consistently over 10,000. Turbulent flows are characterized by fluctuating velocity fields. These fluctuations are very small and of high frequency, therefore they are very difficult to simulate directly. Instead, instantaneous governing equations can be manipulated to remove these fluctuations, resulted in modified set of equations which are computationally less expensive.

To obtain a numerical solution for turbulence, Reynolds decomposition is applied to N-S equations. This technique employed the decomposition of turbulent component into instantaneous (Fluctuating) and mean (Time averaged) component. There are many models to compute solution of turbulent flow using Reynolds Decomposition.

2.3.1 K-$\boldsymbol{\varepsilon}$ Turbulence Model:

The standard K-$\boldsymbol{\varepsilon}$ turbulence model was proposed by Launder and Spalding in 1974 [32]. It is the most used turbulence model for predicting internal flows. i.e., flows inside the buildings and data centers. Standard K-$\boldsymbol{\varepsilon}$ model is based on transport equations for turbulence kinetic energy (*K)* and its rate of dissipation (ε). In derivation of this model, it is assumed that the flow is fully turbulent and molecular viscosity effects are negligible. *K* and ε are obtained from following transport equations

$$\rho \frac{\partial}{\partial x_i}(K v_i) = \frac{\partial}{\partial x_j}\left[\left(\mu + \frac{\mu_t}{\sigma_k}\right)\frac{\partial K}{\partial x_j}\right] + G_K + G_b - \rho\varepsilon - Y_M + S_K \quad \text{……..Eq. 1}$$

And

$$\rho \frac{\partial}{\partial x_i}(\varepsilon v_i) = \frac{\partial}{\partial x_j}\left[\left(\mu + \frac{\mu_t}{\sigma_\varepsilon}\right)\frac{\partial \varepsilon}{\partial x_j}\right] + C_{1\varepsilon}\frac{\varepsilon}{K}(G_K + C_{3\varepsilon}G_b) - C_{2\varepsilon}\rho\frac{\varepsilon^2}{K} + S_\varepsilon \quad \text{……..Eq. 2}$$

Where

G_K = Generation of K due to mean velocity gradient

G_b = Generation of K due to buoyancy

Y_M = Contribution of the fluctuating dilatation to overall dissipation rate (Neglected for incompressible flow)

σ_k & σ_ε = Turbulence Prandtl numbers

S_K & S_ε = User Defined Source Terms

$C_{1\varepsilon}$, $C_{2\varepsilon}$ & $C_{3\varepsilon}$ = Constants

2.3.2 Spalart-Allmaras Model

The Spalart-Allmaras model is used to solve the turbulent viscosity equation. This is one equation model. This is effective for low Reynolds number flows. Mesh requirement for this model is $y^+ > 30$. Near Wall Treatment ($3 < y^+ < 30$) should be avoided for this model.

The transported variable in SA model is similar to the turbulent kinematic viscosity term except in viscosity affected region. The governing equation for this model is

$$\frac{\partial}{\partial x_i}(\rho v u_i) = G_v + \frac{1}{\sigma_v}\left[\frac{\partial}{\partial x_i}\left\{(\mu + \rho v)\frac{\partial v}{\partial x_j}\right\} + C_{b2}\,\rho\left(\frac{\partial v}{\partial x_j}\right)^2\right] - Y_v + S_v$$

Where G_v is the production of turbulent viscosity, Y_v is the destruction of turbulent viscosity, σ_v and C_{b2} are constants and S_v is a user defined source term.

At walls the modified turbulent viscosity $\tilde{\nu}$ is set to zero. When grid is fine enough so that it can resolve the viscosity dominated sublayer, the wall shear stress is obtained from the laminar stress-strain relationship given as

$$\frac{u}{u_\tau} = \frac{\rho u_\tau y}{\mu}$$

If grid is too coarse so that it cannot resolve the sublayer, then it is assumed that the centroid of the wall adjacent cell falls within the logarithmic region of the sublayer. Now, the law of wall is employed which is given as

$$\frac{u}{u_\tau} = \frac{1}{k}\ln_E\left(\frac{\rho u_\tau y}{\mu}\right)$$

Where u is velocity parallel to the wall, u_τ is the shear velocity, y is the distance from the wall, k is Von Karman constant (0.4178) and E = 9.793

2.3.3 Standard, RNG and Realizable *K–ε* Models:

This section presents the use of standard, RNG and realizable K–ε models. All three models have similar forms of transport equation for K and ε. Following are the major differences in the models

i. The method of calculating turbulent viscosity
ii. The turbulent Prandtl numbers governing the turbulent diffusion of K and ε
iii. The generation and destruction terms in the ε equation

The features that are common to all models include turbulent generation due to shear buoyancy, accounting effects of compressibility and modeling heat and mass transfer.

Standard K–ε Model:

Modeling the Turbulent Viscosity:

The turbulent or eddy viscosity μ_τ is calculated by combining K and ε as follows

$$\mu_\tau = \rho C_\mu \frac{K^2}{\epsilon}$$

Where C_μ is the constant.

RNG K–ε Model:

The RNG model is similar to the standard K–ε model except following refinements

i. RNG has an additional term in ε equation which improve the accuracy
ii. The RNG provides an analytical formula for turbulent Prandtl numbers, while standard model used user specified values

Modeling the Effective Viscosity:

For low Reynolds number and near wall flows, RNG theory results in differential equation for turbulent viscosity and is given as

$$d\left(\frac{\rho^2 K}{\sqrt{\mu\epsilon}}\right) = 1.72\ \frac{v}{\sqrt{v^3}-1+C_v}\,dv$$

$$v = \frac{\mu_{eff}}{\mu}\ and\ C_v = 100$$

For high Reynolds number, equation becomes

$$\mu_t = \rho C_\mu \frac{K^2}{\epsilon}$$

With C_μ = 0.845. This value is very close to the one for standard K–ε model where it is0.09.

2.4 SIMPLE Algorithm:

The SIMPLE (Semi-Implicit Method for Pressure-Linked Equations) allows coupling the Navier-Stokes equations with an iterative procedure. This method has been discussed by Patankar and Spalding [33]. In this method, we initially guess the pressure field P^*. This P^* is the assumed pressure and using its value we solve the Navier Stoke's equation and find u^*, v^* and w^*. Now we use pressure correction equation and find values of corrected pressure *P'*. Then we calculate *P* by adding P^* and *P'*. Also find *u, v* and *w* from their assumed values using respective formulas. Solve the discretization equation and find other unknowns such as temperature concentration, turbulence quantities etc. Treat the corrected pressure as assumed pressure *P*. Find starred velocities and the whole process repeated until a converged solution is obtained.

2.5 Boundary Conditions:

Boundary conditions that are frequently used in our studies are discussed in detail in this section. These conditions include Fan boundary condition, Porous jump boundary condition, and interior boundary condition and outflow boundary condition.

Fan Boundary Condition:

Fan boundary condition is used to determine the impact of fan with known characteristics. This boundary condition allows inputting an empirical fan curve which is governed by relationship between head (pressure rise) and flow rate (velocity) across a fan element. In this model, we don't need to model the fan blades. We assign the pressure velocity relationship on a simple flat

surface. This relationship can be constant, linear or a polynomial function. General form of relationship is given in following equation

$$\Delta P = \sum_{n=1}^{N} f_n v^{n-1}$$

Where ΔP is the pressure jump, f_n are the pressure jump polynomial coefficients and v is the magnitude of the local fluid velocity normal to the fan. In our model, this boundary condition is used to model the fans inside the servers.

Porous Jump Boundary Condition:

It is very difficult to model small openings of perforated tiles, rack rear and front, server front etc. There are 768 small opening in four square foot area of tile of our model, and this number increases while modeling rack. In order to avoid this difficulty, porous jump boundary condition is used. This boundary condition actually accounts the pressure loss due to resistance of the perforations. Thus eliminate the requirement to model the perforations. Darcy Law is the governing equation for this condition which is given as

$$S_i = -\left(\frac{\mu}{\sigma} v_i + C_2 \frac{1}{2} \rho |v| v_i\right)$$

Where σ is permeability, C_2 is inertial resistance factor, $|v|$ is the magnitude of velocity and S_i is the source term. In our model, this boundary condition is employed for server inlet perforations.

Interior Boundary Condition:

Whenever there is some interface between two or more fluids, either one of the following two boundary conditions can be employed to that

Porous Jump: Whenever there are perforations between two fluids or there is some porous media

Interior: When we just want to intermix both fluids freely and there is no blocking between them. So interior is a surface without any function. In our model, this condition is employed at server inlet and outlet.

Outflow Boundary Condition:

Outflow boundary condition is employed where flow exits and we don't know the details of velocity and pressure of the fluid before solution. We don't define any conditions at outlet boundaries and solver extrapolates the required information from the interior. In our model, this condition is employed at the outlet of the room or data center.

Heat Flux Boundary Condition:

When the constant heat flux from a device is known, boundary condition employed for that surface in numerical study is heat flux boundary condition. In our model, this condition is used to model heat generated by servers in the racks.

Velocity Inlet Boundary Condition:

This boundary condition is used to define the flow velocity along with other scalar properties of the flow at the flow inlets. This boundary condition is intended to be used for incompressible flows. In our model, this condition is used at air entrance surfaces of room or data center.

Chapter # 3

Validation Studies

In this chapter, we perform few validation studies in order to verify our CFD simulations. We initially take the simplest case and increase the complexity of flow domains step by step. We perform three validation studies. First case is the simplest 2D empty room and flow is just coming from one side and leaves the room from opposite wall. In next case, we consider a 3D empty room with a wall partition inside it. In case three, we performed 3D analysis of a data center test cell, with two fully packed server racks. Details of each case is discussed in this chapter.

3.1 Case 1: Numerical Simulation of Forced Convection Flow Inside 2D empty room

Objectives:

a) Validation of CFD codes
b) Comparison of analysis from different turbulent flows
c) Grid Independent Study
d) Understanding the flow physics

3.1.1 Room Configuration:

Figure 3.1 shows the description of room with data extraction lines (dotted). Room is of 9m by 3m. But for non dimensional analysis, we use the following data

$$L / H = 3;\ h / H = 0.056;\ t / H = 0.16 \text{ where } H = 3m$$

Experimental data for this case was obtained from a scale model room using LDA by Nielsen [34]. They obtain horizontal velocity (u) component data at two vertical lines at x = H and x = 2H. Similarly, u was also obtained at two horizontal line with y = h / 2 and y = H – h / 2. These lines are shown as dotted in Figure 3.1.

3.1.2 Boundary Conditions:

There are two main boundary conditions used in this numerical study; Velocity inlet and outflow. All side walls of the room are given wall boundary condition with no slip condition and no heat flux is generated from them. Outflow boundary condition is used at the surface where flow is leaving the room where as at the inlet surface of the room, velocity boundary condition is employed with following x and y components

$$\mathbf{U_o = 0.455\ m/s \text{ And } V_o = 0}$$

K_0 And ε_0 are obtained by using equation [3-5]

$$K_0 = 1.5\ (0.04 * U_0)^2 \quad \text{…….. } \textit{Eq. 3}$$

$$\varepsilon_0 = \frac{{K_0}^{1.5}}{l_0} \quad \text{…….. } \textit{Eq. 4}$$

Where

$$l_0 = \frac{h}{10} \quad \text{…….. } \textit{Eq. 5}$$

3.1.3 Data Collection points

There are four regions where velocity data is compared with the experimental data. These regions are shown as dotted straight lines in Figure 3.1. First two lines are parallel to x-axis and y component are at 0.84m and 2.914m respectively. Other two lines are parallel to y-axis with x component equal to 3m and 6m respectively. U velocity component is calculated at all the lines and then compared with the experimental data.

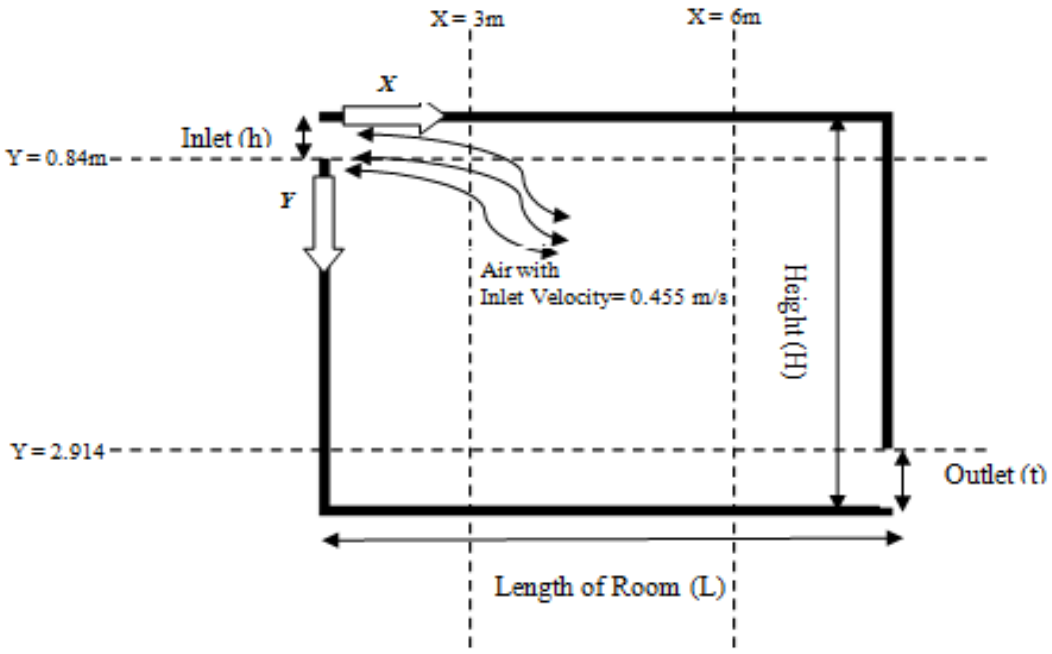

Figure 3.1: Configuration of 2D test room

3.1.4 Grid Independent Study:

In order to check grid independence, we performed simulations on several grid sizes. The results for very coarse and very fine meshes diverge from experimental data. So we choose intermediate range of grid sizes. The results for three different meshes are shown below from Figure 3.2 to Figure 3.5. The most relevant results were obtained from 300 * 100 grid size.

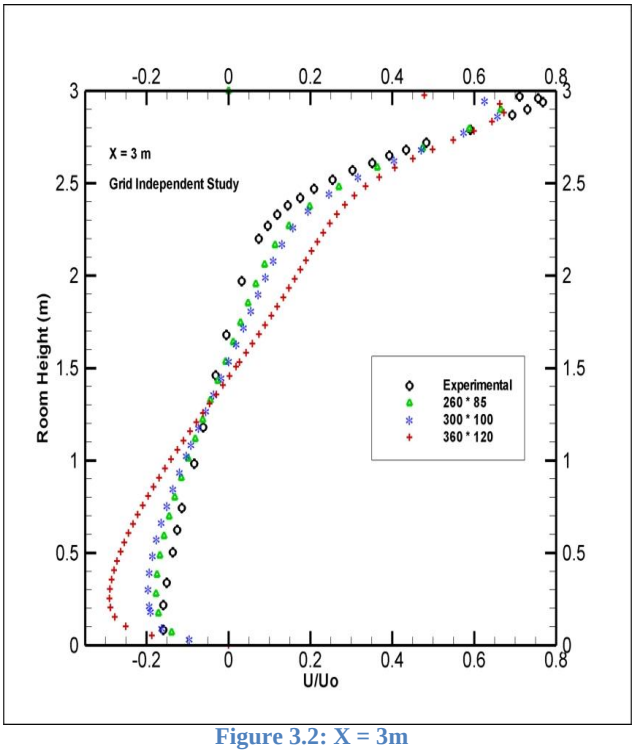

Figure 3.2: X = 3m

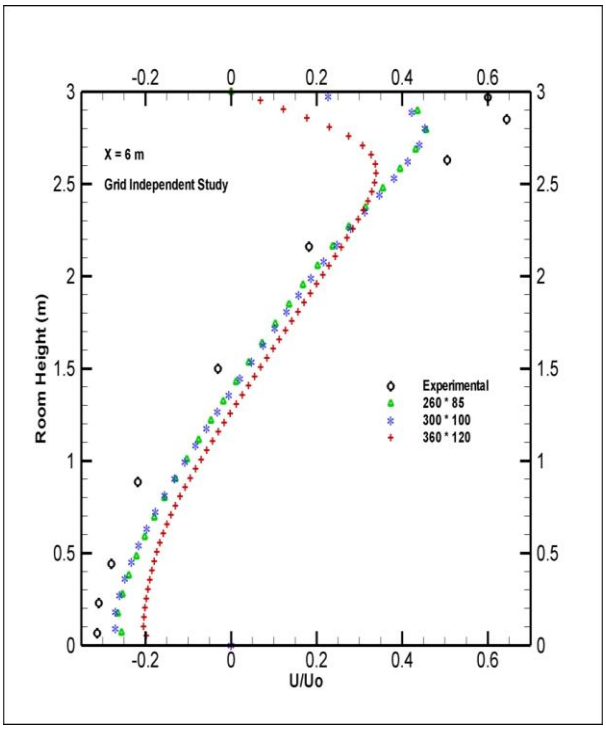

Figure 3.3: X = 6m

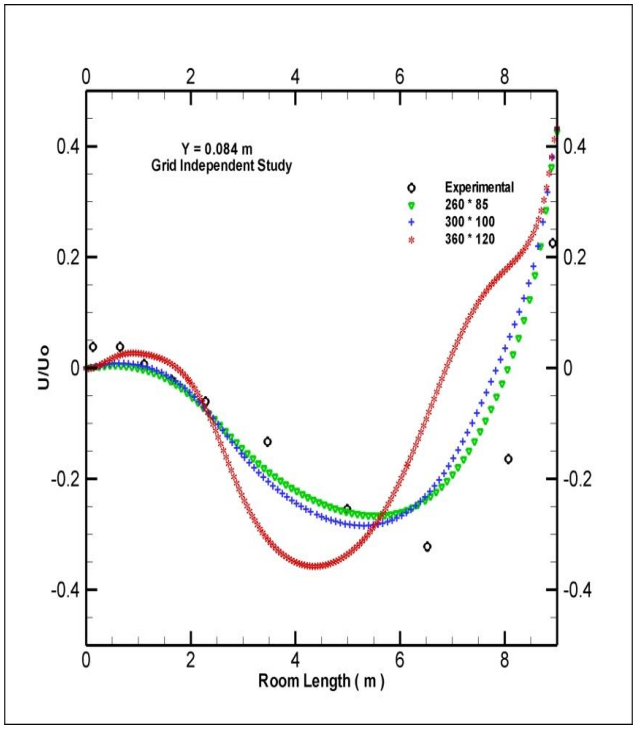

Figure 3.4: Y = 0.084m

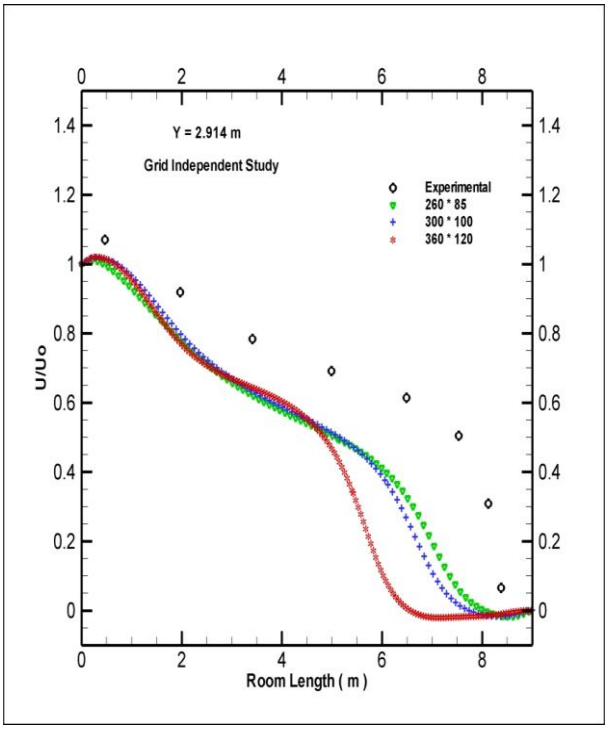

Figure 3.5: Y = 2.916m

Table 3.1: Grid Independent Study

3.1.5 Comparison of All Turbulence Models

Numerical simulation of the above case is performed by Standard K-Epsilon Model, Standard K-Omega Model and Sparlet Allmaras Model. U Velocity in non dimensional form is obtained on all the four lines mentioned above. Results are shown in Table 3.2.

It is found that K-Omega model gives the worst results of all. While K-Epsilon and Sparlet Allmaras model shows good agreement with experimental data. Both K-*E* and SA model under predict the x throughout domain in inlet region. This is shown in Figure 3.6 and Figure 3.7. Results are under predicted in the top region. A strange behavior is obtained when velocities are computed at y = 0.084m and y = 2.916m. Although the pattern is similar in case of K-*E* and SA model, but velocities are much lesser than experimental data. Again, K-O model shows strange results for both of these lines.

3.1.6 Comparison of All K-Epsilon Turbulence Models:

We found from above discussion that K-*E* gives best results as compared to other models. So we obtain all results from all K-E models (Standard, RNG and Realizable) and compare them. Results are shown in Table 3.3. Standard and RNG K-E model show almost similar behavior and their results are close to experimental data. Realizable K-E model show strange behavior for x = 3m and y = 0.084m. It over predicts the results throughout domain.

3.1.7 Comparison of Wall Treatments for Standard K – Epsilon Model:

Above discussion shows that standard K-E provides best results for our domain problem. In this section different wall treatments (Standard Wall Treatment: SWT; Non Equilibrium Wall Treatment: NEWF and Enhanced Wall Treatment: EWT) are studied to analyze their affects on flow dynamics. Results of x velocity (U/Uo) on all the lines are shown in Table 3.4. All the treatments under predict x velocity throughout domain. This pattern is shown in Figure 3.14 to Figure 3.17. Moreover, no strange behavior is obtained in these results. All treatments show almost similar results.

3.1.8 Standard K-Epsilon Model with SWF:

We can conclude from results and discussion that Standard K-Epsilon model with Standard Wall Function gives best results for 2D room Forced Convection flow. X velocity and Y velocity contours are shown in Figure 3.18 and Figure 3.19. Streamlines on both contours are shown in

Figure 3.20 and Figure 3.21. Due to very small inlet and outlet zones, strong recirculation flow occurs within the room. Velocity of inlet jet is high enough to reach up to the center of room. Y velocity (V/Vo) contours are almost symmetric around the center line of room. This shows that most part of the inlet jet is recirculated within room before leaving out.

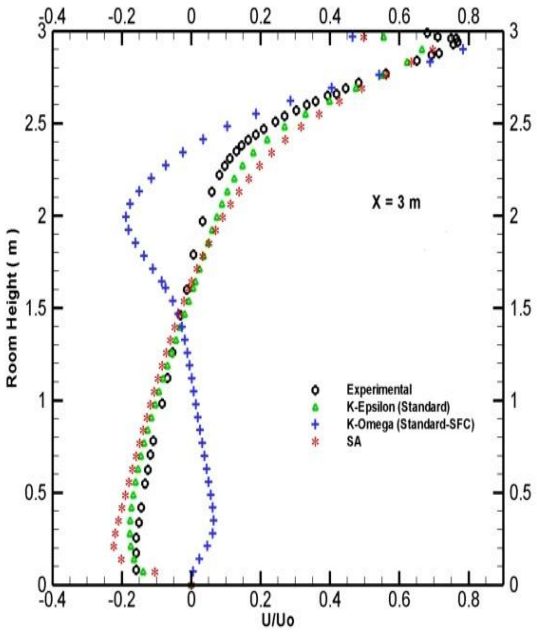

Figure 3.6: X = 3m

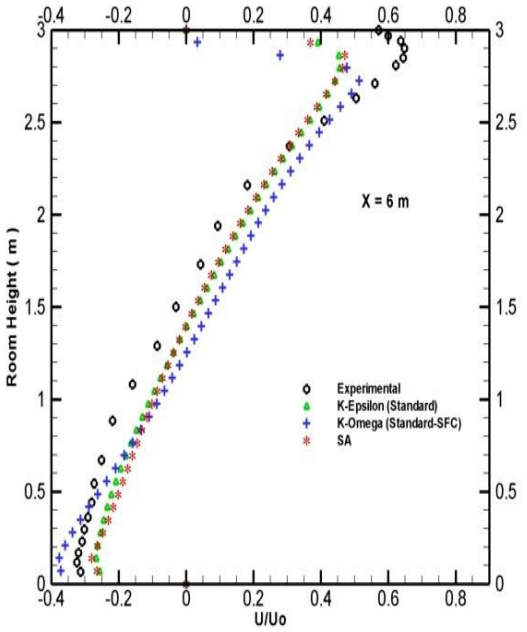

Figure 3.7: X = 6m

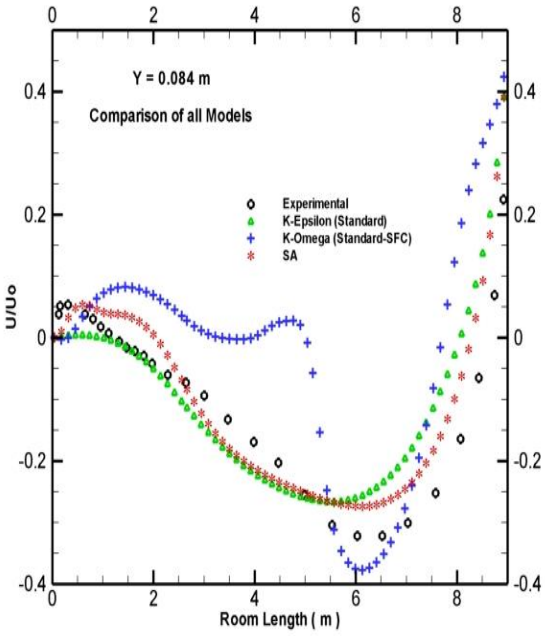

Figure 3.8: Y = 0.084m

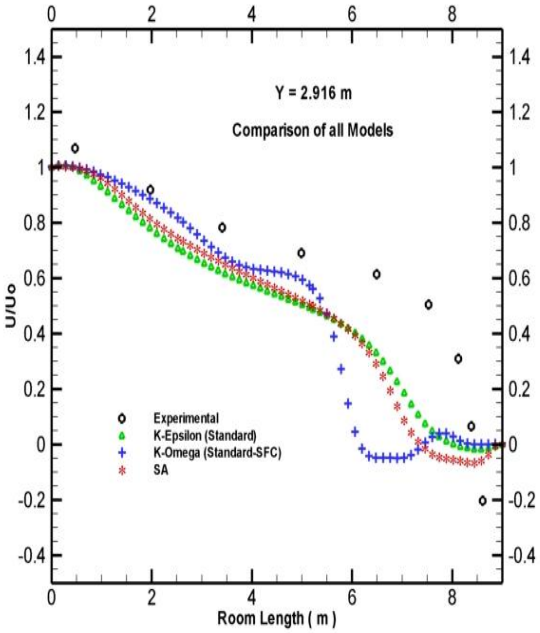

Figure 3.9: Y = 2.916m

Table 3.2: Comparison of All Turbulence Model

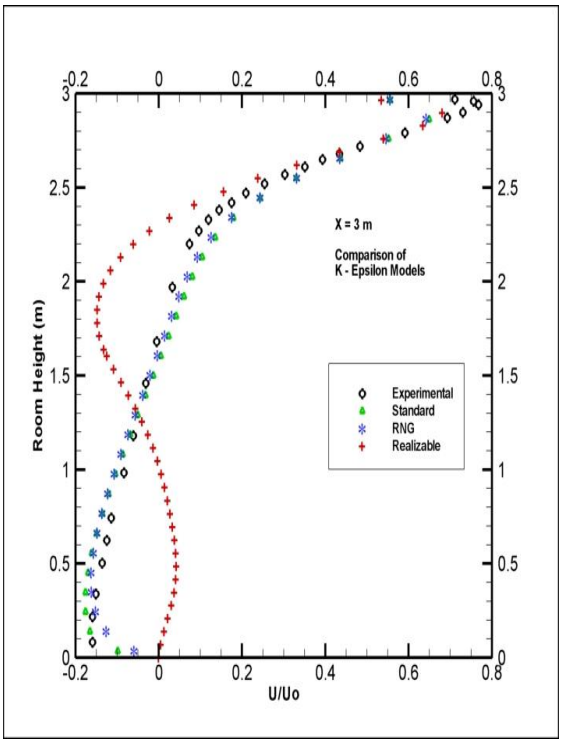

Figure 3.10: X = 3m

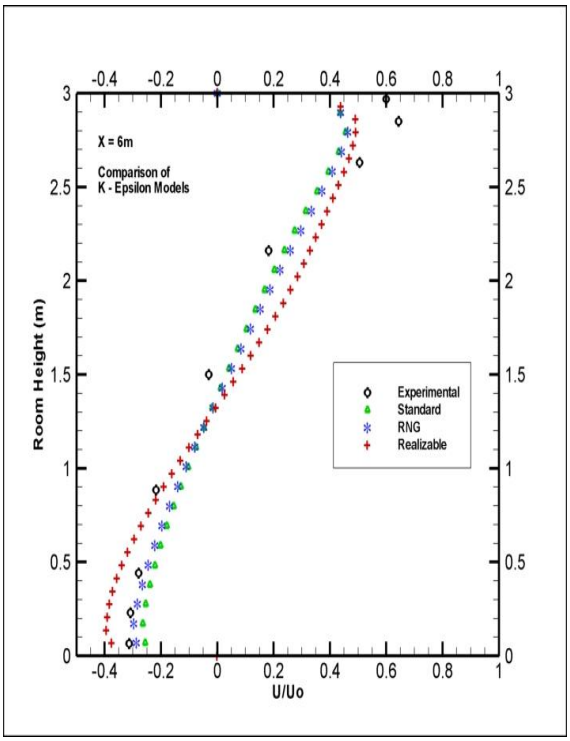

Figure 3.11: X = 6m

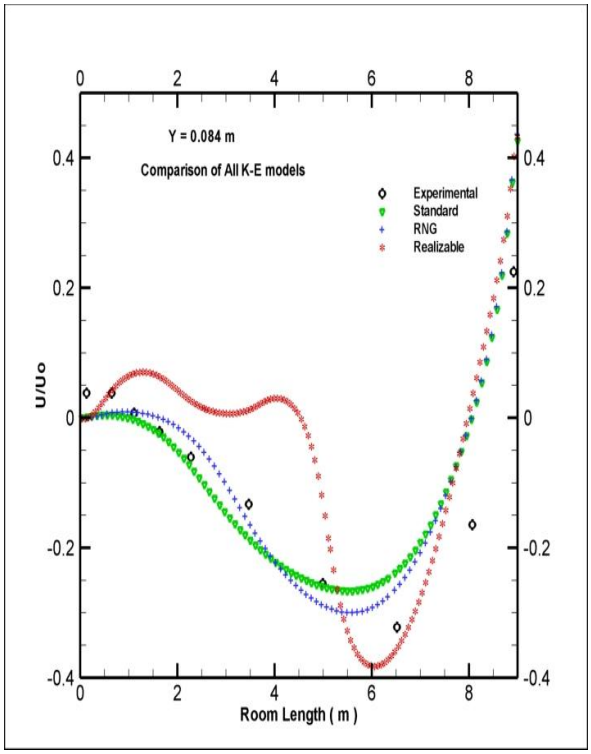

Figure 3.12: Y = 0.084m

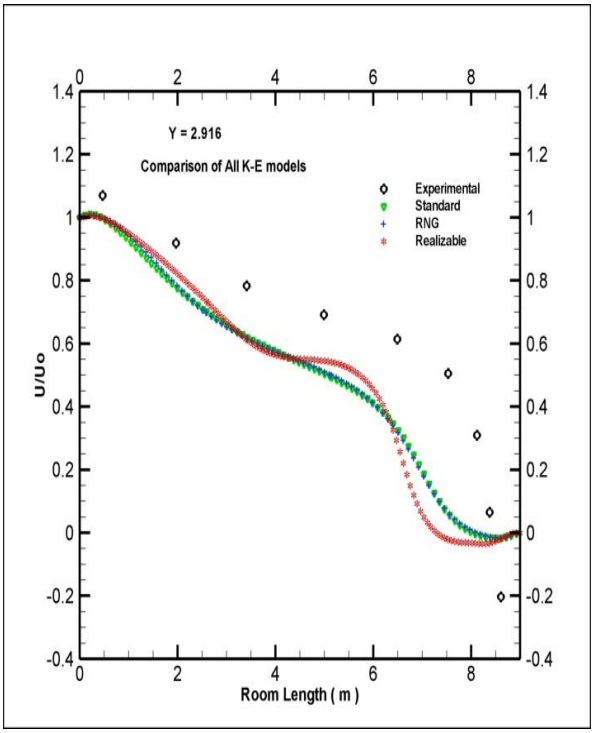

Figure 3.13: Y = 2.916m

Table 3.3: Comparison of All K - Epsilon Turbulence Models

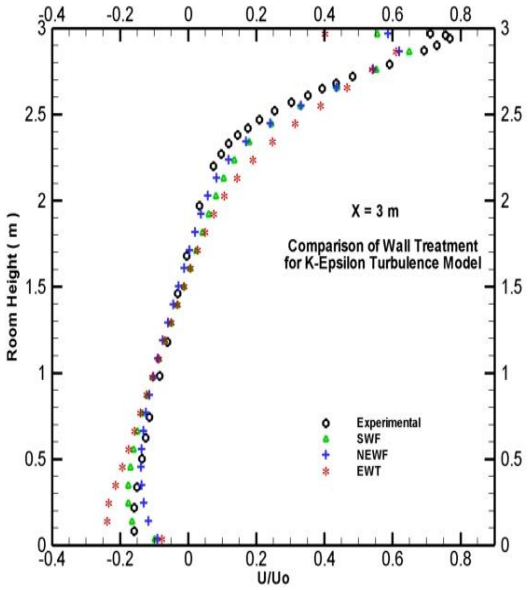

Figure 3.14: X= 3m

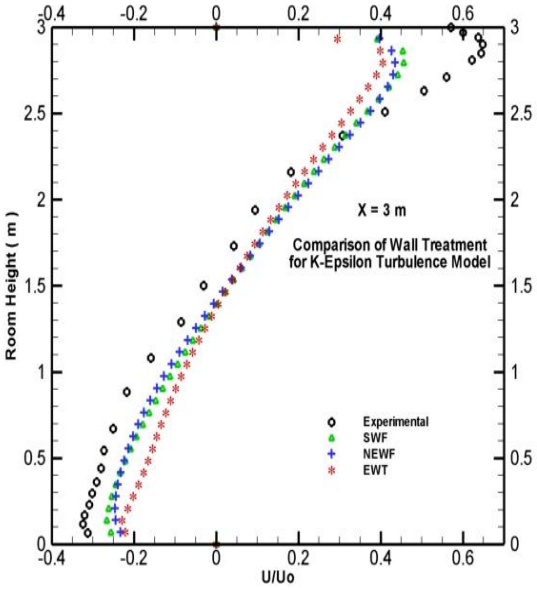

Figure 3.15: X = 6m

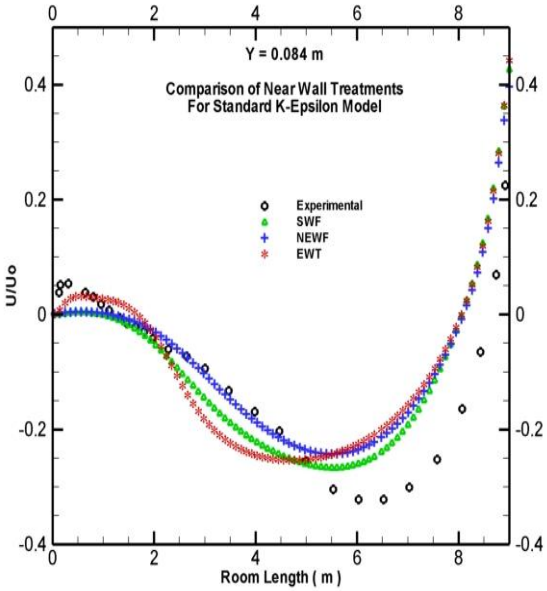

Figure 3.16: Y = 0.084m

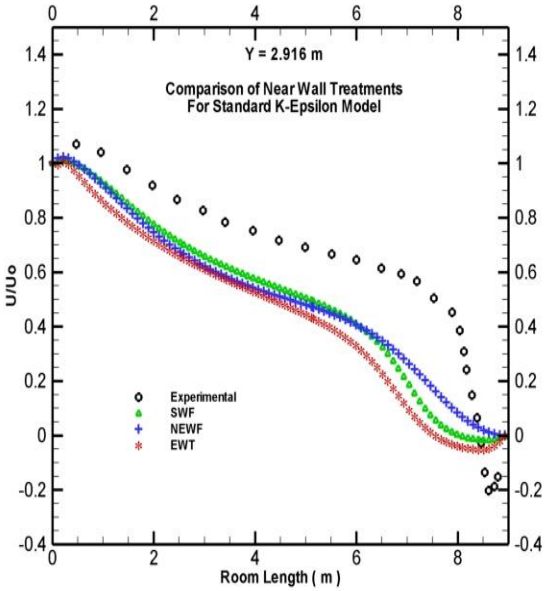

Figure 3.17: Y = 2.916m

Table 3.4: Comparison of Wall Treatments for Standard K-Epsilon Model

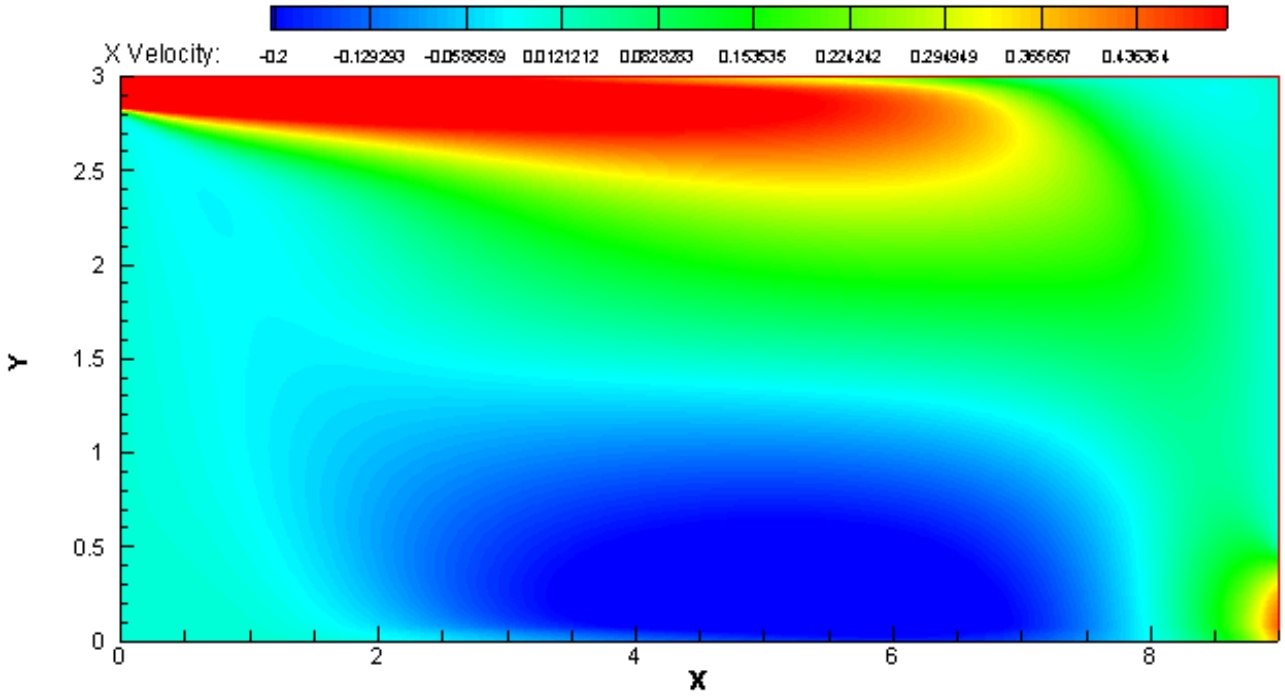

Figure 3.18: X Velocity (U/Uo) Contours

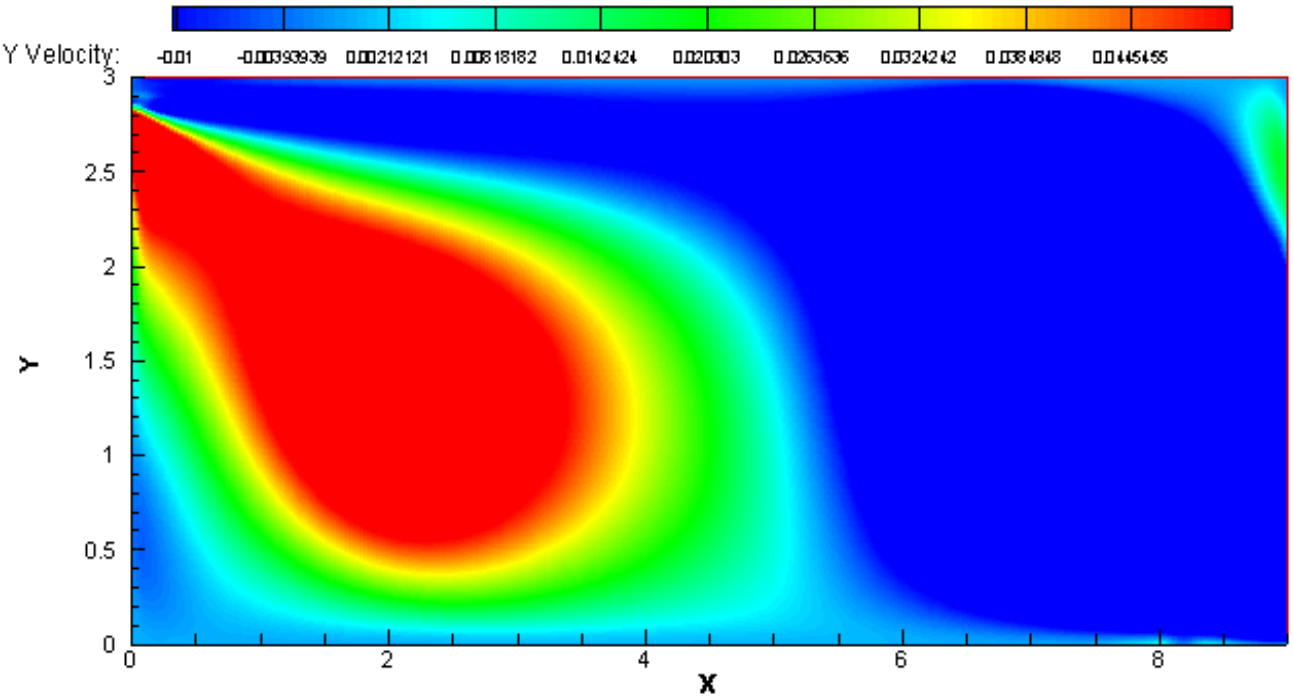

Figure 3.19: Y Velocity (V/Vo) Contours

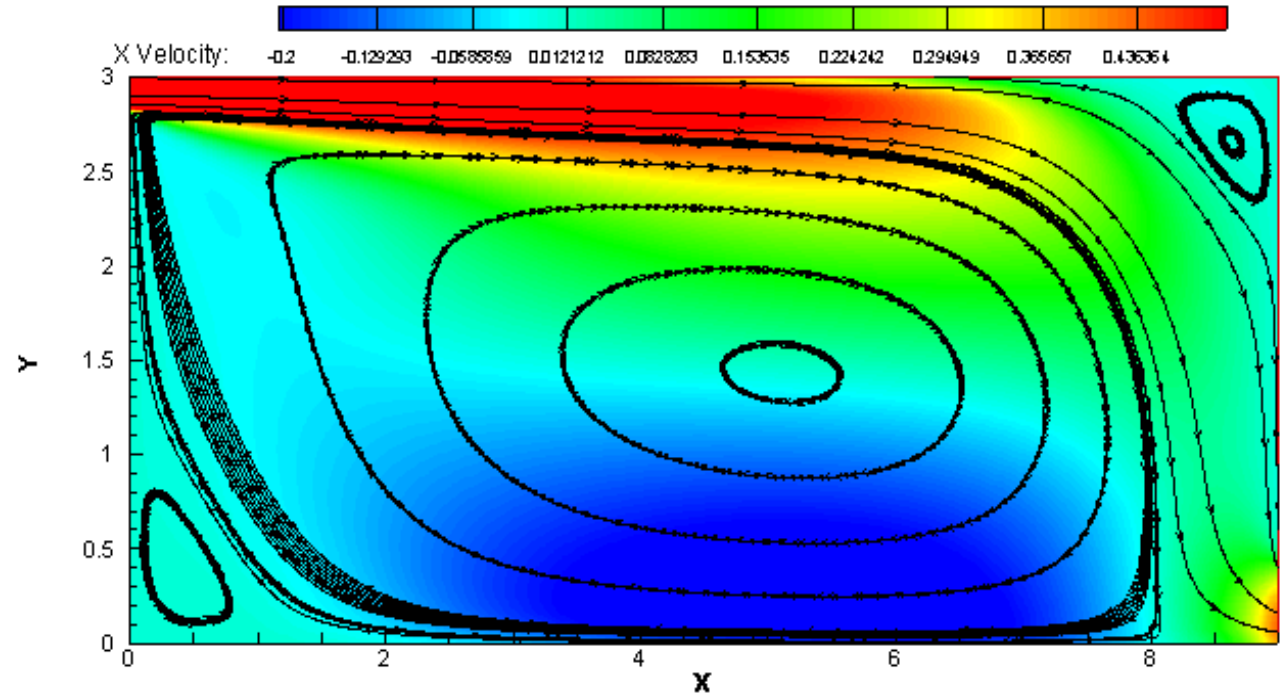

Figure 3.20: Streamlines on X Velocity Contours

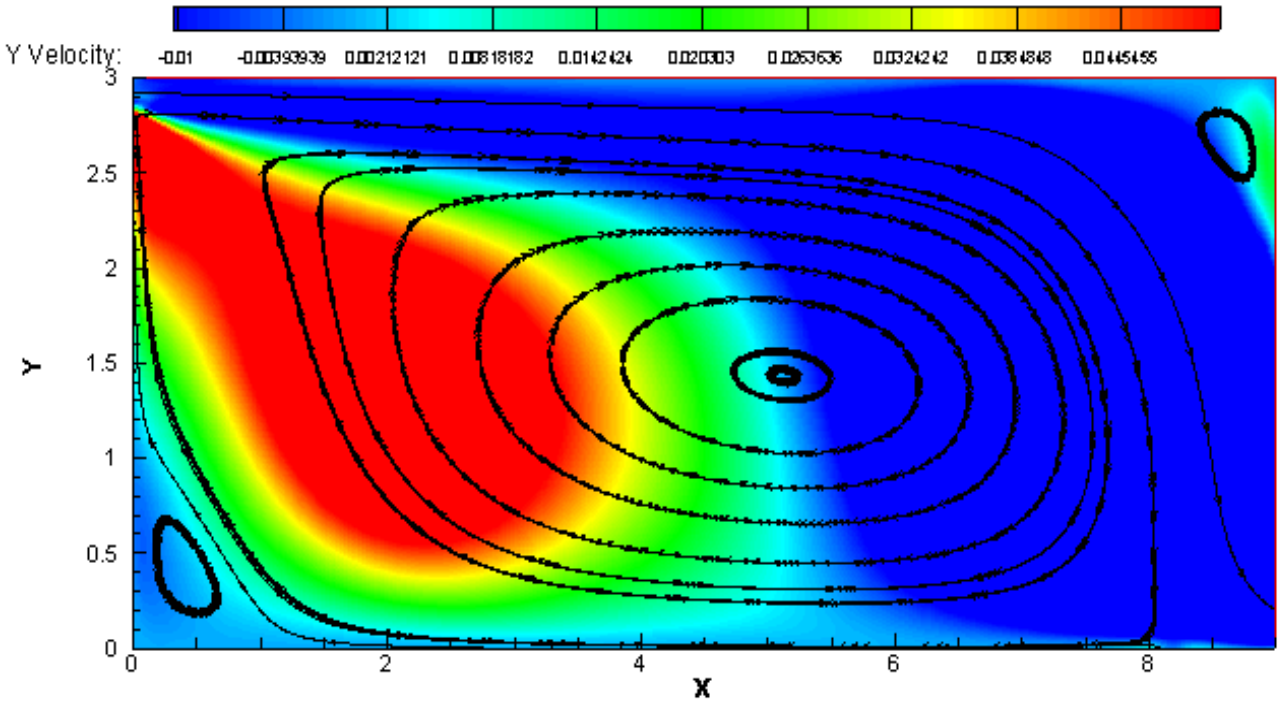

Figure 3.21: Streamlines on Y Velocity Contours

3.2 Case 2: Isothermal Forced Convection Flow inside 3D Room with a Partition Wall

To further evaluate the indoor flows, we take 3D Room Force Convection Flow. This test case is presented by Buchanan [35]. Experiment is conducted in a model room of dimension 0.95m * 0.46m * 0.3m. This represents 1/10 of a modern office room. It has an inlet and outlet; both are 0.1m * 0.1m and are located at the top wall of the model room. There is a wall of very small thickness (0.01m) and of height 0.15m located at the center of the room. Configuration of room is shown in Figure 3.22. Air enters the room from inlet with a velocity of 0.235 m/s and leaves from the outlet. Vertical velocity components are obtained at Jet Center Line and Mid Height Line. Both the lines are shown in Figure 3.23.

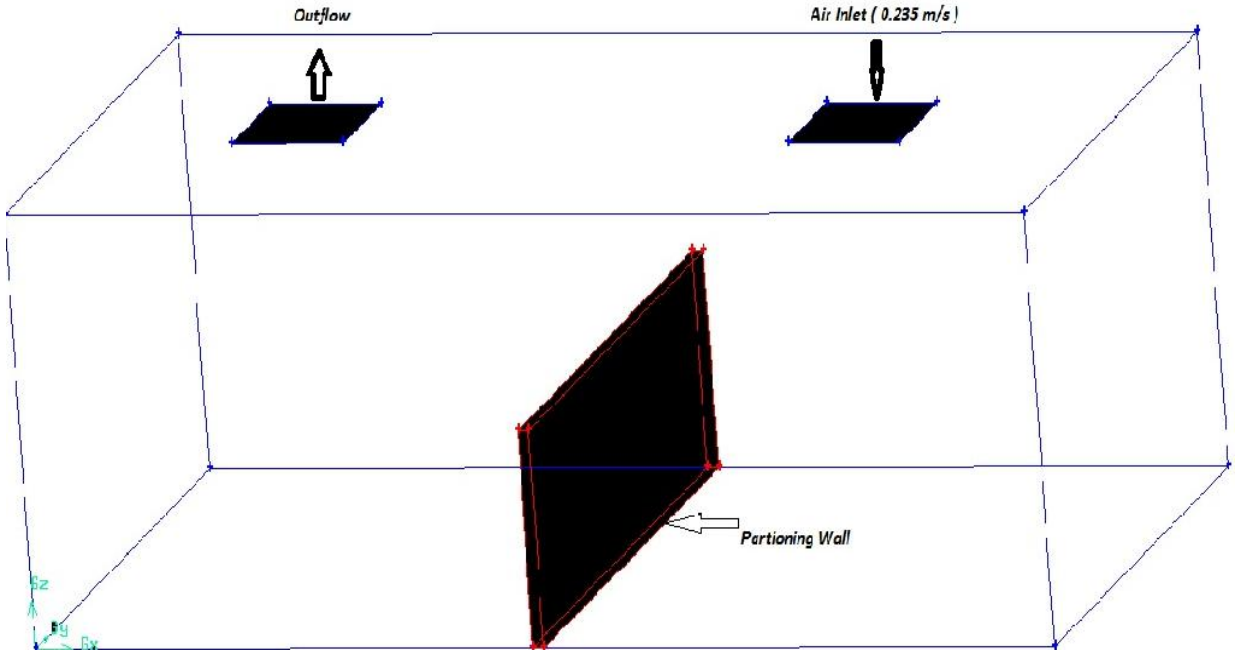

Figure 3.22: Configuration of Case 2 Room

Figure 3.23: Data Collection Lines (Blue) for Case 2

3.2.1 Boundary Conditions:

Following Boundary Conditions are employed in numerical simulations

Inlet:

Velocity Inlet; Vx = 0, V_y = o, V_z = 0.235 m/s

Outlet:

Pressure Outlet; Gauge Pressure = 0

Walls:

No slip Boundary Condition

3.2.2 Comparison of all Turbulence Models:

Vertical Velocity component for jet center line and mid height line obtained from all turbulence models are presented in Figure 3.24 and Figure 3.25. All turbulence models show similar behavior for jet center line case. Results are quite close to experimental data. For mid height line, there are two interesting regions, the center wall region (upper circle) and jet inlet region (lower circle) as shown in Figure 3.25. Around center wall K-Omega model best predicts the velocity peaks, while at jet inlet region all models shows little under prediction from experimental data.

3.2.3 Comparison of all K-Epsilon Turbulence Models:

K-Epsilon model gives better results as compared to other turbulence model except near center wall region. This behavior can be seen in Figure 3.26 and Figure 3.27. Standard K-Epsilon again shows better agreement to experimental data as compared to RNG and Realizable models.

3.2.4 Comparison of Near Wall Treatment for Standard K-Epsilon Turbulence Model:

Figure 3.28 and Figure 3.29 shows Z velocity component at jet center line and mid height line for different wall treatments in K-Epsilon turbulence model. Enhanced wall treatment (EWT) shows little different behavior as compared to Standard wall function (SWF) and Non Equilibrium wall function (NEWF). This is due to the fact that EWT requires very fine mesh near the wall to capture viscous sub layer affects. We did not employ very fine mesh in our model due to computational time issue. Therefore we see much less velocities for EWT case rather than SWF and NEWF.

3.2.5 Contours and Vector Plots in Y Plane:

Z Velocity contour along mid Y plane is shown in Figure 3.30, while vector plots on similar plane near mid wall and near right wall of room are shown in Figure 3.31and Figure 3.32 respectively. From contour, it’s found that velocity is high near the right wall and near right side of mid wall. From vector plots, the reason for this high velocity is found that when inlet air strikes the floor, it moves in upward direction.

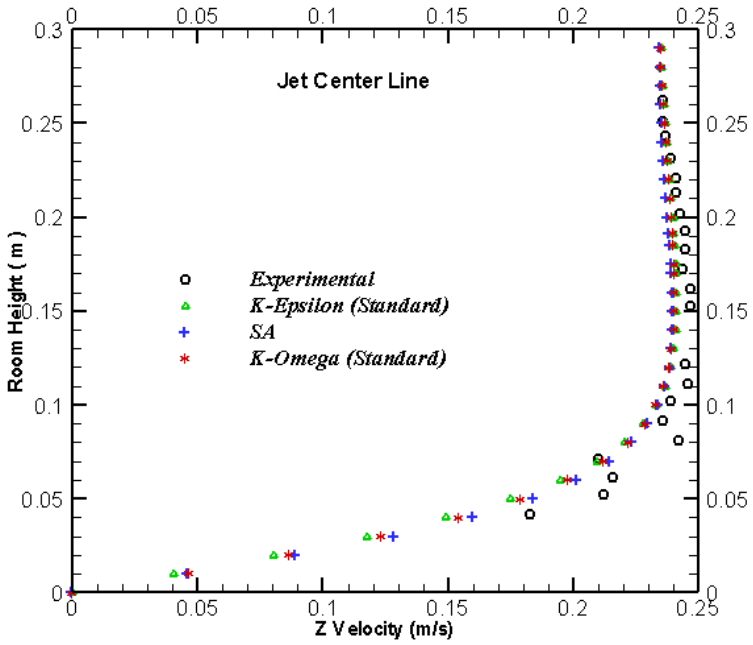

Figure 3.24: Comparison of all Turbulence Models

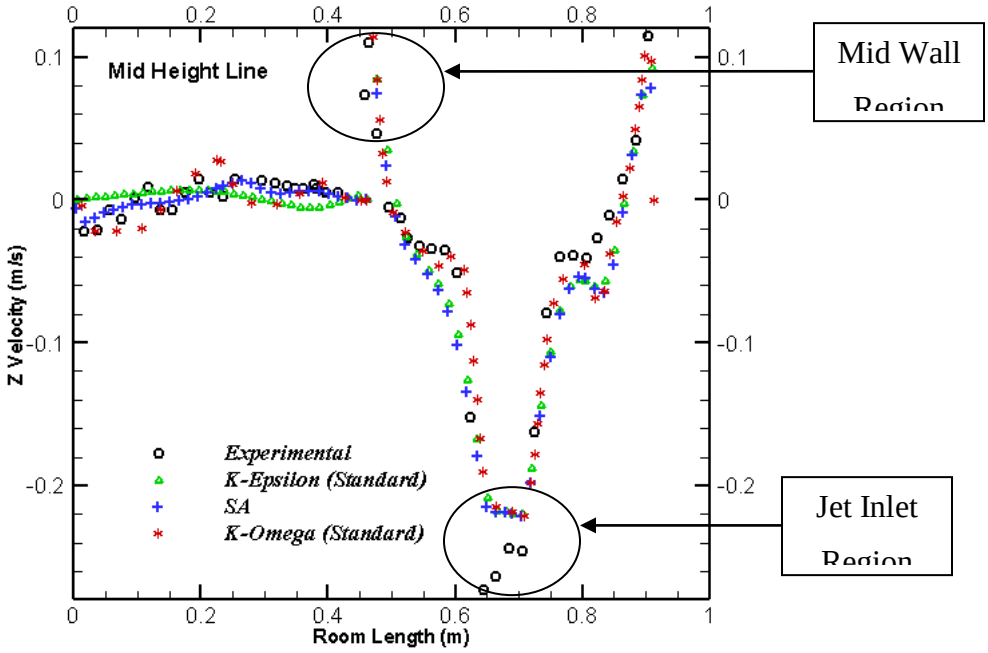

Figure 3.25: Comparison of all Turbulence Models

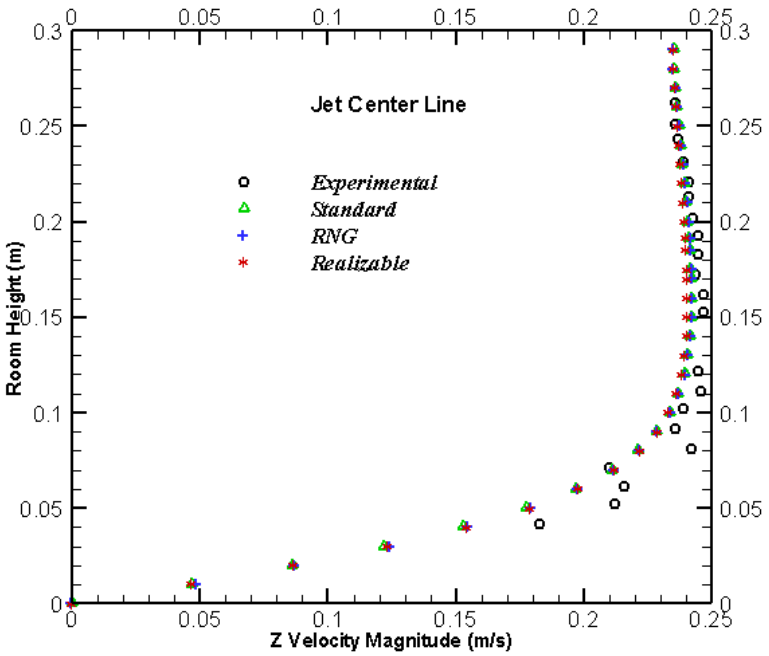

Figure 3.26: Comparison of K-Epsilon Models

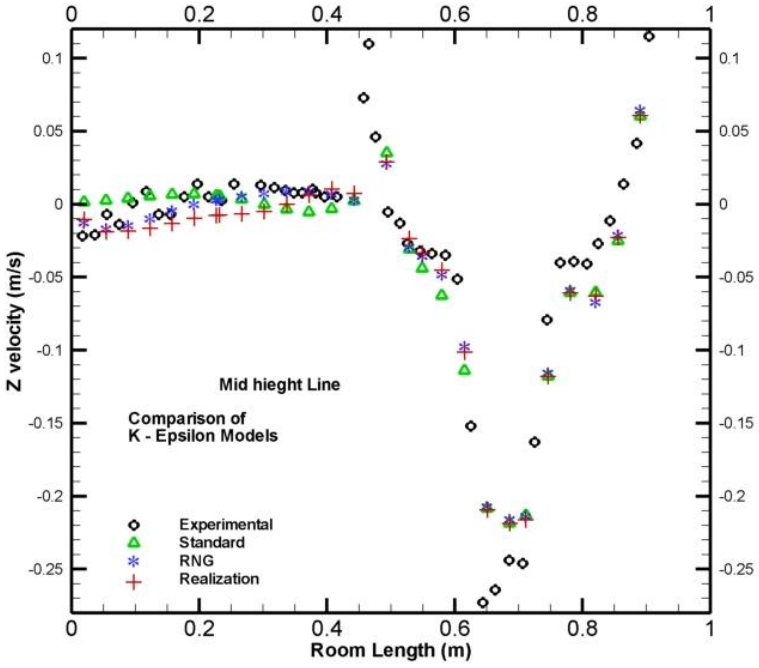

Figure 3.27: Comparison of K-Epsilon Models

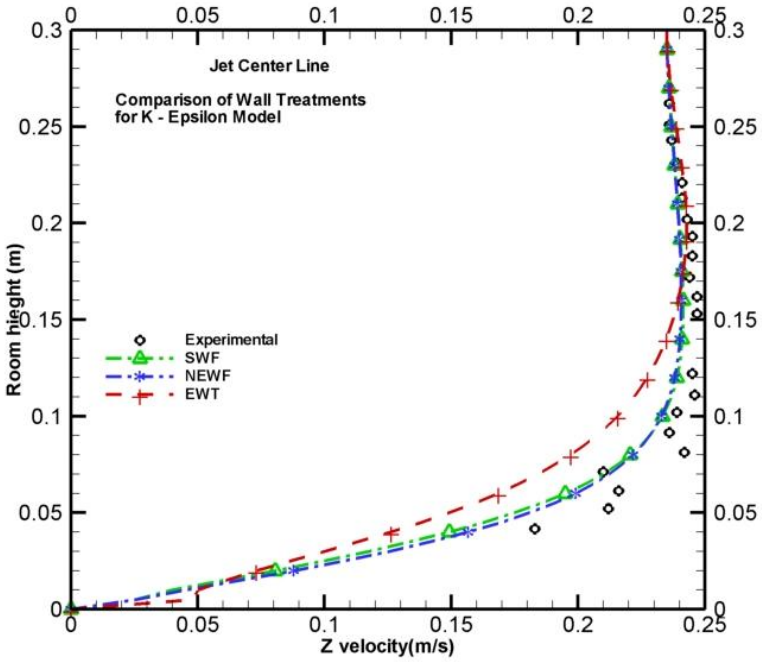

Figure 3.28: Comparison of Near Wall Treatments for K-Epsilon Models

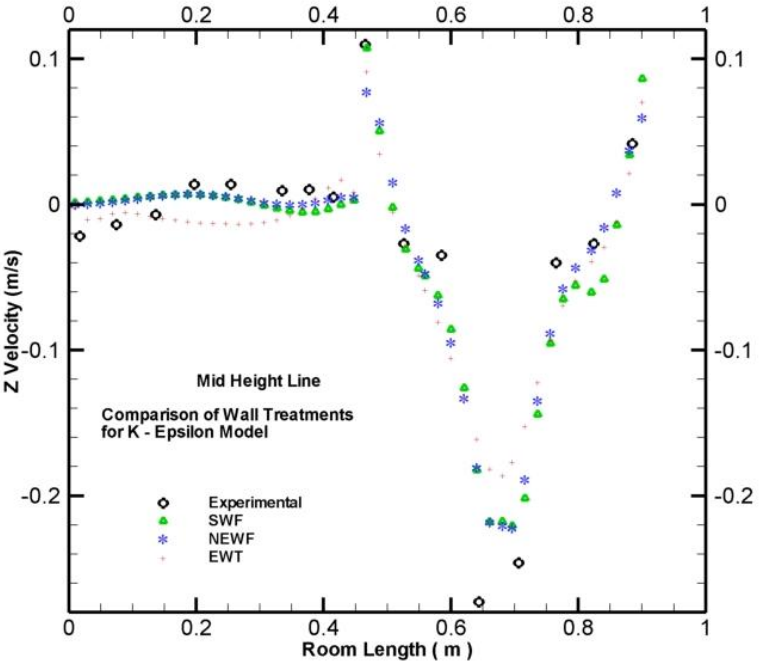

Figure 3.29: Comparison of Near Wall Treatments for K-Epsilon Models

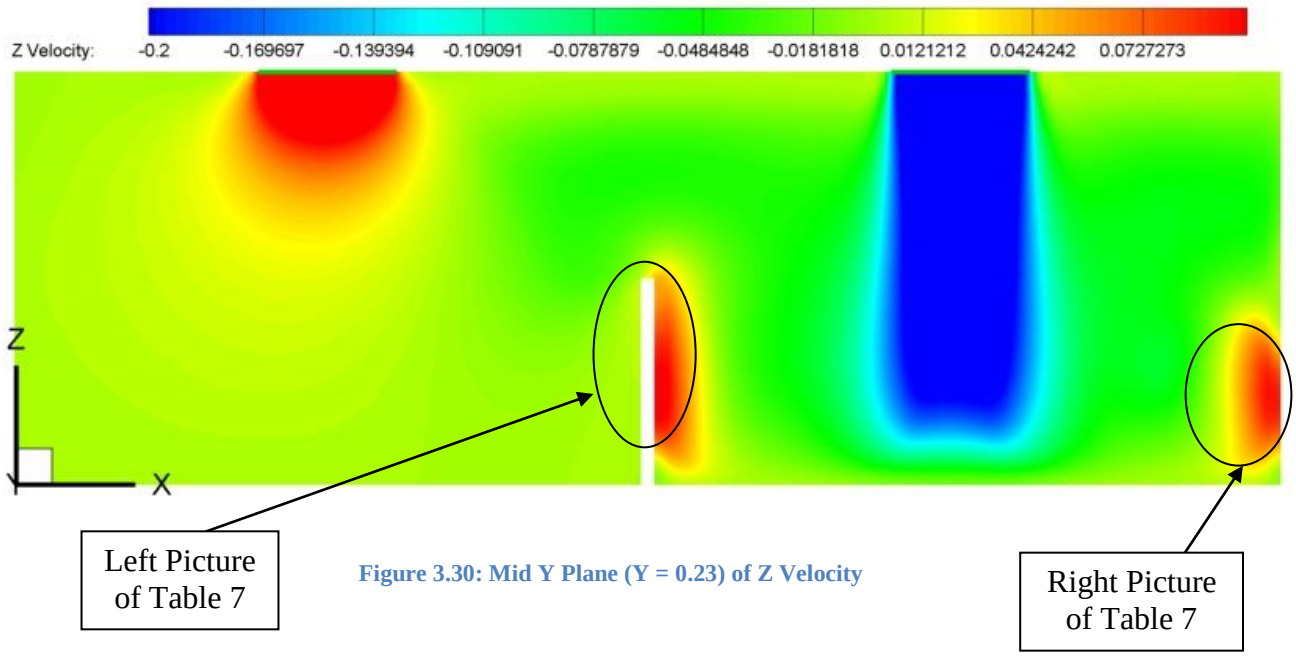

Figure 3.30: Mid Y Plane (Y = 0.23) of Z Velocity

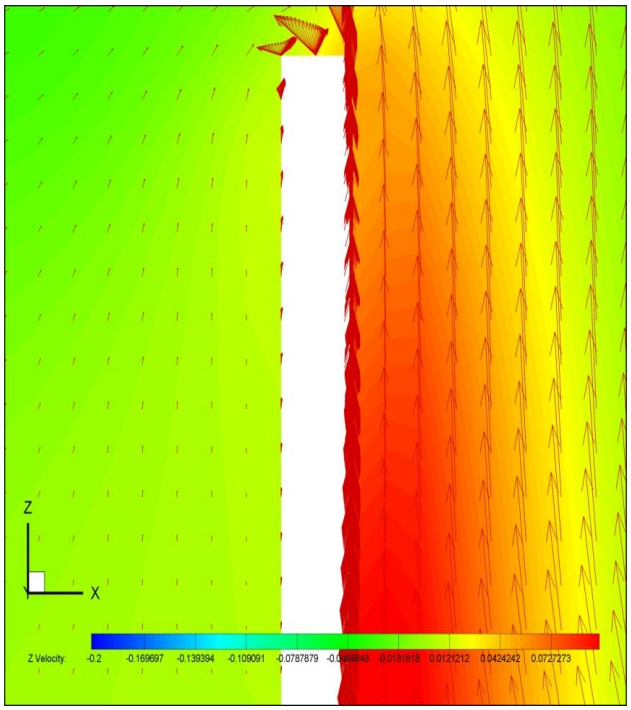

Figure 3.31: Vector Plots near mid partition wall

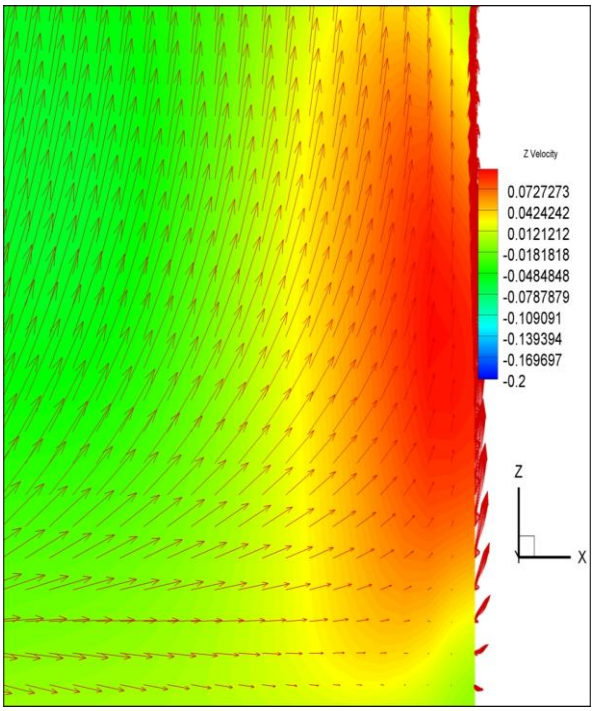

Figure 3.32: Vector plots near right wall of room

Table 3.5: Vector Plots of the regions mentioned in Figure 39

3.3 Case 3: Validation of Above Plenum Small Data Center

Experimental studies are performed on small test data center shown in Figure 3.33 located at Cambridge, Massachusetts by M. D. Lloyd in 2010 [28]. He calculated point velocities and temperature at different planes in front and back of racks. Uniform and Non uniform velocity distribution is employed in CFD models. We also performed the similar methods to validate the experimental data of lab.

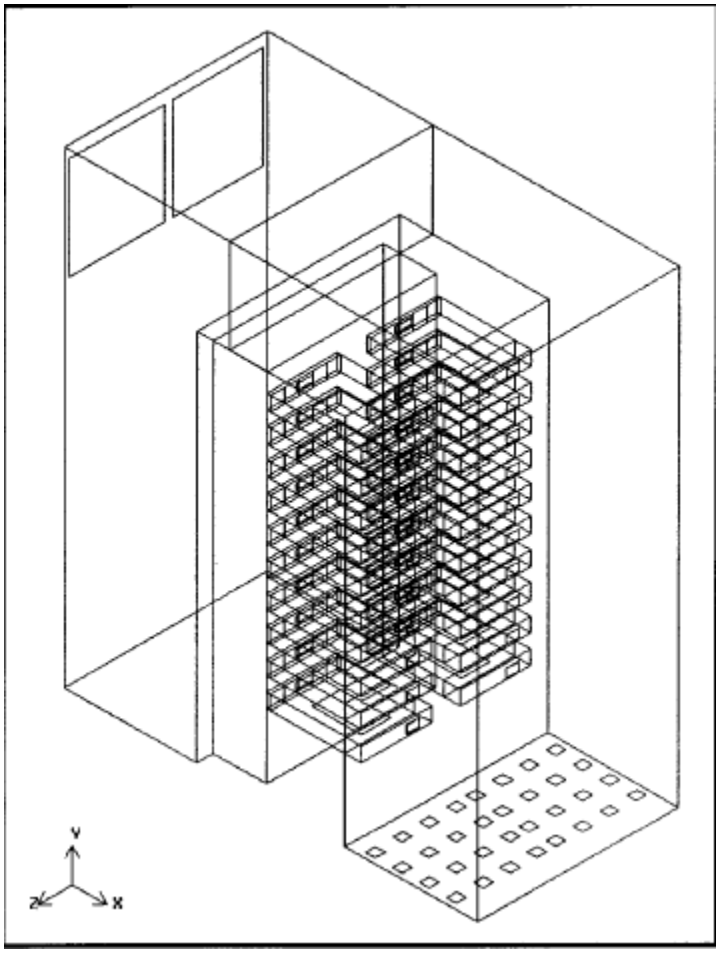

Figure 3.33: Layout of Data Center Test Cell

3.3.1 Data Collection Points:

Calculation of Y Velocity:

Table 3.6: Data Collection points in data center test cell

Height	X Coordinate	Y Coordinate
14’’	5", 10", 15"	4", 12", 20", 28", 36", 44"
38’’	6", 12"	6", 18", 30", 42"
66’’	6", 12"	6", 18", 30", 42"

Calculation of Temperature Difference:

Temperature is obtained at rack inlet and outlet of each server and finally average temperature difference is calculated. Velocity and Temperature calculation points are shown in Figure 3.35.

3.3.2 Boundary Conditions:

Room Inlet:

Each perforated tile is modeled as sixteen small openings. Sum of all openings are equal to total open area of each tile. Velocity Inlet Boundary Condition is employed at each opening.

There are two models used to simulate the data center test cell. In model number 1, uniform velocity of 3.75 m/s and at 284 K is employed at each tile opening, while in model number two, different values of velocity are given to each opening in order to have better agreement with real data. Details of these velocities are given in Figure 3.34.

Room Outlet:

Outflow Boundary condition is used for outlet of room.

Rack Inlet and Outlet:

Interior Boundary Condition is used to allow the flow going into and out of rack.

Heat Generation by Server:

In order to model heat transfer from server, each server is modeled as wall, located at the bottom of surface of server. Constant heat flux of 1400 W/m^2 is employed to that wall in order simulate the effects of heat transfer accurately.

Modeling of fan Inside Servers:

In order to simulate the fans inside a server, Pressure Velocity curve of a real fan is obtained. Using that curve, a linear relationship between Pressure Difference (ΔP) and velocity (v) is obtained, which is

$$\Delta P = 41.2 - 14.3\,v$$

There are five fans inside each server. So five faces are produced near the back of server and Fan boundary Condition is given to them.

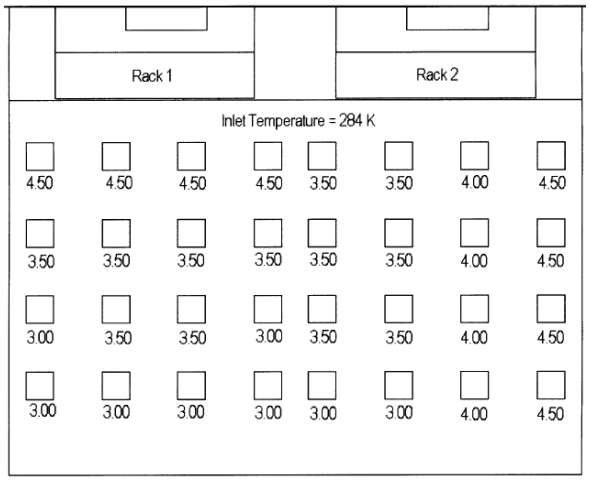

Figure 3.34: Velocity Inlet Values for Model Number 2

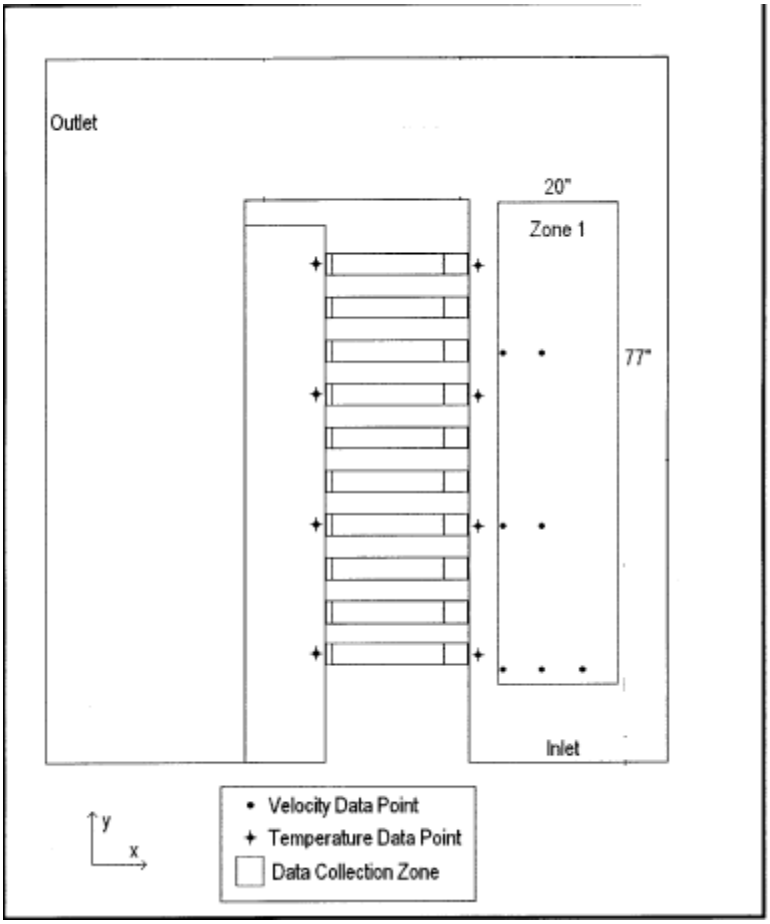

Figure 3.35: Data Collection Points in Test Data Center

3.3.3 Results & Discussion:

Comparison at 14'' Height:

Firstly, y velocities are calculated just below the 1st server (14"). This height is chosen because the flow coming out of small openings merges into one large jet up to this height. This region is just below first server, because flow is highly unsteady in front of servers.

Results for Model Number 1 are given in Table 3.7 and Table 3.8. Model number one does not provide good prediction of experimental data. This pattern can be seen from both M. D. Lloyd and Present Study. This is due to the reason that uniform velocity is employed at each inlet opening. Therefore graphs of comparison are only plotted between M. D. Lloyd and Present study. Table 3.9 shows the Experimental as well as Numerical Studies data of Y Velocity

distribution obtained by Model Number 2. The average absolute difference between Experimental and M. D. Lloyd Model and between experimental and Present Study is shown in Table 3.10. Present Study gives better approximation to experimental study as compared to M. D. Lloyd Model. This is may be due to better quality mesh being used in present study model. Graphical representation of Model Number 2 and experimental data is shown in Figure 3.36, Figure 3.37 and Figure 3.38 while Figure 3.39 represents the Y Velocity Contours at 14'' Height.

Model # 1:

Table 3.7: Velocity Data for Model 1 at 14 Inch Height

	Points	***a***	***b***	***c***	***d***	***e***	***f***	***X***
1	**Experimental**	1.07	1	1.17	0.68	0.61	1.07	***5"***
	M. D. Lloyd	0.5	0.47	0.58	0.68	0.45	0.54	
	Present Study	0.63	0.51	0.48	0.56	0.42	0.42	
2	**Experimental**	0.91	0.76	0.51	0.4	1.12	1.3	***10"***
	M. D. Lloyd	0.7	0.64	0.64	0.8	0.6	0.67	
	Present Study	0.79	0.73	0.72	0.72	0.66	0.73	
3	**Experimental**	0.73	0.53	0.61	0.4	0.88	0.76	***15"***
	M. D. Lloyd	0.82	0.69	0.77	0.83	0.75	0.87	
	Present Study	0.89	0.83	0.82	0.77	0.71	0.82	
	Z	***4"***	***12"***	***20"***	***28"***	***36"***	***44"***	

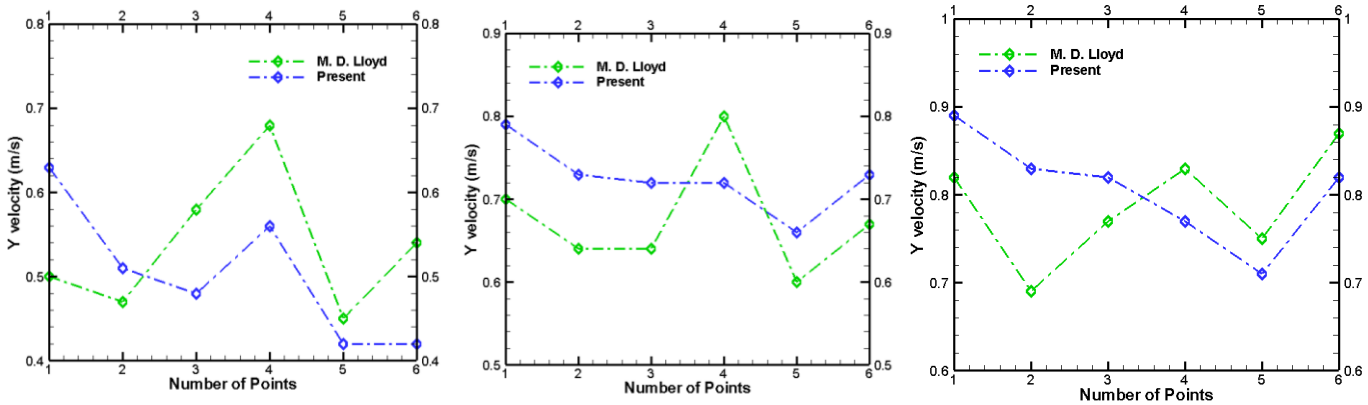

Table 3.8: Velocity Comparison for Model 1 at 14'' Height

Model # 2:

Table 3.9: Velocity data For Model 2 at 14 Inch Height

Points		a	b	c	d	e	f	X
1	Experimental	1.07	1	1.17	0.68	0.61	1.07	5"
	M. D. Lloyd	1.01	0.89	1.07	0.7	0.43	0.93	
	Present Study	1.18	1.02	1.09	0.43	0.39	1.08	
2	Experimental	0.91	0.76	0.51	0.4	1.12	1.3	10"
	M. D. Lloyd	0.56	0.6	0.56	0.74	0.61	1.05	
	Present Study	0.56	0.65	0.59	0.59	0.66	1.29	
3	Experimental	0.73	0.53	0.61	0.4	0.88	0.76	15"
	M. D. Lloyd	0.43	0.44	0.46	0.72	0.55	1.22	
	Present Study	0.46	0.66	0.48	0.64	0.71	1.33	
	Z	4"	12"	20"	28"	36"	44"	

Table 3.10: Average Absolute Difference between Experimental & Different Studies

Exp-Lloyd	0.10	5"
Exp-Present	0.12	
Exp-Lloyd	0.28	10"
Exp-Present	0.20	
Exp-Lloyd	0.28	15"
Exp-Present	0.25	

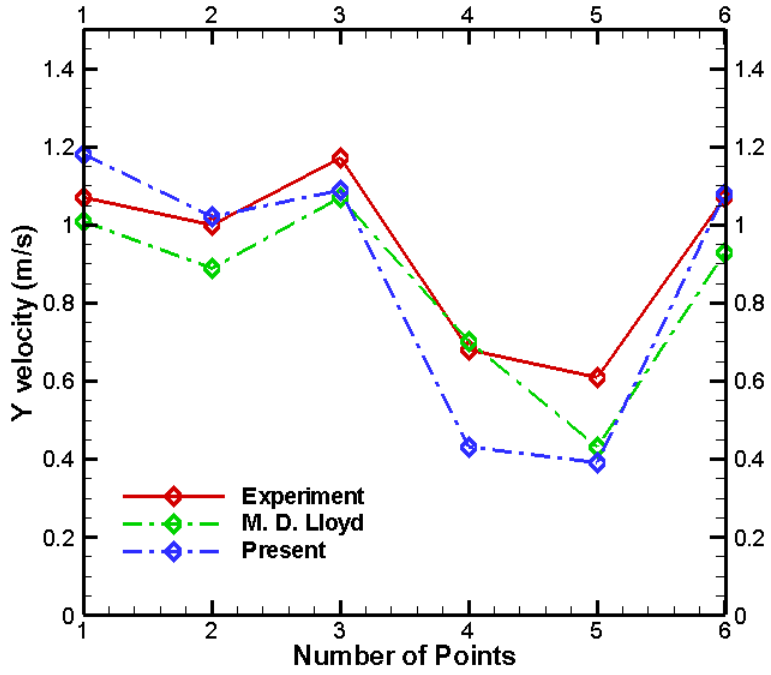

Figure 3.36: Velocity Comparison at X=5'' and 14 inch height

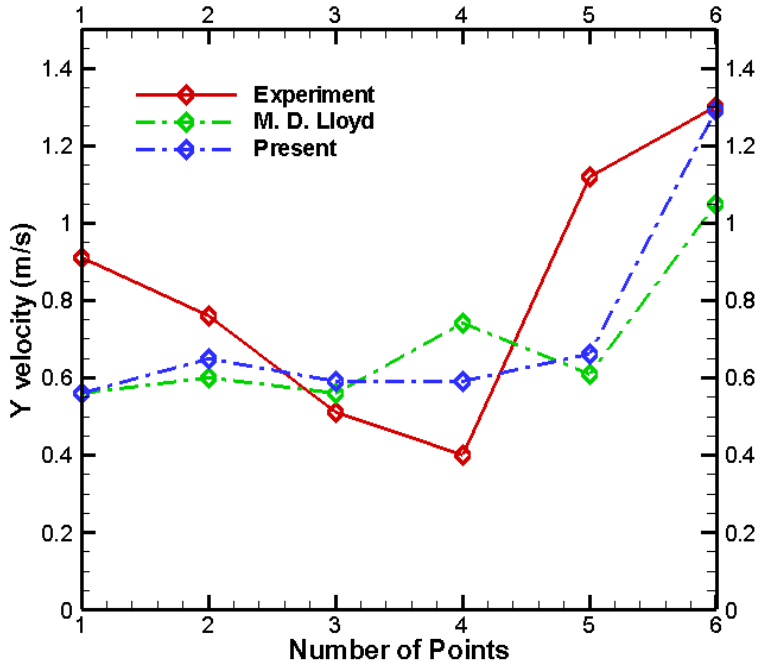

Figure 3.37: Velocity Comparison at X=10'' and 14 inch height

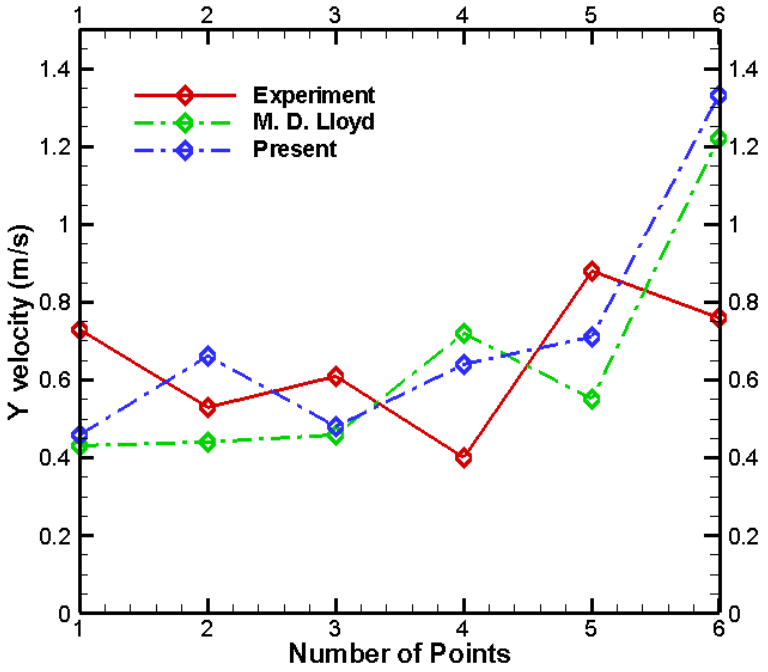

Figure 3.38: Velocity Comparison at X=15'' and 14 inch height

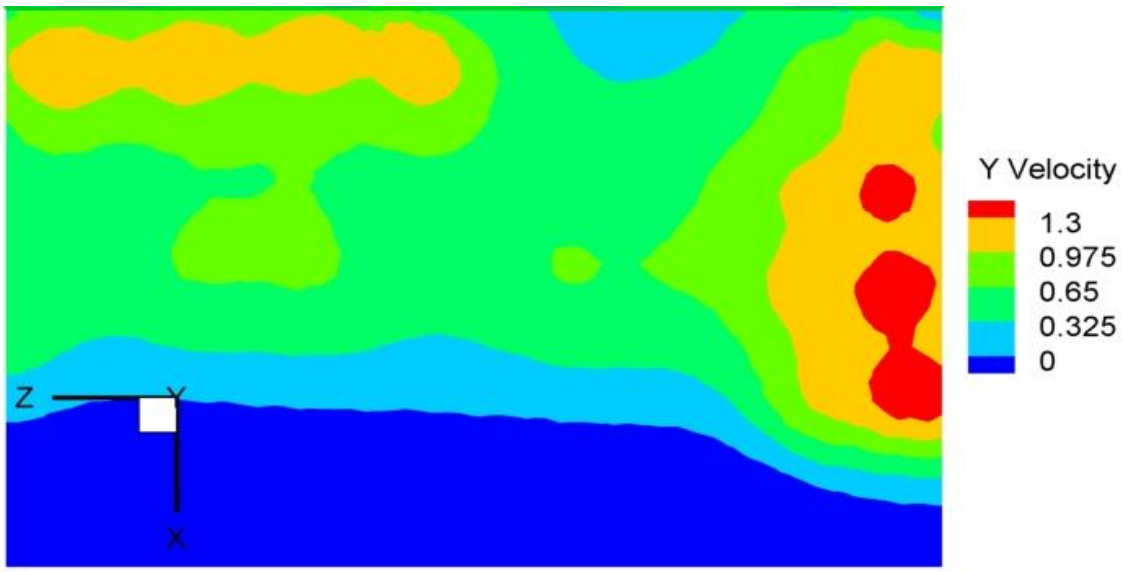

Figure 3.39: Y velocity Contours at 14'' Height

Comparison at 38'' Height:

Table 3.11 shows results of Y Velocity distribution at about mid height of rack (38''). More uniformity in results for Model 1 is seen here as compared to 14'' height. Table 3.12 shows graphical representation of results. Velocity distribution at this height from Model 2 is presented

in Table 3.13. Higher velocities near corners (z = 6'' and z=42'') is seen as expected (Due to higher inlet velocities around corners). Table 3.14 presents the average absolute difference of both studies (Present and M. D. Lloyd) from experimental results. Again present study show less difference as compared to M. D. Lloyd model. Graphical comparison of Numerical Experimental studies is presented in Figure 3.40and Figure 3.41. Contour of Y Velocity for Model 2 at 38'' height is shown in Figure 3.42.

Model # 1:

Table 3.11: Velocity data for Model 1 at 38'' Height

	Points	*a*	*b*	*c*	*d*	*X*
1	**Experimental**	0.37	0.26	0.11	0.58	*6''*
	M. D. Lloyd	0.36	0.38	0.4	0.37	
	Present Study	0.42	0.44	0.4	0.36	
2	**Experimental**	0.16	0.07	0.08	0.74	*12''*
	M. D. Lloyd	0.38	0.42	0.42	0.41	
	Present Study	0.34	0.44	0.4	0.45	
	Z	*6''*	*18''*	*30''*	*42''*	

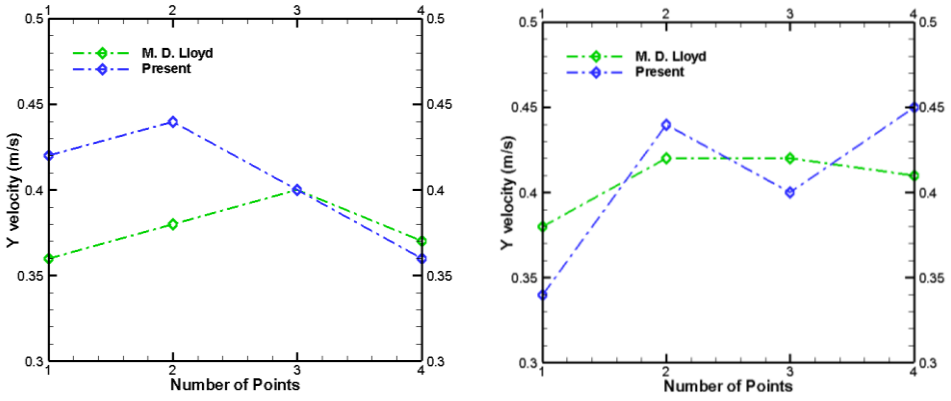

Table 3.12: Velocity Comparison for Model 1 at 38'' Height

Model # 2:

Table 3.13: Velocity Data for Model 2 at 38'' Height

	Points	*a*	*b*	*c*	*d*	*X*
1	**Experimental**	0.6	0.6	0.18	0.9	*6''*
	M. D. Lloyd	0.94	0.7	0.73	0.91	
	Present Study	0.8	0.46	0.43	0.87	
2	**Experimental**	0.11	0.19	0.15	1.04	*12''*
	M. D. Lloyd	0.47	0.36	0.56	0.9	
	Present Study	0.25	0.08	0.19	0.85	
	Z	*6''*	*18''*	*30''*	*42''*	

Table 3.14: Average Absolute Difference at 38'' Height

Exp-Lloyd	0.22	*6''*
Exp-Present	0.14	
Exp-Lloyd	0.24	*12''*
Exp-Present	0.11	

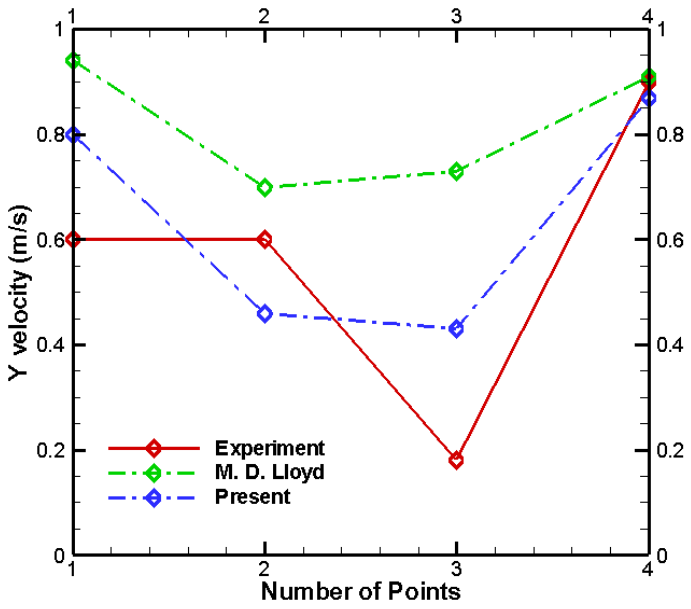

Figure 3.40: Comparison at X=6'' and 38'' Height

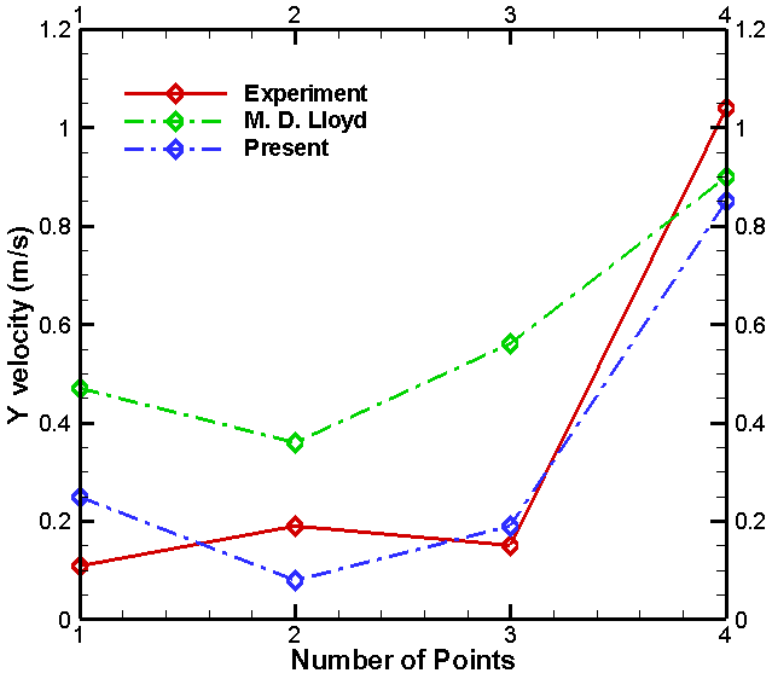

Figure 3.41: Comparison at X=12'' and 38'' Height

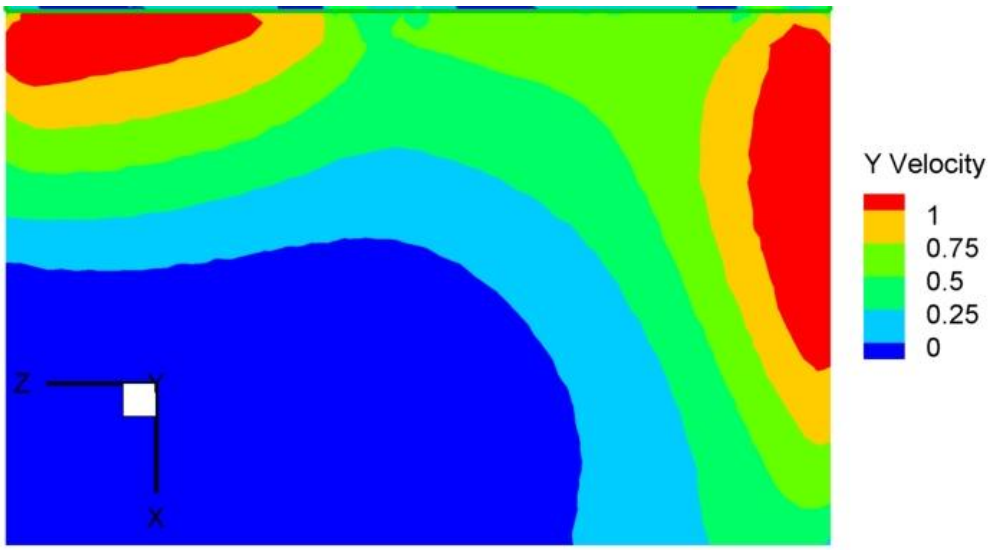

Figure 3.42: Y Velocity Contours for Model 2 at 28'' Height

Comparison at 66'' Height:

At 66'' height (about height of Eighth server), Model Number 1 again predicts uniform velocity distribution. This pattern can be seen from Table 3.15 and Table 3.16. Again, Model 1 shows significant variation from experimental data. On the other hand, Model Number 2 shows good agreement with experimental data at this height. This can be seen from

Table 3.17. Again, Present study provides good prediction of experimental data than Lloyd Model as can be seen from

Table 3.18. Figure 3.43 and Figure 3.44 presents graphical distribution of velocity data. Y Velocity contour is presented in Figure 3.45.

Model # 1:

Table 3.15: Velocity Data for Model 1 at 66'' Height

Points		*a*	*b*	*c*	*d*	*X*
1	**Experimental**	0.37	0.26	0.11	0.58	*6''*
	M. D. Lloyd	0.22	0.24	0.23	0.24	
	Present Study	0.17	0.24	0.24	0.26	
2	**Experimental**	0.16	0.07	0.08	0.74	*12''*
	M. D. Lloyd	0.24	0.25	0.25	0.24	

	Present Study	0.11	0.22	0.21	0.33	
	Z	***6''***	***18''***	***30''***	***42''***	

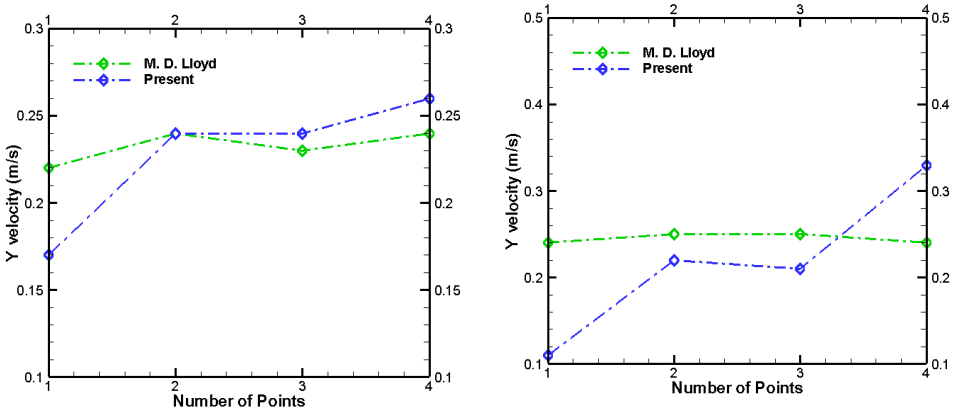

Table 3.16: Velocity Comparison for Model 1 at 66'' Height

Model # 2:

Table 3.17: Velocity Data for Model 2 at 66'' Height

	Points	***a***	***b***	***c***	***d***	***X***
1	**Experimental**	0.37	0.26	0.11	0.58	***6''***
	M. D. Lloyd	0.68	0.29	0.51	0.81	
	Present Study	0.64	0.12	0.12	0.58	
2	**Experimental**	0.16	0.07	0.08	0.74	***12''***
	M. D. Lloyd	0	0.03	0.28	0.72	
	Present Study	0.096	0.13	0.001	0.59	
	Z	***6''***	***18''***	***30''***	***42''***	

Table 3.18: Average Absolute Difference at 66'' Height

Exp-Lloyd	0.22	6''
Exp-Present	0.05	

Exp-Lloyd	0.09	12''
Exp-Present	0.10	

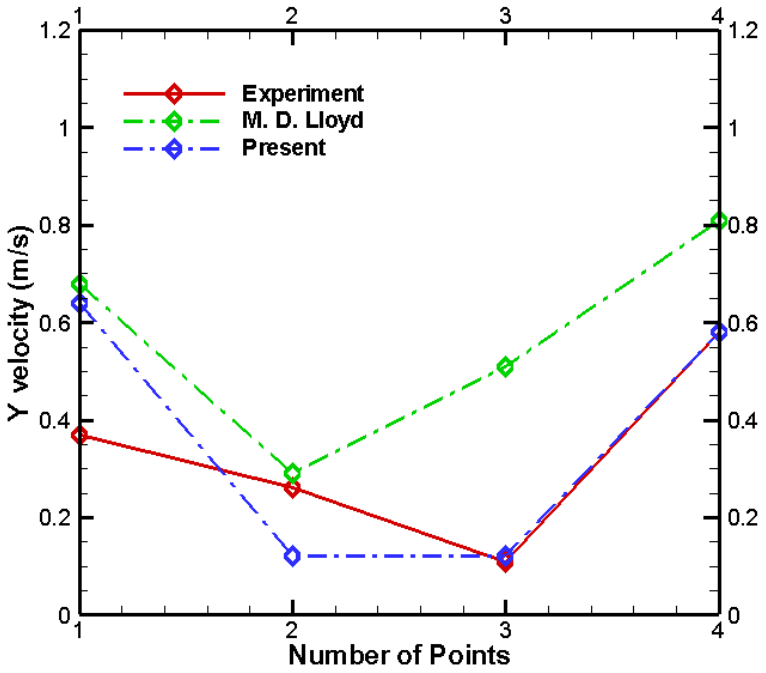

Figure 3.43: Velocity Comparison at X=6'' and 66'' Height

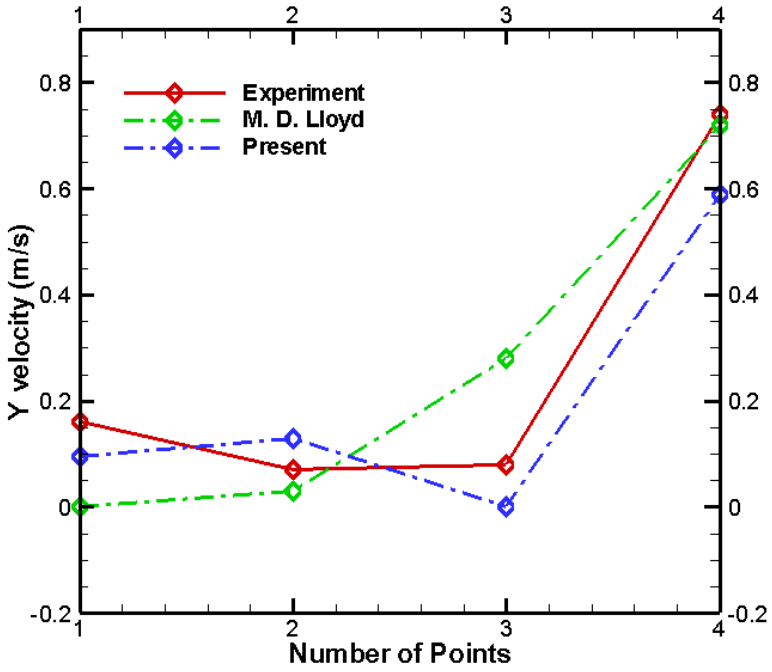

Figure 3.44: Velocity Comparison at X=12'' and 66'' Height

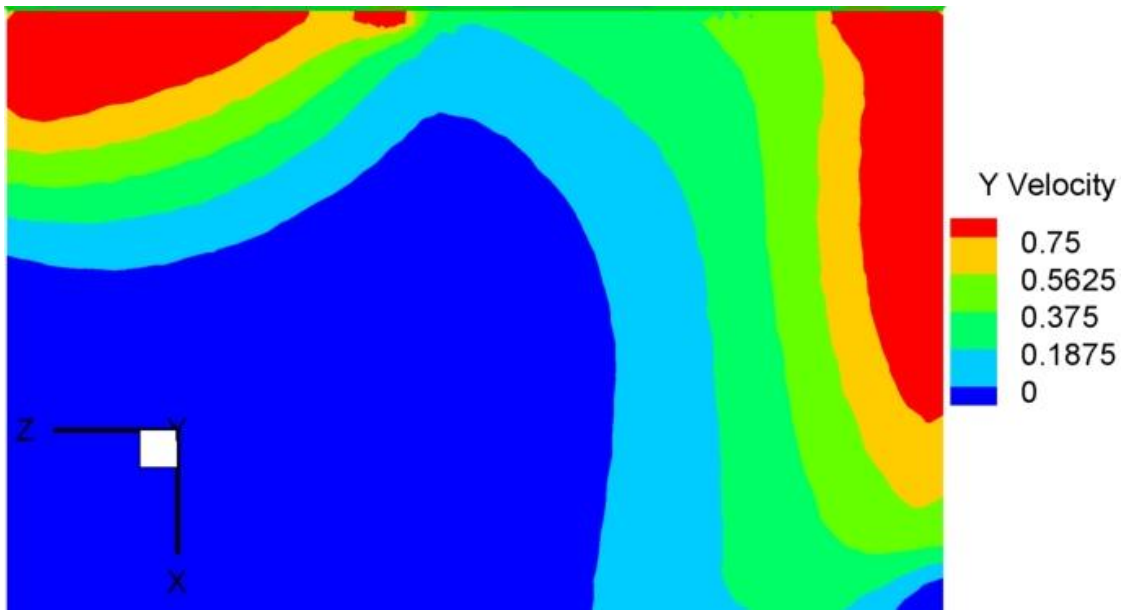

Figure 3.45: Y Velocity Contour at 66'' Height

Average Temperature Difference between Rack Inlet and outlet:

From above discussion, it is found that Model Number 2 best predicts the velocity distribution with experimental data. Therefore, for Thermal Validation, we use only Model Number 2 results.

Average inlet and outlet temperatures of racks are calculated and their difference represents the increase in temperature of air as it passes through servers in racks.

Average Inlet Temperature is equal to the room inlet temperature. This is due to the reason that there is no open space around racks in Test Cell, and due to this, there is no recirculation of hot air into cold aisle. So, Temperature in cold aisle remains constant. Table 3.19 presents temperature distribution at back of racks and their average. Table 3.20 presents the average temperature values obtained from experimental as well as numerical studies. Results show that both numerical studies (Present and M. D. Lloyd) are in well agreement with experimental data. This means that both studies well predicted the flow rate and heat transfer phenomena inside the racks.

Server No.	***Temperature (K)***
1	288.14
2	288.13
3	288.19
4	288.31
5	288.43
6	288.68
7	289.17
8	289.69
9	289.25
10	288.76

Average	**288.675**

Table 3.19: Temperature at Back of Each Server

	Temperature (K)		
	Experiment	***M. D. Lloyd***	***Present Study***
Average Server Inlet	284	284	284
Average Server Outlet	288.9	288.8	288.7
Temperature Difference	***4.9***	***4.8***	***4.7***

Table 3.20: Comparison of Average Temperature

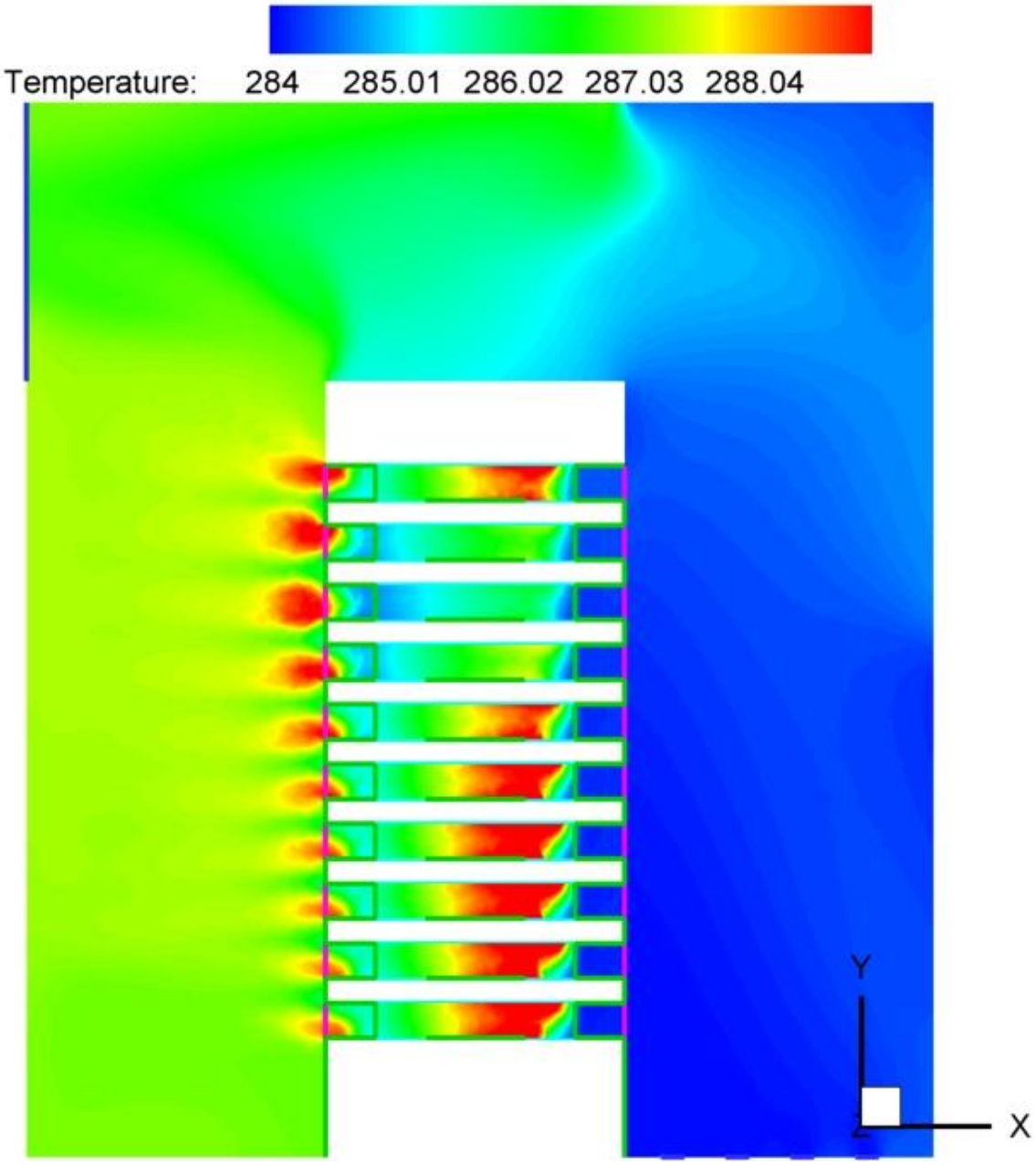

Figure 3.46: Temperature Contour at mid Z Plane

Chapter # 4

Experimental Setup

4.1 Experimental Space

In order to obtain accurate velocity and temperature data in an operating data center, experiment is conducted in the High Performance Computing (HPC) Lab at the Research Center for Modeling and Simulation (RCMS), NUST. This data served as the basis for the CFD model. The data center holds three identical racks along with a CRAC unit. The uninterruptable power supply along with the batteries is located in a nearby room. The racks present in the center had determinable server configurations, which aided in both CFD modeling and experimental data acquisition. The system has the following technical specifications:

- 66 NODE supercomputer with 30,992 processor cores
- 2 Head Node (16 Processor Cores)
- 32 Dual Quad Core Computer Nodes (256 Processor Cores)
- 32 NVidia Tesla Computing Processors
- QDR Infiniband Interconnections
- 21.6TB SAN storage
- Power Backup and Cooling System

Figure 4.1: Physical Data Center at RCMS, NUST

Figure 4.1 shows the physical setup of the model data center. CRAC is located at the right wall of the room. Center row has three racks, each with an inlet tile on the floor in front of it. The first two racks are adjacent while the third rack is offset by 1'. There are a total of five inlet tiles, each 2' by 2' with 2048, 6 mm holes, which render an open area of 15.5%. A schematic is shown in Figure 4.2**.** The room dimensions, location of dimensions of operating equipment and tile configurations are shown in Figure 4.3. Figure 4.4 represent the details of perforation of a tile.

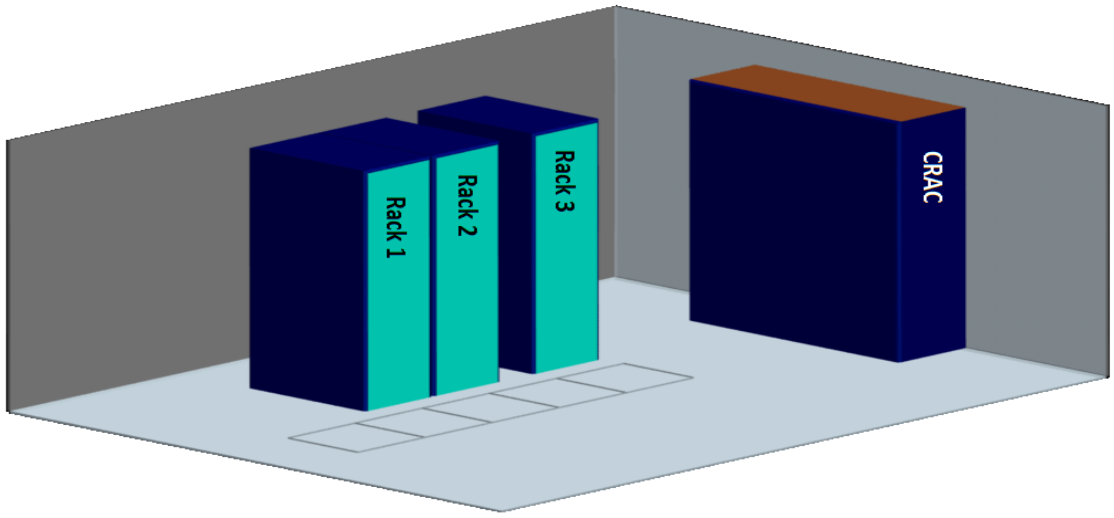

Figure 4.2: Computer generated model of RCMS Data Center

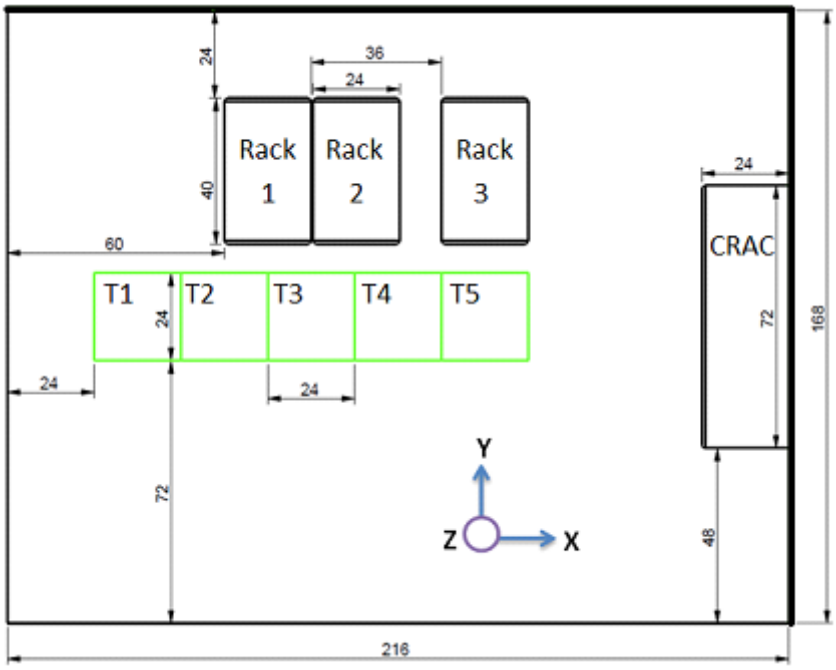

Figure 4.3: Plan View of the Data Center Room

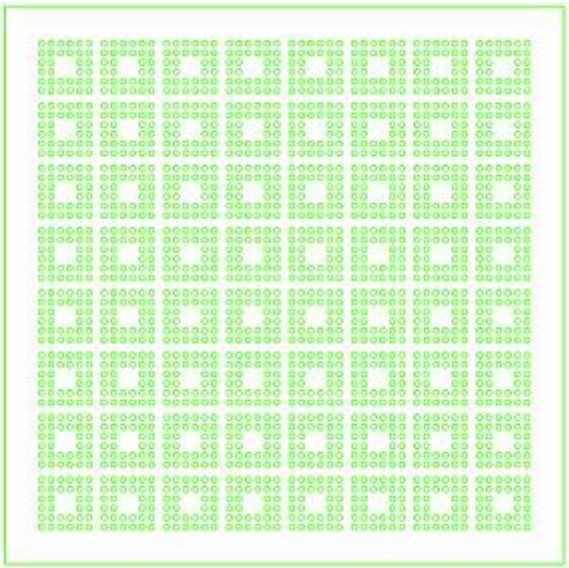

Figure 4.4: Layout of the Perforated Tile

4.2 Data Acquisition

For comparison with CFD results, air velocity and temperature data has to be acquired throughout the data center at specific points in space. An anemometer with a temperature probe was used to find the air speed and the temperature at the points of interest. The points selected were based on the areas of interest in the data center, specifically around the inlet tiles and the computer racks.

Ground Level:

For inlet boundary conditions in CFD model, temperature and velocity data is obtained at each perforated tile surface. It is computationally inexpensive to model all the perforations of the tile. 17 show that modeling tile as multiple opening yield better results as compared to single opening. We employed similar technique in our study and each tile is modeled as 16 square openings. These points are shown as dots in Figure 4.5.

Zone 1:

This is the region parallel to perforated tile and located just above (16 inches) the ground level. Small jets coming out of inlet opening will suppose to merge into one jet up to this height and velocity data at this height will tell us about impact of rack suction on inlet jet. Data is obtained at nine points as shown in Figure 4.6.

Zone 2:

Zone 2 is located about midway (38 inches) of rack and parallel to perforated tile surface. Data is obtained at four points above each tile as shown in Figure 4.7.

Zone 3:

This is located along the back side of rack. Temperature data is obtained at the center of each rack to get average outlet temperature of rack. Data is obtained at ten points behind each rack as shown in Figure 4.8.

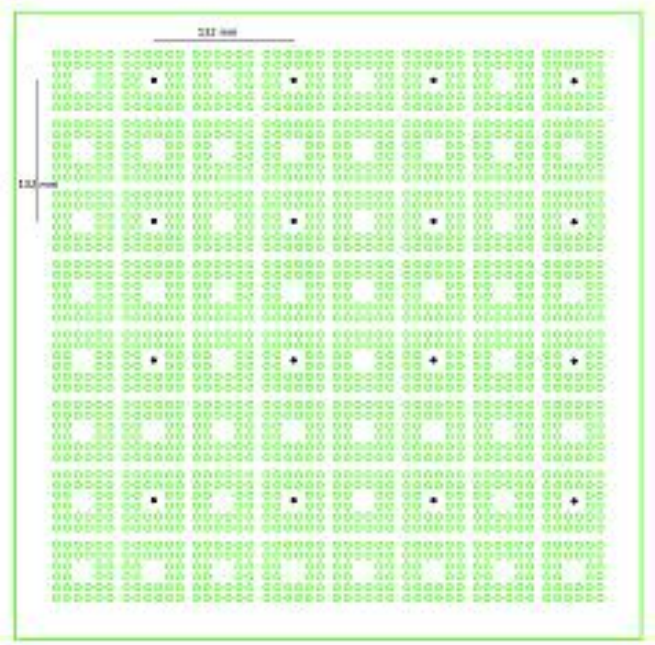

Figure 4.5: Data Collection points on Ground Level

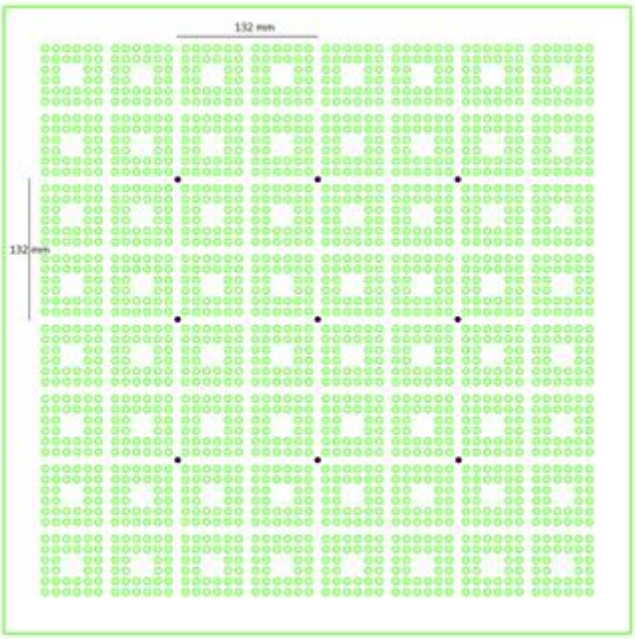

Figure 4.6: Data Collection points for zone 1

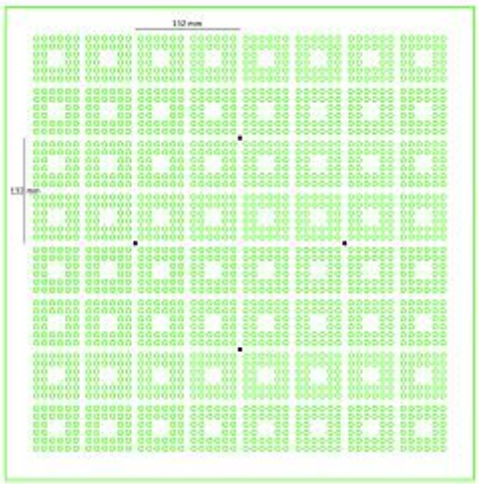

Figure 4.7: Data Collection Points for zone 2

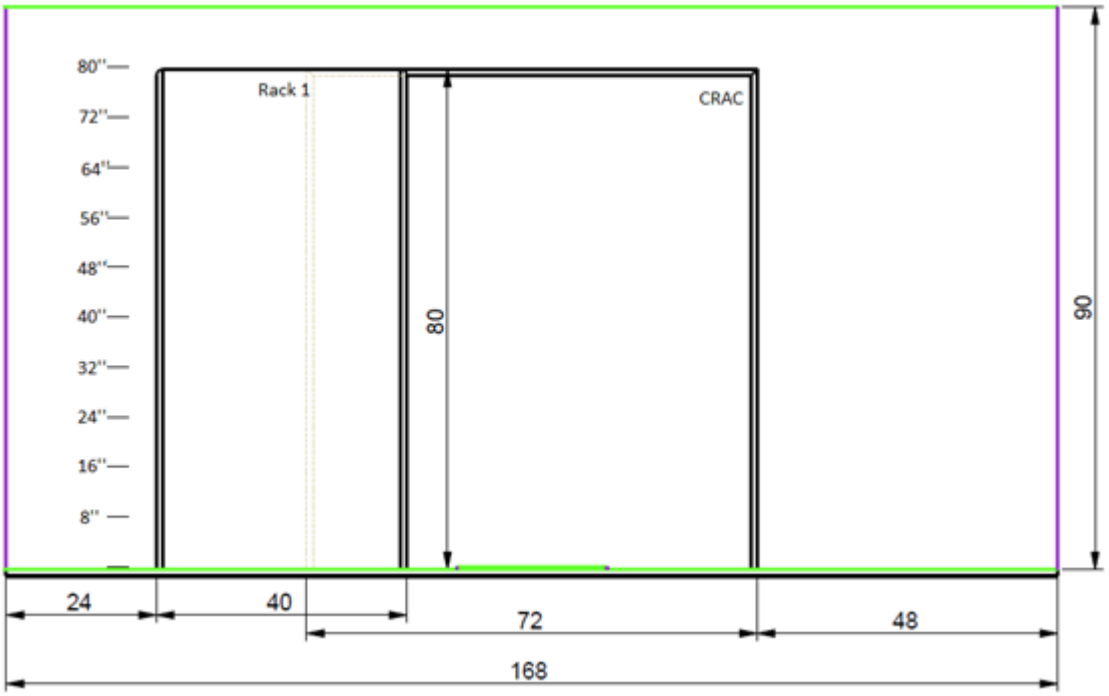

Figure 4.8: Data Collection points for zone 3

4.3 Equipment and Setup

The apparatus used to hold the anemometer at the required point in space consisted of a modified tripod assembly supporting the anemometer. The point in space was located with the help of a laser level. The dimensions were first measured along the reference surfaces (i.e. the tile edges for x and y dimensions, and along the rack front (from the floor) for the z direction). The leveling device ensured that our anemometer/tripod assembly was properly aligned with the measured points on the references. Two laser pointers further confirmed proper alignment of the anemometer vane over the points on the tile and its altitude above ground level. Laser B in Figure 4.9, mounted horizontally, ensured proper height and laser A, mounted vertically, ensured proper alignment with respect to a point marked on the tile below. The apparatus itself was calibrated using set squares and adjustable mounts to fine tune its position in space as required.

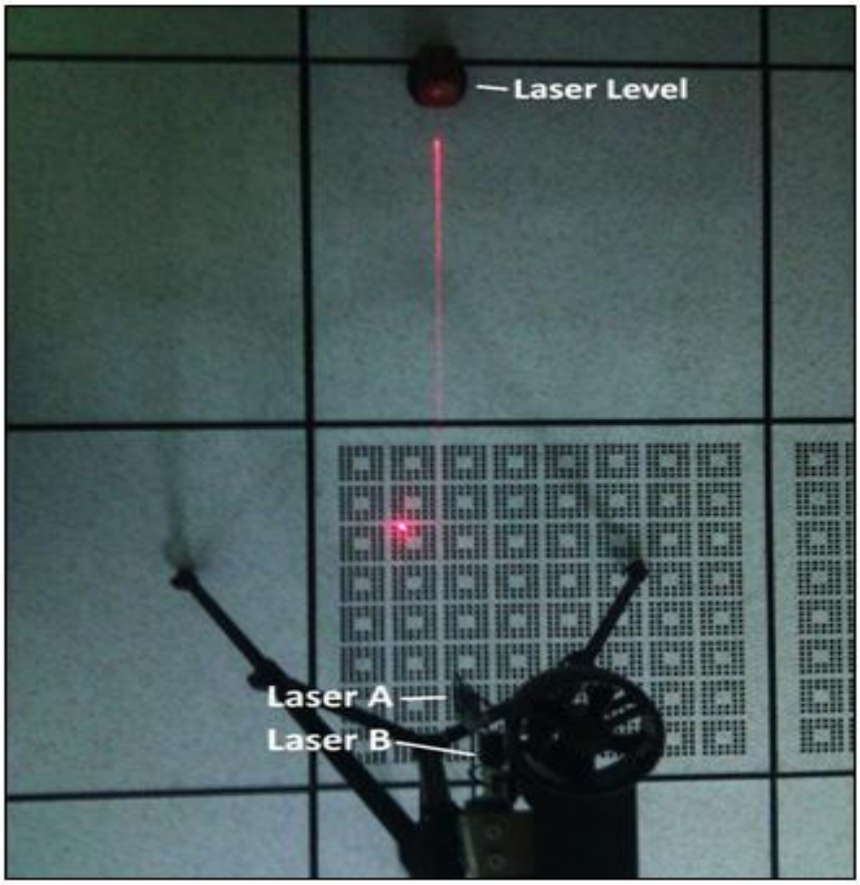

Figure 4.9: Alignment of apparatus using Laser Beams

The anemometer used was of a simple windmill design with an adjoining handheld unit. The unit displayed a real time output that was stored over a period of time at a user-set sample rate. The stored values could then be transferred to a spreadsheet for processing.

Figure 4.10: Temperature probe used for obtaining temperature data behind racks

4.4 Observations and data obtained at Ground Level:

Table 4.1 to Table 4.5 represents the experimental data obtained at ground level for each tile. A 16 point transverse data is being taken. These points are shown in Figure 4.5. At each point, anemometer is placed and used to obtain averaged z velocity and temperature data every second for two minutes. Average velocities and temperatures are shown as bold while standard deviations are shown as italic numbers in tables.

Table 4.1: Experimental data of tile 1

	i = 1			i = 2			i = 3			i = 4		
j	Velocity	Std. Dev	Temp	Velocity	Std. Dev	Temp	Velocity	Std. Dev	Temp	Velocity	Std. Dev	Temp
1	2.67	*0.01*	16.9	2.49	*0.02*	16.5	2.53	*0.02*	16.3	2.71	*0.02*	16.5
2	2.44	*0.02*	16.3	2.48	*0.01*	16.1	2.52	*0.02*	16.1	2.48	*0.02*	16.3
3	2.36	*0.1*	16.1	2.5	*0.03*	15.9	2.46	*0.03*	16.1	2.37	*0.02*	15.9
4	2.42	*0.02*	16.7	2.45	*0.02*	16.7	2.43	*0.03*	16.7	2.52	*0.02*	16.9

Table 4.2: Experimental data of tile 2

	i = 1			i = 2			i = 3			i = 4		
j	Velocity	Std. Dev	Temp	Velocity	Std. Dev	Temp	Velocity	Std. Dev	Temp	Velocity	Std. Dev	Temp
1	2.36	*0.02*	16.3	2.35	*0.02*	16.1	2.34	*0.01*	16.5	2.33	*0.06*	17.1
2	2.54	*0.02*	17.1	2.46	*0.02*	17.5	2.42	*0.02*	17.5	2.51	*0.03*	17.69
3	2.53	*0.02*	17.3	2.54	*0.03*	17.69	2.45	*0.02*	17.3	2.49	*0.02*	16.9
4	2.47	*0.02*	16.5	2.4	*0.02*	16.3	2.28	*0.01*	16.1	2.52	*0.03*	16.1

Table 4.3: Experimental data of tile 3

	i = 1			i = 2			i = 3			i = 4		
j	Velocity	Std. Dev	Temp	Velocity	Std. Dev	Temp	Velocity	Std. Dev	Temp	Velocity	Std. Dev	Temp
1	2.32	*0.02*	16.7	2.19	*0.03*	16.7	2.03	*0.02*	16.5	2.1	*0.02*	16.3
2	2.22	*0.01*	16.1	2.29	*0.02*	15.9	2.04	*0.02*	15.9	2.15	*0.02*	15.9
3	2.24	*0.02*	15.9	2.41	*0.03*	16.1	2.1	*0.02*	16.5	2	*0.02*	16.5
4	2.29	*0.03*	16.9	2.3	*0.03*	17.1	2.01	*0.02*	17.3	2.15	*0.02*	17.5

Table 4.4: Experimental data of tile 4

	i = 1			i = 2			i = 3			i = 4		
j	Velocity	Std. Dev	Temp	Velocity	Std. Dev	Temp	Velocity	Std. Dev	Temp	Velocity	Std. Dev	Temp
1	2.48	*0.03*	16.5	2.4	*0.02*	16.3	2.27	*0.02*	16.1	2.43	*0.03*	16.1
2	2.3	*0.01*	16.1	2.48	*0.02*	15.9	2.42	*0.02*	16.5	2.5	*0.02*	16.5
3	2.48	*0.02*	16.7	2.42	*0.02*	16.7	2.35	*0.02*	17.1	2.46	*0.02*	17.1
4	2.42	*0.02*	17.5	2.43	*0.02*	17.5	2.3	*0.03*	17.1	2.43	*0.03*	16.7

Table 4.5: Experimental data of tile 5

	i = 1			i = 2			i = 3			i = 4		
j	Velocity	Std. Dev	Temp	Velocity	Std. Dev	Temp	Velocity	Std. Dev	Temp	Velocity	Std. Dev	Temp
1	2.28	*0.03*	16.1	2.27	*0.03*	15.9	2.27	*0.02*	15.9	2.37	*0.02*	15.71
2	2.26	*0.02*	15.9	2.31	*0.03*	15.71	2.14	*0.02*	16.3	2.28	*0.03*	16.3
3	2.28	*0.01*	16.9	2.33	*0.03*	16.9	2.21	*0.02*	17.3	2.29	*0.02*	17.1
4	2.29	*0.02*	17.5	2.33	*0.03*	17.5	2.3	*0.02*	17.1	2.36	*0.04*	17.3

4.5 Observations and data obtained at 18 inch Level:

At 18'' height, experimental velocity data is taken using the anemometer. As stated earlier, anemometer is fixed on the height adjustable stand and height of the stand is changed as required. Velocity data obtained at this height is shown in Table 4.6 to Table 4.10 for tiles 1 to 5 respectively. This height is chosen on the basis of assumption that flow streams coming out of tile are being converted into a single jet of flow up to this height. And also suction effects up to this height are not much prominent, so velocity data here shows that how much loss of Kinetic energy is occurred so far due to flow of air. On the basis of data obtained, it is found that in most of the region, (tile 2, 3 and 4) about 50% of the velocity of the flow is being loosed while reaching to this height. Other two tiles show much variation in data and reason of this variation is explained in detail in next chapter.

Table 4.6: Z-Velocity for Tile 1 at 38'' height

	i = 1	i = 2	i=3
j=1	0.28	0.91	0.51
j=2	0.79	0.83	0.85
j=3	0.23	0.51	0.82

Table 4.7: Z-Velocity for Tile 2 at 38'' height

	i = 1	i = 2	i=3
j=1	0.98	0.67	0.68
j=2	1.14	0.85	0.75
j=3	1.09	0.9	0.57

Table 4.8: Z-Velocity for Tile 3 at 38'' height

	i = 1	i = 2	i=3
j=1	0.69	0.72	0.64
j=2	0.55	0.51	0.61
j=3	0.76	0.33	0.65

Table 4.9: Z-Velocity for Tile 4 at 38'' height

	i = 1	i = 2	i=3
j=1	0.94	0.65	0.88
j=2	1.19	1.22	1.3
j=3	0.67	0.88	1.45

Table 4.10: Z-Velocity for Tile 5 at 38'' height

	i = 1	i = 2	i=3
j=1	1.33	1.28	0.91
j=2	1.18	1.43	0.29
j=3	1.45	1.2	0.68

Chapter # 5

Numerical Study of RCMS Data Center

In this study, a CFD model of the experimental setup was used to understand the flow patterns inside the data center as well as validation of the experimental data. This chapter starts with explanation of CFD model. Results obtained by numerical study were then discussed and compared with the experimental data.

Six types of boundary conditions were used in this study. Summary of these boundary conditions are given in Table 6.2. Velocity inlet boundary condition is employed at the room inlet surface. There are three ways to model these perforated tiles as explained by [17]. If entire face of tile was modeled as uniform velocity, the flow rate will be satisfied, but neither velocity distribution nor initial momentum of flow would be satisfied. Therefore each tile is modeled as sixteen small openings. The area of each opening is 5.52 in2. This corresponds to total open area of 86.6 in2, which is equal to the total open area of real perforated tile. Outflow boundary condition is employed at the outlet surface of the room.

Last four boundary conditions in Table 6.2 are used inside each server of the data center. Interior boundary condition is used for inlet and outlet of each server. Area of these surfaces is equal to sum of all small openings present at front and rear of actual server. Heat flux boundary condition is employed to model the heat generated by each server. Pressure loss due to component-packed server is accounted using porous jump boundary condition. Fans are modeled using a pressure velocity relationship given in

$$\Delta P = 41.3 - 14.3v$$

5.1 Comparison at 18 inch height

Numerical study is performed to validate the experimental data obtained in lab. Results are shown in Table 5.1 to Table 5.11 for all tiles. Increase in velocity at this height from left most tiles to right most tile, as seen in experimental results is not much prominent in numerical study. This can be due to the fact that in experimental setup, CRAC is quite close to the tile 5. So, throughout the room, air tends to move towards the CRAC which cause velocities to be higher in the right half of the data center. Moreover, in real data centers, velocities are relatively higher in tiles near to the CRAC. While in Numerical study, velocities at the surfaces of perforated tiles are almost uniform which is the reason for uniform velocities just above the tile surfaces (18'' height). Also there are much low velocities above tile 1 in numerical study. This can be due to the reason that suction effects of racks on tile 1 are much higher. But experimental results did not give such behavior. This can be due to the fact in real data center; door of room is located very near to the tile 1. So the suction of racks is balanced by the effects of infiltrations in door. While in numerical study, there is no infiltration and due to this more air is sucked towards racks.

Table 5.1: Tile 1 Comparison Data

Points		*a*	*b*	*c*	*Y*
1	**Experimental**	0.28	0.91	0.51	***6''***
	Numerical	0.41	0.19	0.1	
2	**Experimental**	0.79	0.83	0.85	***12''***
	Numerical	0.24	0.14	0.17	
3	**Experimental**	0.23	0.51	0.82	***18''***
	Numerical	0.22	0.19	0.23	
	X	***6''***	***12''***	***18''***	

Table 5.2: Tile 2 Comparison Data

Points		*a*	*b*	*c*	*Y*
1	**Experimental**	0.98	0.67	0.68	***6''***
	Numerical	0.89	0.74	0.59	
2	**Experimental**	1.14	0.85	0.75	***12''***
	Numerical	1.06	0.96	0.54	
3	**Experimental**	1.09	0.9	0.57	***18''***
	Numerical	0.88	0.74	0.59	
	X	***6''***	***12''***	***18''***	

Table 5.3: Tile 3 Comparison Data

Points		a	b	c	Y
1	Experimental	0.69	0.72	0.64	6''
	Numerical	0.51	0.89	0.44	
2	Experimental	0.55	0.51	0.61	12''
	Numerical	0.64	0.86	0.62	
3	Experimental	0.76	0.33	0.65	18''
	Numerical	0.6	0.8	0.37	
	X	6''	12''	18''	

Table 5.4: Tile 4 Comparison Data

Points		a	b	c	Y
1	Experimental	0.94	0.65	0.88	6''
	Numerical	0.68	0.79	0.46	
2	Experimental	1.19	1.22	1.3	12''
	Numerical	0.98	1.03	0.72	
3	Experimental	0.67	0.88	1.45	18''
	Numerical	0.78	1.01	0.65	
	X	6''	12''	18''	

Table 5.5: Tile 5 Comparison Data

Points		a	b	c	Y
1	Experimental	1.33	1.28	0.91	6''
	Numerical	0.67	0.78	0	
2	Experimental	1.18	1.43	0.29	12''
	Numerical	0.78	0.84	0.18	
3	Experimental	1.45	1.2	0.68	18''
	Numerical	0.67	0.75	0.41	
	X	6''	12''	18''	

Table 5.6: Average velocities (m/s) at 18'' height

	Experimental	Numerical
Tile 1	0.64	0.21
Tile 2	0.85	0.78
Tile 3	0.61	0.64
Tile 4	1.02	0.79
Tile 5	1.08	0.56

Table 5.6 shows average velocities above each tile. From table, this is clear that error between numerical and experimental values is much more pronounced in tile 1 and tile 5. Average vertical velocity component at this height is 0.84 m/s while from numerical study it is 0.6 m/s. This shows that overall numerical study results show good agreement with experimental data.

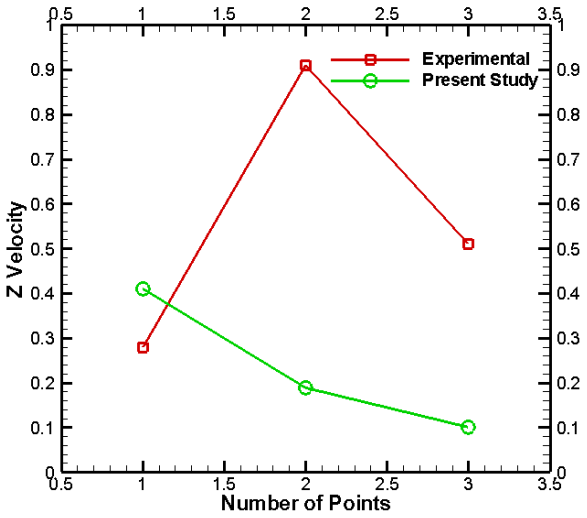

Figure 5.1: Tile 1 (T-1), Y = 6''

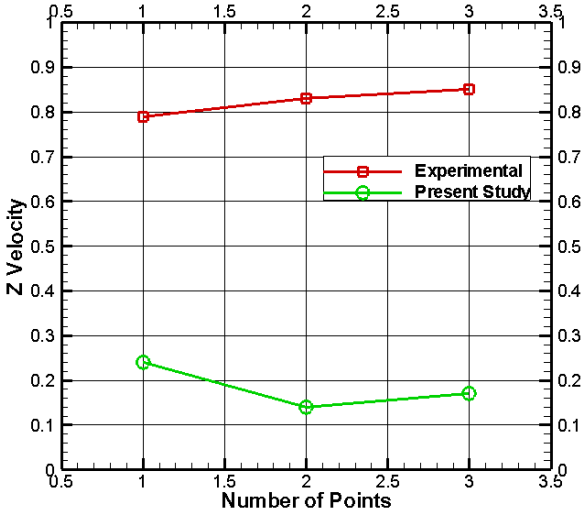

Figure 5.2: T-1, Y = 12''

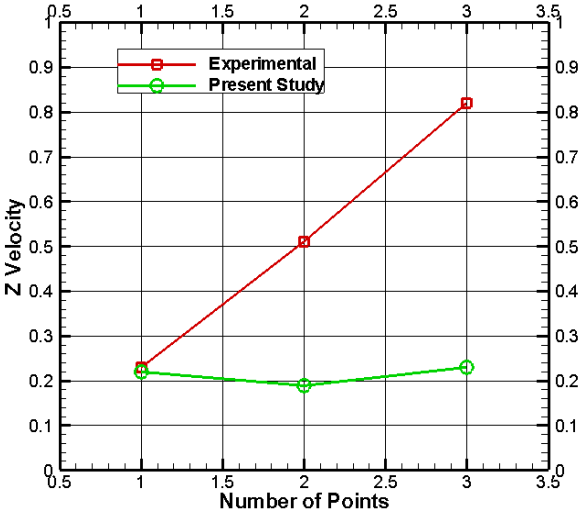

Figure 5.3: T-1, Y = 18''

Table 5.7: Experimental-Numerical comparison of Z-Velocity for tile 1

Table 5.7 shows the distribution of z component of velocity over tile 1 for x = 6'', 12'' and 18''. It can be seen that at x = 6'', both studies are in good agreement. Results for other two values differ a lot. Numerical study was much under predicted, but over all distribution patterns from both studies remain almost similar. Reason for difference in results from both studies is infiltration effects near this tile in real data center and is discussed in detail already.

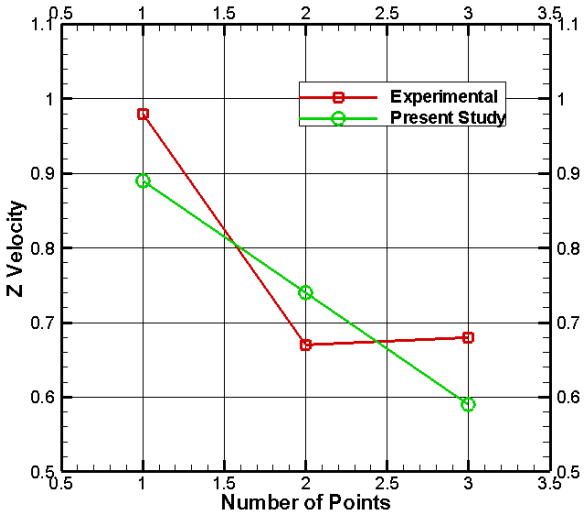

Figure 5.4: T-2, Y = 6''

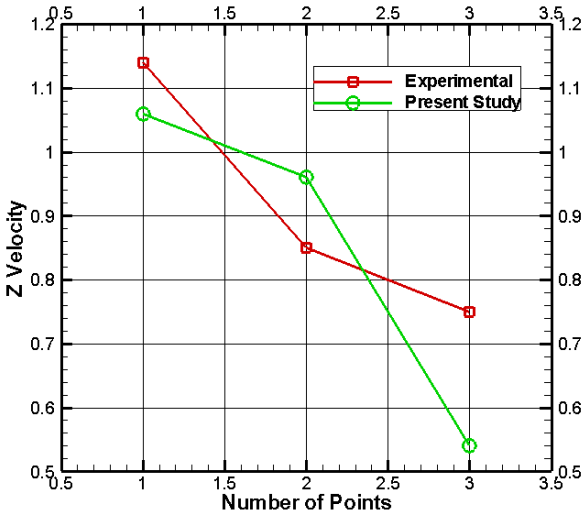

Figure 5.5: T-2, Y = 12''

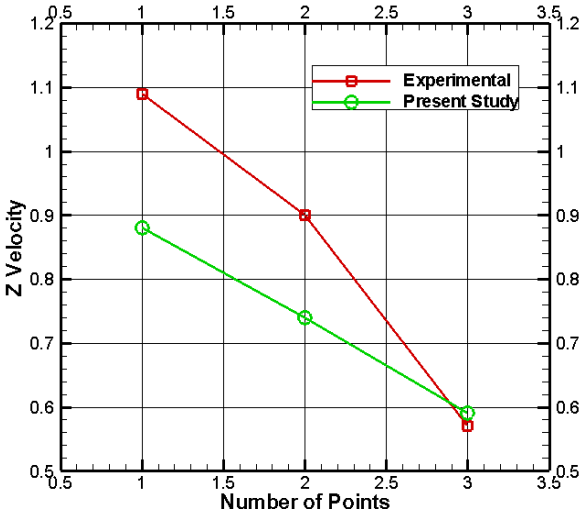

Figure 5.6: T-2, Y = 18''

Table 5.8: Experimental-Numerical comparison of Z-Velocity for tile 2

Figure 5.4 to Figure 5.6 represent the results of velocity distribution just above tile 2. Both studies show good agreement. Left side of tile 2 is jet flow region (higher velocity). This is due to the fact that the left side of tile 2 has no blockage or rack suction as compared to other two portions of the tile (middle and right side)

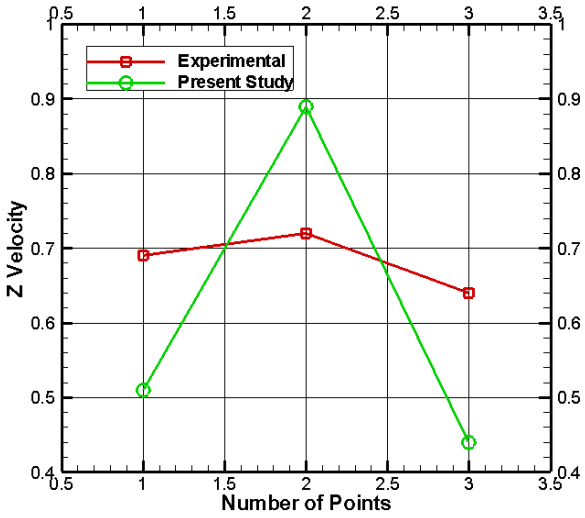

Figure 5.7: T-3, Y = 6''

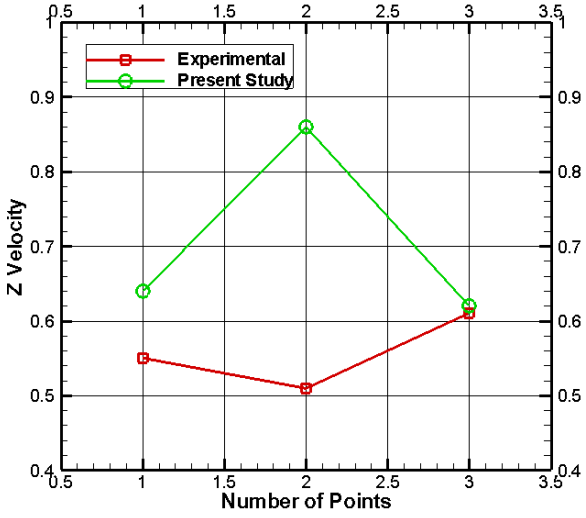

Figure 5.8: T-3, Y = 12''

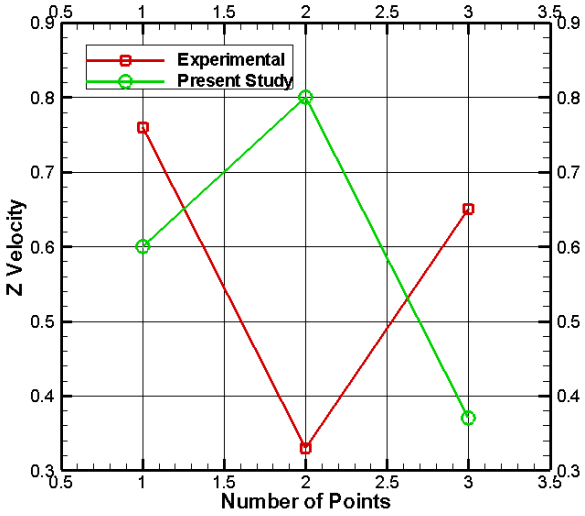

Figure 5.9: T-3, Y = 18''

Table 5.9: Experimental-Numerical comparison of Z-Velocity for tile 3

Figure 5.7 to Figure 5.9 shows velocity distribution above tile 3. This tile is fully blocked by Rack 1 and Rack 2. These are high powered racks and there are much suction effects in front of them. This results in much lover velocities at 18'' height above this tile. Due to high velocity gradients on all points above this tile, both studies show much discrepancy. Average difference

between numerical-experimental results at this surface is about 0.2 m/s, which is comparable to the difference of tile 1 and tile 5. The bottom of tile (Y= 18'' and X= 6'', 12'' and 18'') show least velocities and this will also explain the high suction effects of rack on this tile.

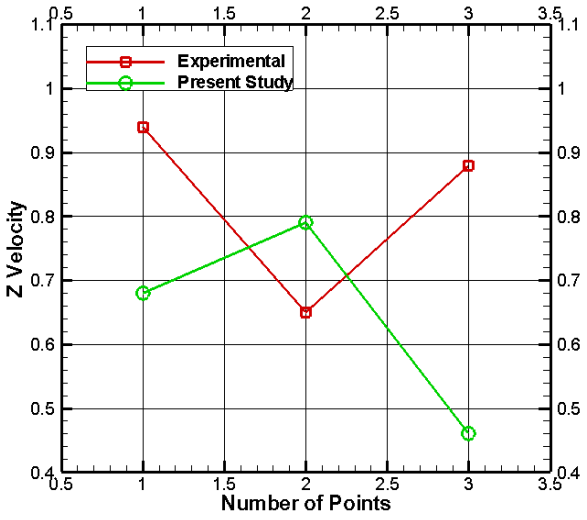

Figure 5.10: T-4, Y = 6''

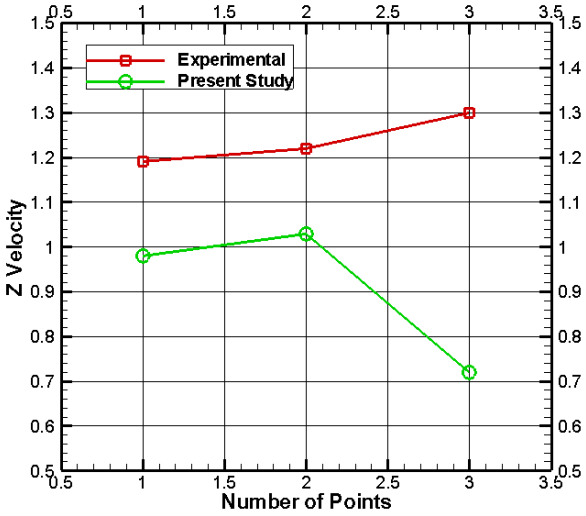

Figure 5.11: T-4, Y = 12''

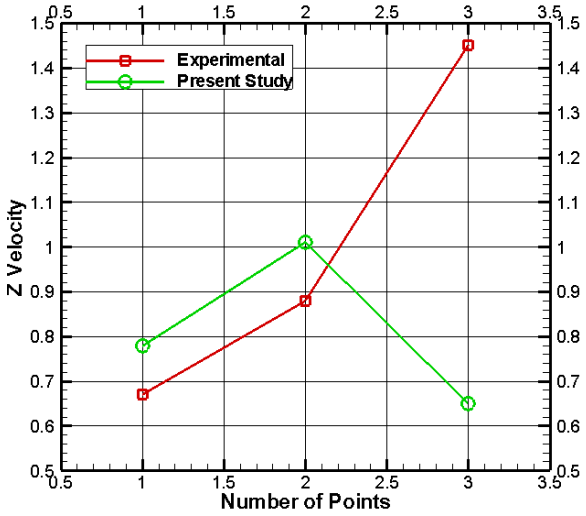

Figure 5.12: T-4, Y = 18''

Table 5.10: Experimental-Numerical comparison of Z-Velocity for tile 4

Figure 5.10 and Figure 5.12 shows the distribution of velocities at 18'' height above tile 4. Relatively high velocities are seen in this region. This is due to the CRAC location and is already explained. Average velocity on this surface is 1.02 experimentally and 0.79 numerically. There is

strong jet flow region in right half plane of this tile and again this can be explained due to the reason that there is no rack in front of this half. So no suction will lead to higher velocity.

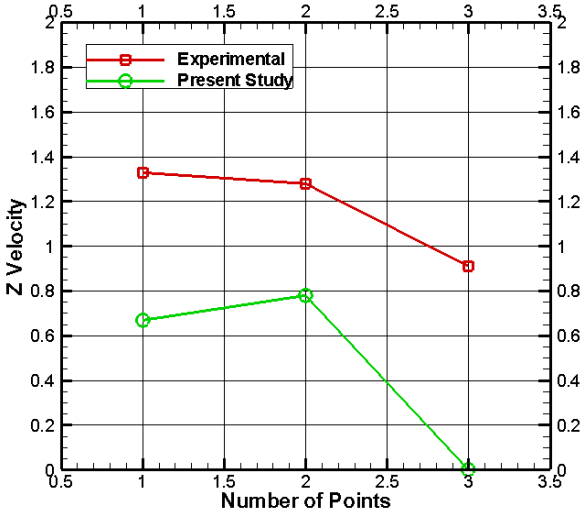

Figure 5.13: T-5, Y = 6''

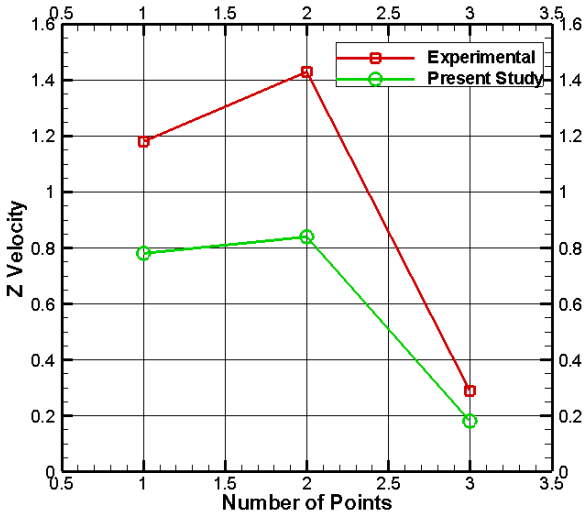

Figure 5.14: T-5, Y = 12''

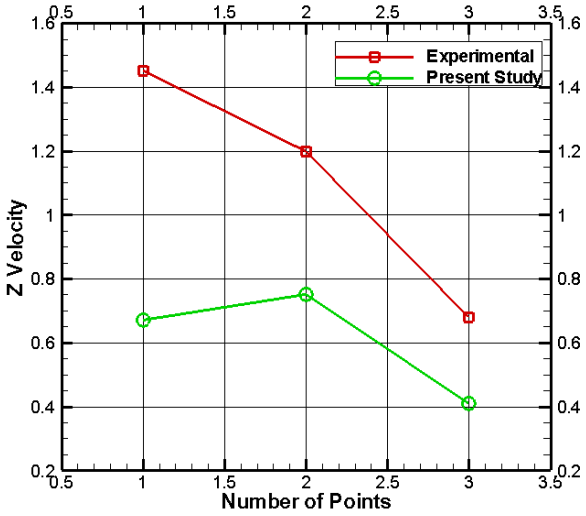

Figure 5.15: T-5, Y = 18''

Table 5.11: Experimental-Numerical comparison of Z-Velocity for tile 5

Tile 5 is fully covered by rack 3. But most part of this rack is empty and all the sides of rack are closed. So, in this case rack is acting as a black box and no flow passes through it. This blockage cause high velocities above tile 5 and two jet flow regions are seen at 18'' height. Average velocity is 1.08 m/s at this height. As we explained earlier, numerical results did not show good

agreement with the experimental data. Although, the pattern are quite similar as can be seen from Figure 5.13 to Figure 5.15, but numerical results are much under predicted in this region.

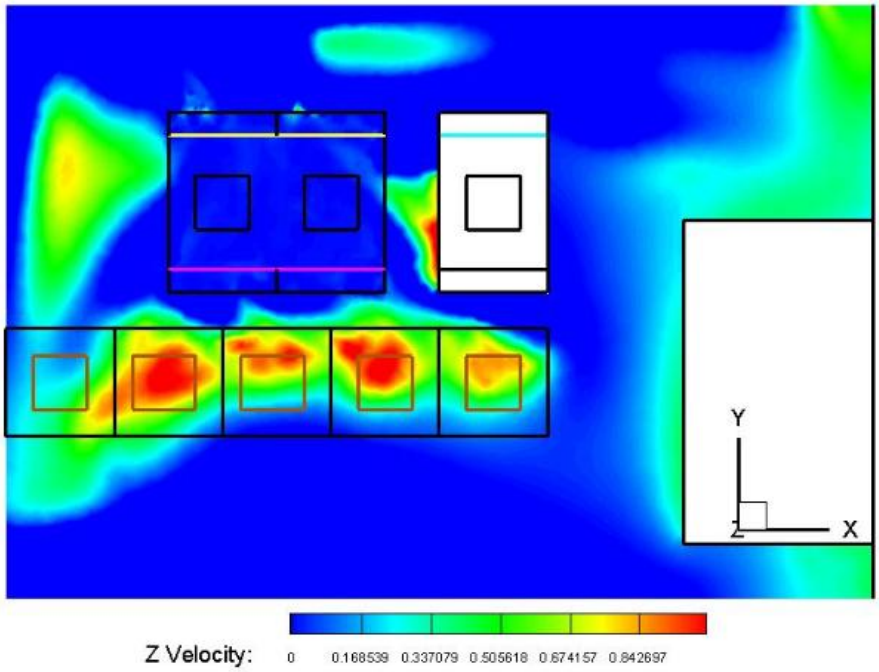

Figure 5.16: Z velocity contour at 18'' height

Figure 5.16 shows the distribution of z velocity throughout the data center at18'' height. This contour graph verifies above discussion of high jet velocities at tile 2, 3 and 4. Moreover relatively high velocities are seen near CRAC at this height and at the right side of the data center. High velocities of right extreme of data center (near rack 1) will explain the reason of low velocities above tile 1. This shows that flow coming out of tile 1 rushes towards the back side of rack rather than moving upwards. Figure 5.17 represents the different slices of contours of temperatures within the data center. Low temperature can be seen in front of rack and high temperatures are present at back side of racks. Intermixing of hot air into cold aisle is also observed through slices, as the temperature contours along sides of racks show relatively high temperature. Figure 5.18 represents the Iso Surfaces for z velocity component equal to 0.5 m/s. Surfaces are colored according to distribution of temperature. Again, flow at front of racks shows much less temperature as compared to temperature of rack back flow.

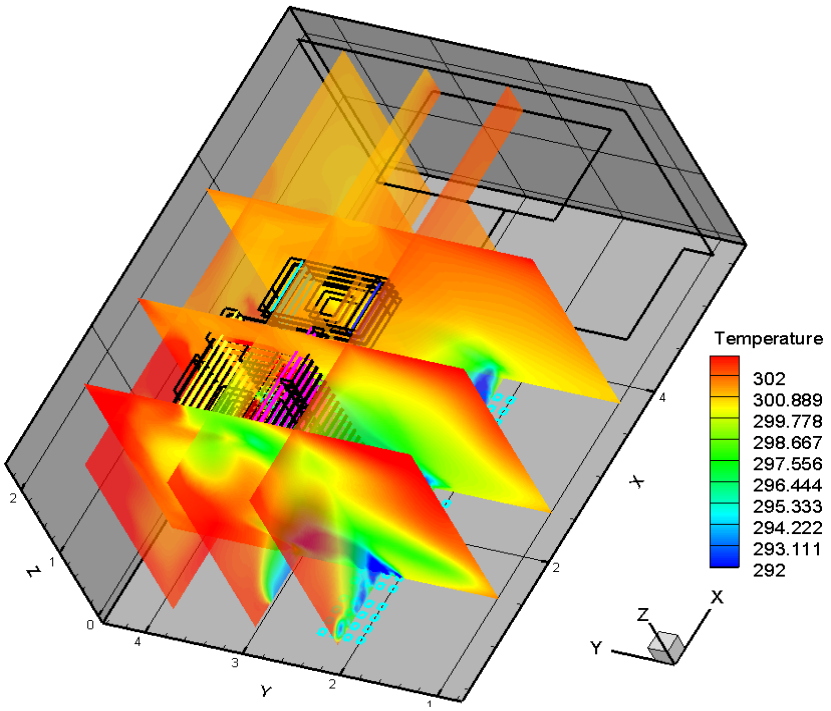

Figure 5.17: Temperature contours along X & Y axis slices

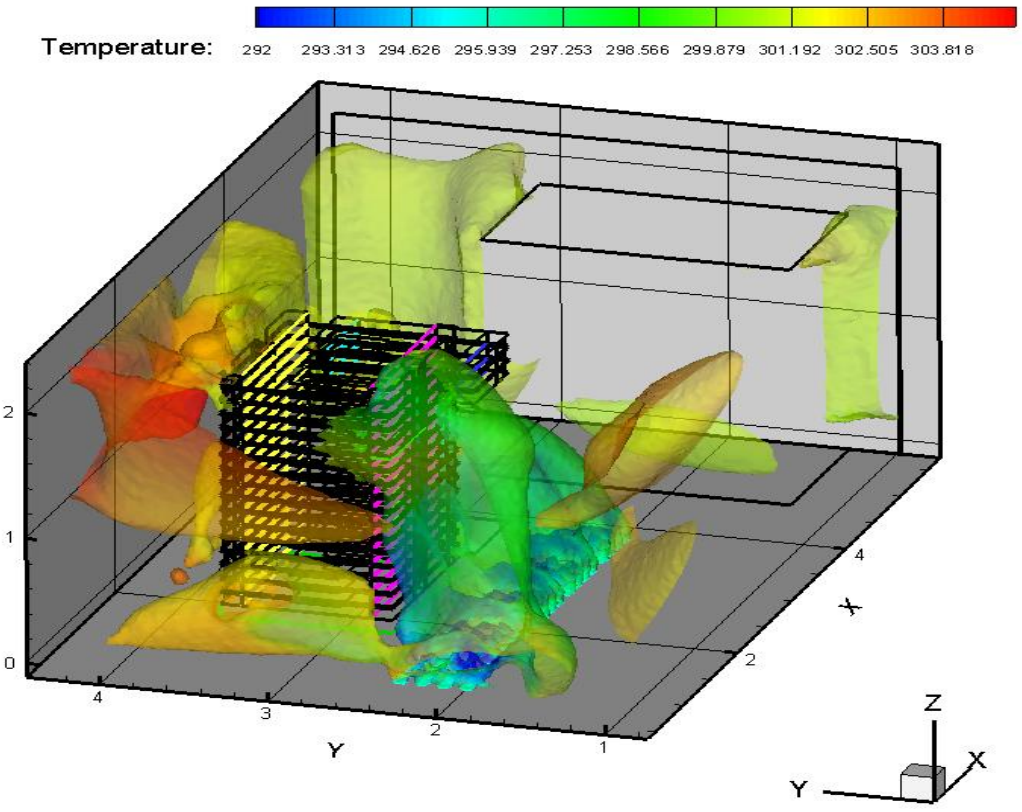

Figure 5.18: Z Velocity Iso-Surfaces for w=0.5 m/s

Chapter # 6

Hot/Cold Aisle Configuration Effect

6.1 Data center design details

A raised floor data center with conventional cooling system is considered in present study. Two even numbered rows of racks configurations are studied; one with two rows of racks (case 1) and other with four rows of racks (case 2). In our simulations, we use one rack as a representative of a complete row of racks. Each case further consists of two more arrangements. For two racks data center, two further configurations are studied. There are two cold aisles (T-1 & T-2) and one hot aisle (present between both racks) in first configuration. We termed this situation as case 1A. In second configuration, there is one cold aisle and two hot aisles. This is termed as case 1B. Figure 6.1 represent plan view of both configurations. Both rooms are 84 × 152 × 90 inches. Dimension of racks are 24 × 40 × 78 inches. There is one CRAC of 24 × 48 × 66 inches. Tiles have four square foot area. For four racks data center, there will be either 3CA-2HA (case 2A) or 2CA-3HA (case 2B) configuration. Figure 6.2 represent top view of both configurations. Room has foot print area of 72 × 280 inches. Racks and tiles are of same dimensions as used for case 1A and case 1B. There are two CRAC's in these data centers. Both are of 12 × 94 × 66 inches. Figure 6.3 represents the 3D view of 2 and 4 racks data center. Summary of configurations is given in Table 6.1. Racks used in our study are similar to the one reported in [13].

Table 6.1: Configurations used in present study

Case	No. of racks	Details of configuration
case 1A	2	2CA & 1 HA
case 1B	2	1CA & 2 HA
case 2A	4	3CA & 2HA
case 2B	4	2CA & 3HA

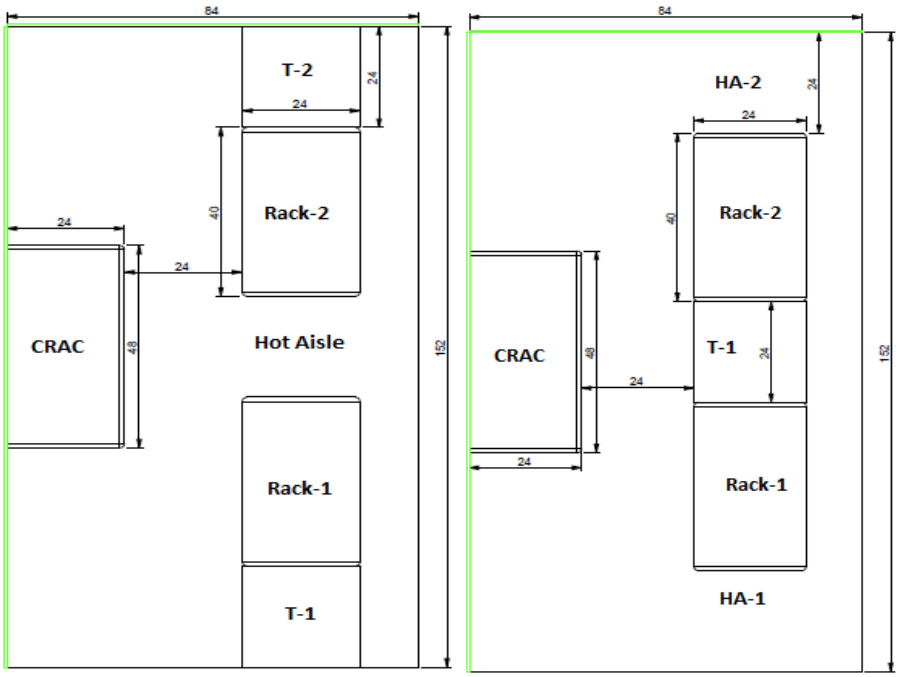

Figure 6.1: Plan view of case 1A (Left) and case 1B (Right)

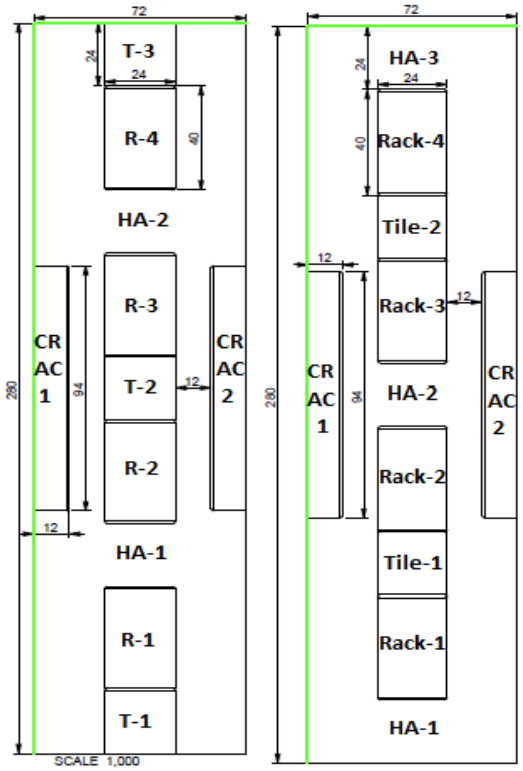

Figure 6.2: Plan view of case 2A (Left) and case 2B (Right)

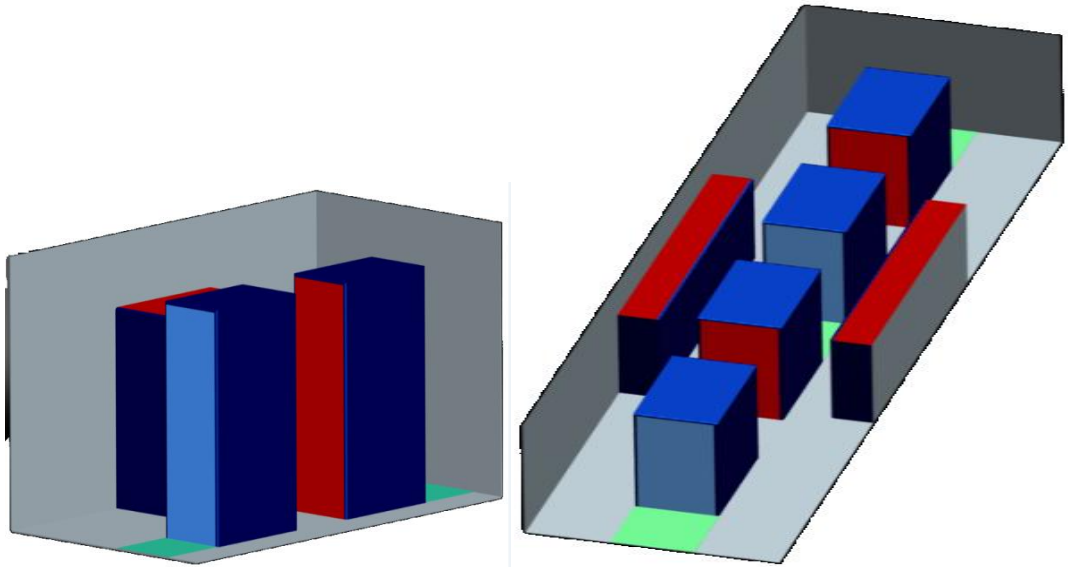

Figure 6.3: 3D views of case 1 & case 2

There are small openings in tiles and at the rear and front of each rack. Modeling them is computationally much expensive, so we followed the technique proposed in [7]. They propose that modeling of a tile as multiple openings gives better results as compared to modeling a tile as a single opening or using Body Force Model. We employed similar technique in our study and used sixteen openings in each tile to represent perforations of tiles. Also, there is one extra tile in case 1A and case 2A as compared to case 1B and case 2B. So, in order to keep constant mass flow rate of cold air coming to the room, we increase area of openings accordingly. Percentage open area of a tile in case 1A is 20% while in case 1B, it is 40%. Figure 6.4 & Figure 6.5 represent the layout of a tile for case 1 and case 2 respectively. In order to model perforations at the front of a rack, we use single opening and created a porous zone near it to get the pressure gradient created by perforations. This technique of modeling rack front is discussed in detail by [13]. Details of boundary conditions used in our study are given in Table 6.2.

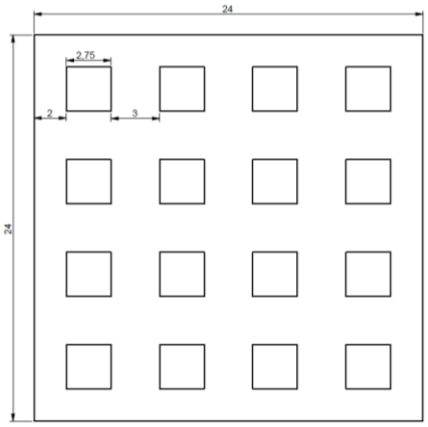

Figure 6.4: Layout of tile for case 1

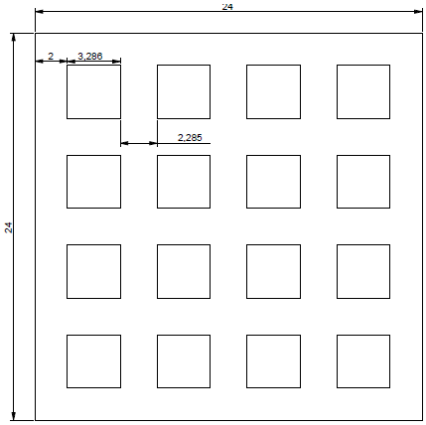

Figure 6.5: Layout of tile for case 2

Table 6.2: Boundary Conditions

Face Name	Boundary Condition	Value
Room Inlet	Velocity Inlet	3.75 m/s & 284K
Room Outlet	Outflow	1
Rack Inlet/Outlet	Interior	
Server Fans	Fan	P(v) = 41.2 - 14.3v
Porous Zone	Porous Jump	$1e^{+10}$ m^2; 1 m; 30
Server	Heat Flux	1400 W/m

We present the effects of cold and hot aisle configurations explained in Table 6.1 on heat transfer phenomenon inside racks. In order to see which case provide higher heat transfer inside racks, we obtain average inlet and outlet temperatures for each rack. By using following equation, we can see which case provides higher ΔT, and in other words gives higher heat transfer inside racks. These results are summarized in Figure 6.8 and Figure 6.9.

$$\Delta T = T_{Outlet} - T_{Inlet}$$

Figure 6.6 shows the inlet and outlet temperatures of both racks for case 1A & case 1B, while Figure 6.7 presents the temperatures for case 2A & case 2B. From Figure 6.6, it is found that inlet temperatures for case 1A are little higher than case 1B. Average difference between them is 1.5K for rack 1 and 1.2K for rack 2. Table 6.3 indicates that ΔT of both racks for case 1A is about 1K higher than case 1B. This shows that more heat transfer occurs when there are more cold aisles than hot aisles (case 1A). This is may be due to the fact that when there are more cold aisles than hot aisles, suction of servers on cold air is from one side. But when there are less cold aisles, although the flow rate of cold air coming into room remains same in that case as compared to previous one, but now cold aisle is sandwiched between two racks. Therefore, suction on cold air is from both sides and this will lead to inefficient heat transfer inside servers.

In case of four racks data center (case 2A & case 2B), Figure 6.7 represents the inlet and outlet temperatures for all racks. Difference between average inlet temperatures for both cases is about 1.5K. This behavior is similar to the one seen in case 1A & case 1B. But the difference between average outlet temperatures for all racks is magnified here. Outlet temperatures of all racks for case 2A are about 5K higher than case 2B. This indicates that heat transfer across servers in case 2A is much more than case 2B. These results are summarized in Table 6.4.

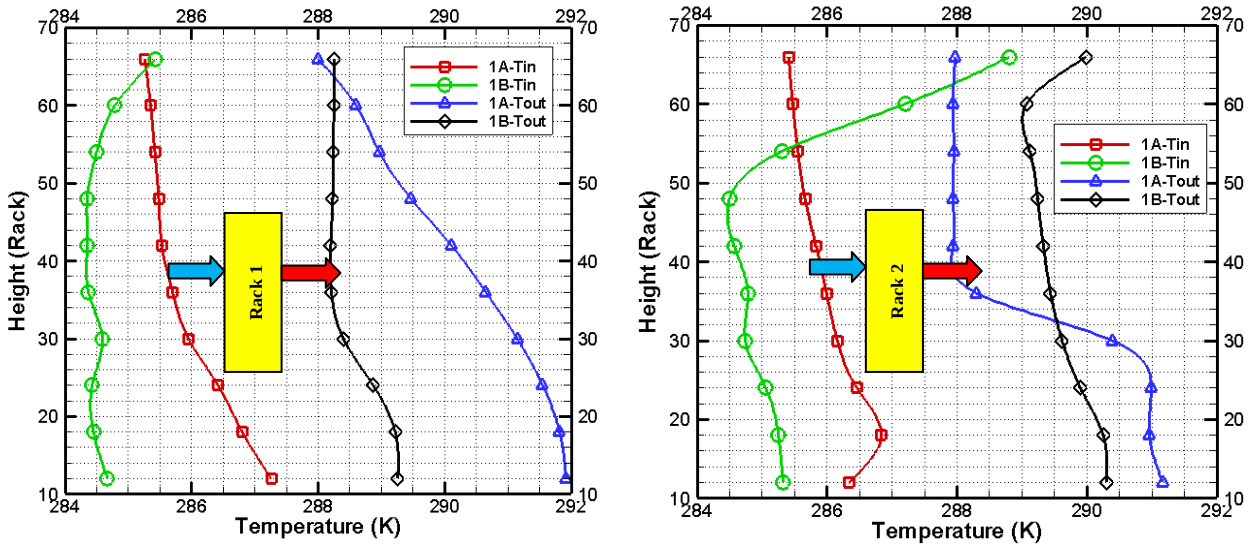

Figure 6.6: Rack Inlet & Outlet Temperature for case 1A & case 1B

Figure 6.8 and Figure 6.9 represent the temperature contours of vertical plane that bisects the rack for all cases. For case 1A, recirculation of hot air into cold aisle seem to be much less than case 1B, because cold aisle contour of case 1A does not show much variation in temperatures. In case 1B, temperature is much less in lower half region of the cold aisle. This is due to the reason that large jet of cold air is coming into room in this case (double than case 1A). But this temperature rises very quickly in upper half region of the cold aisle. This shows that there is very strong recirculation of hot air in this case. For hot aisle contours, case 1A show much uniformity than case 1B. Figure 6.9 represents temperature contours for four rack data center. Rack outlet temperatures for case 2A are much higher than case 2B. We already mention this behavior while discussing the inlet and outlet temperature plots of both cases.

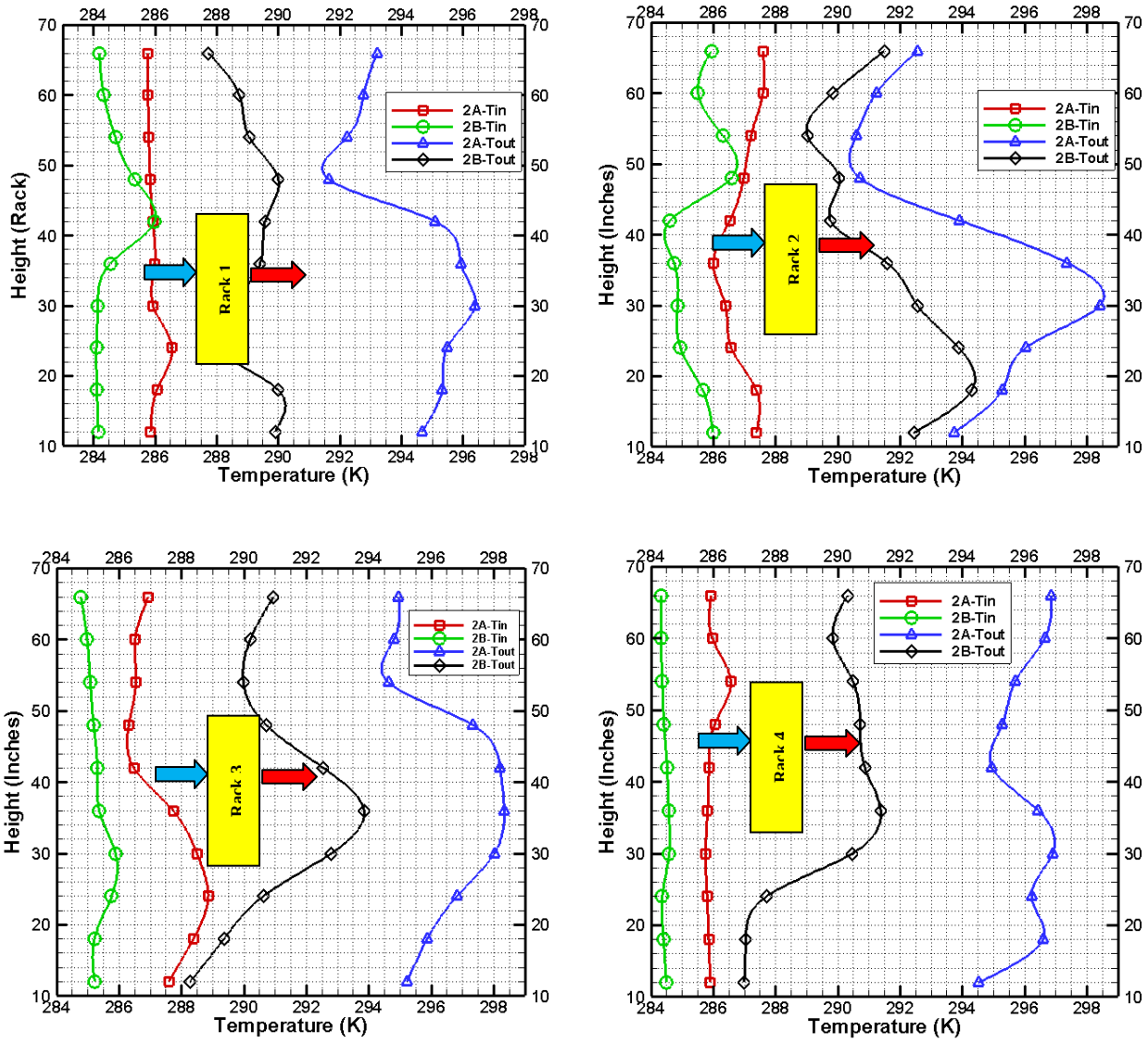

Figure 6.7: Rack Inlet & Outlet Temperature for case 2A & case 2B

The more heat transfer in above cases means that more cold air passes over servers as compared to other cases. Therefore, in order to validate the idea of more heat transfer, we obtain magnitude of x-velocity at each rack outlet for all cases. It is found that case 1A and case 2A has high velocities as compared to case 1B and case 2B. As outlet area of all racks is same, therefore, we can say that case 1A and 2A has more mass flow rate as compared to case 1B and case 2B. Due to higher mass flow rate, more intermixing of hot and cold air occurs across servers, which lead to higher heat transfer rate. This validates the reason why case A has more heat transfer than case B.

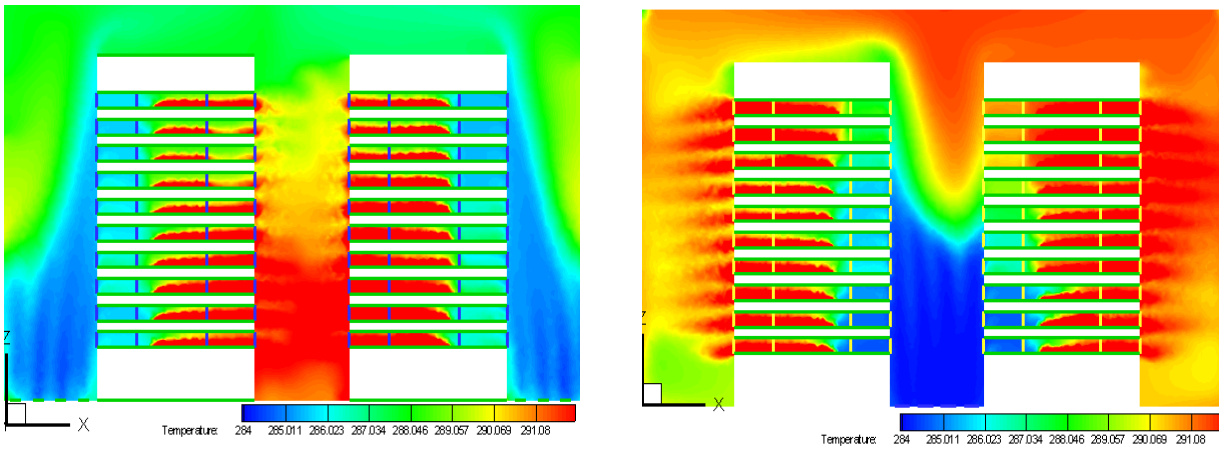

Figure 6.8: Temperature contour of mid Y plane for case 1A (Left) & case 1B (Right)

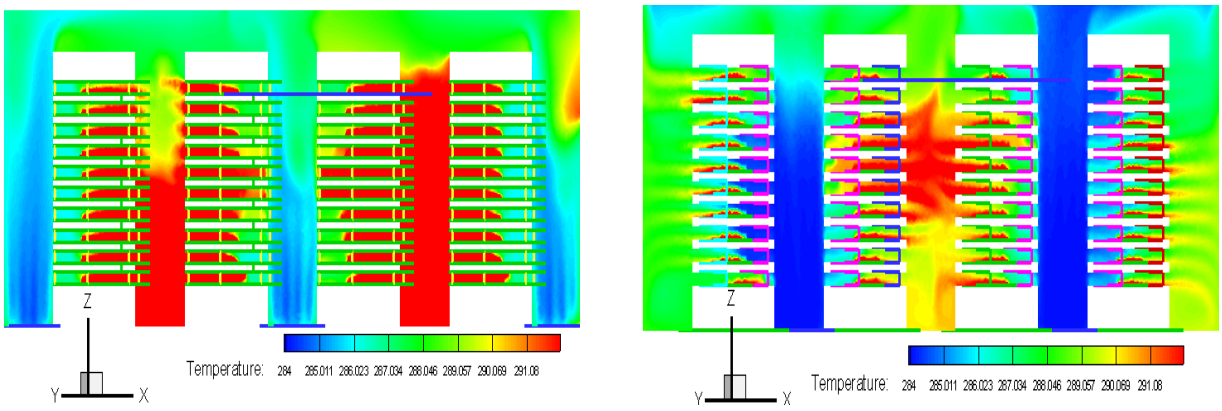

Figure 6.9: Temperature contour of mid Y plane for case 2A (Left) & case 2B (Right)

Table 6.3: Average ΔT of all racks for case 1

Rack	ΔT (case 1a)	ΔT (case 1b)
1	4.31	3.92
2	4.07	3.18

Table 6.4: Average ΔT of all racks for case 2

Rack	ΔT (case 2a)	ΔT (case 2b)
1	8.33	4.52
2	7.02	5.99
3	9.04	5.66
4	10.07	5.15

6.2 Summary of chapter

This paper investigates the effects of cold/hot aisle configurations on temperature difference across racks in a data centre having even number of racks. Numerical study is performed for a data center having two and four racks.

Results showed that whatever configuration will be used, the inlet temperatures for racks did not show much variation. On the other hand, outlet temperatures show much difference for both cases. This will explain that the configuration change will affect the heat transfer efficiency inside servers. In order to see which configuration will give more heat transfer, we find temperature difference between inlet and outlet temperatures for both cases. It is found that, whenever cold aisles are more than hot aisles, that configuration provide higher heat transfer as compared to other case. This can be due to the reason that for higher cold aisles case, suction effects of servers on cold air are single sided. While in other cases, suction is from both sides. This suction causes mass flow rate across servers to be less in case 1B and 2B. In order to validate that concept, we obtain magnitude of x-velocities at outlet of all racks. These velocities are more for case 1A and 2A. In other words, there is more mass flow rate. Therefore, cold air will be efficiently served to all servers of racks in these cases, which results in higher heat transfer in these cases.

6.3 **Effect on Energy Efficiency:**

On the basis of above discussion, we found that for the same flow rate (CFM) of cool air into the data center, one configuration (n (CA) = n (HA) + 1) provides higher heat transfer than other (n (CA) = n (HA) – 1). In other words, one system is providing cooling more efficiently than other. So, in order to obtain the same delta T across racks from both cases, case A needs less amount of cool air into the data center. In other words, for case A, we need less tonnage of CRAC as compared to case B to obtain a specific temperature across servers, which will result in low electricity bills.

Conclusion and Future Work

7.1 Conclusion:

Above plenum CFD models are usually validated against temperature measurements. The temperature only CFD model gives complete picture of the thermal behavior of a data center, but it did not give any idea about air flow patterns like recirculation problem, stagnation regions, jet flow regions etc. As a result, better validation techniques are required to properly verify the air flow patterns of a CFD model. Validation of a full scale data center is presented in this thesis.

An experimental space with two highly dense racks and a partially filled rack in a data center located at RCMS is selected. Point velocities and temperature distribution measurements are obtained using anemometer. A CFD model of the experimental space is created. The boundary conditions were determined from the experimental space. Results of numerical study are then compared with the experimental data and it was found that CFD model shows good agreement with the experimental data.

In order to analyze the effects of aisle configurations on energy efficiency of a data center, a numerical study for two even numbered rows of racks data center is then performed. Racks density and boundary conditions were chosen on the basis of study performed in [28]. It was found that whenever there are even number rows of racks in a data center, it is better to have one cold aisle than number of hot aisles.

7.2 **Future Work:**

Although this thesis concludes that there are notable benefits for using air flow focused validation techniques to confirm the airflow patterns in a CFD model, the benefit of using these techniques for different cooling scenarios are still unknown. We can use this technique for some of the following situations

1. Supply less air than the servers demand. This will magnify the recirculation effects
2. Drastically imbalance the flow rates
3. Use different kind of racks (fully and partially loaded, empty etc), and check what effects each will produce

In addition, experimental setup for aisle configuration study should be generated and tested either that will provide the same effect or not. Also, expansion of RCMS data center should be done according to the recommendations of Hot/Cold aisle configuration study.

Works Cited

1 Energy Information Administration (EIA), "Use of energy in the United States.", 2008, http://www.eia.gov/energyexplained

2 D. Butler, "Architects of a Low Energy Future.", Nature 452, 520-523, 2008, doi:10.1038/452520a

3 Annual energy outlook 2012, http://www.eia.gov/forecasts/archive/aeo12/sector_residential.cfm

4 W. Bhutto, M. Yasin, 25-27 Oct 2010; "Overcoming the Energy Efficiency gap in Pakistan's Household Sector.", IEEE International Conference on Energy Systems Engineering Conference (ICESE 2010), Islamabad, Pakistan.

5 M. Saghir, Prospects Of Energy Efficiency Business In Pakistan, 2007

6 Energy Efficient Lighting by MD ENERCON Pak, May 2009, www.enercon.gov.pk

7 Energy Outlook for 2008 with Projections to 2030", Report by the US energy Information Administration, Report number: DOE/EIA-0383, 2008

8 M. Iyengar, R. Schmidt, and J. Caricari, 2-5 June 2010, "Reducing Energy usage in data centers through control of room air conditioning units.", 12th IEEE Intersociety Conference on Thermal and Thermomechanical Phenomena in Electronic Systems (ITherm), Las Vegas, NV, pp 1-11

9 R. Schmidt, K. C. Karki, K. M. Kelkar, A. Radmehr, S. V. Patankar, 2001, "Measurements And Predictions Of The Flow Distribution Through Perforated Tiles In Raised-Floor Data

Centers", ASME International Electronic Packaging Technical Conference and Exhibition (IPACK), Kauai

10 K. C. Karki, A. Radmehr & S. V. Patankar, 2003, "Use of Computational Fluid Dynamics for Calculating Flow Rates Through Perforated Tiles in Raised-Floor Data Centers.", HVAC & R Research, Vol 9, No. 2, pp. 153-166.

11 S. Kang, R. Schmidt, 2001, "A Methodology for the Design of Perforated Tiles in Raised Floor Data Centers Using Computational Flow Analysis.", *IEEE Transactions on Components and Packaging Technologies,* Vol. 24, No. 2, pp. 177 -183

12 R. Schmidt, K. C. Karki and S. V. Patankar, 1-4 June 2004, "Raised-Floor Data Center: Perforated Tile Flow Rates for Various Tile Layouts." IEEE The Ninth Intersociety Conference on Thermal and Thermomechanical Phenomena in Electronic Systems (ITHERM), Vol 1, pp 571- 578

13 K. C. Karki, S. V. Patankar, A. Radmehr, 2003, "Techniques for Controlling Air Flow Distribution in Raised Floor Data Centers.", *ASME International Electronic Packaging Technical Conference and Exhibition (INTERPACK),* USA

14 D. Patel, R. Sharma, C. E. Bash and A. Beitelmal, 2002, "Thermal Considerations in Cooling Large Scale High Compute Density Data Centers.", *The Eighth Intersociety Conference on Thermal & Thermomechanical Phenomena in Electronic Systems (ITHERM),* IEEE, USA, Vol. 8, pp. 767 - 776

15 K. C. Karki, A. Radmehr and S. V. Patankar, "Use of Computational Fluid Dynamics for Calculating Flow Rates Through Perforated Tiles in Raised-Floor Data Centers", International Journal of Heating, Ventilation, Air-Conditioning, and Refrigeration Research, Volume 9, Number 2, pp. 153-166, 2003

16 X. Ven, J. Liu, August 1-4 2012, "The Optimization of Airflow in Raised Floor Internet Data Center", The Second International Conference on Building Energy and Environment (COBEE), Colorado, USA

17 W. A. Abdelmaksoud, H. E. Khalifa and T. Q. Dang, 2010, " Improved CFD Modeling of a Small Data Center Test Cell", *The 12th Intersociety Conference on Thermal & Thermomechanical Phenomena in Electronic Systems (ITHERM)*, IEEE, USA, Vol. 12, pp. 1 - 9

18 P. Kumar, V. Sundaralingam, Y. Joshi, 19-22 Dec. 2010, "Dynamics Of Cold Aisle Air Distribution In A Raised Floor Data Center", 3rd International Conference on Thermal Issues in Emerging Technologies Theory and Applications (ThETA), Cairo, Egypt, pp. 95 – 102

19 W. A. Abdelmaksoud, H. E. Khalifa and T. Q. Dang, 2-5 June 2010, " Improved CFD Modeling of a Small Data Center Test Cell", 12th IEEE Intersociety Conference on Thermal & Thermomechanical Phenomena in Electronic Systems (ITHERM), Las Vegas, NV, pp. 1 - 9

20 B. Fakhim, N. Srinarayana, M. Behnia and S. W. Armfield, 2010, "Effect of Under Floor Blockages and Perforated Tile Openings on the Performance of Raised-Floor Data Centers", *17th Australasian Fluid Mechanics Conference*, New Zealand

21 "Facility Design for High Density Data Centers", Intel White Paper, January 2012

22 X. Zhang, J. W. VanGilder, M. Iyengar, R. Schmidt, 2008, "Effect Of Rack Modeling Detail On The Numerical Results Of A Data Center Test Cell", *Intersociety Conference on Thermal and Thermomechanical Phenomena in Electronic Systems* (ITHERM), IEEE, Billerica , Vol. 8, pp. 1183 - 1190

23 P. Kumar, V. Sundaralingam and Y. Joshi, 2011, "Effect of Server Load Variation on Rack Air Flow Distribution in a Raised Floor Data Center", *27th IEEE SEMI-THERM Symposium*, USA, Vol. 27, pp. 90 - 96

24 R. Ghosh, V. Sundaralingam, Y. Joshi, 2012, "Effect of Rack Server Population on Temperatures in Data Centers", The 13th Intersociety *Conference on Thermal & Thermomechanical Phenomena in Electronic Systems (ITHERM)*, USA, Vol. 13, pp. 30 - 37

25 V. Bedekar, S. Karajgikar and D. Agonafer, 2006, "Effect of CRAC Location on Fixed Rack Layout", The 10th Intersociety Conference on Thermal & Thermomechanical Phenomena in Electronic Systems (ITHERM), IEEE, USA, Vol. 10, , pp. 420 – 425

26 G. Tan, K. S. Venerable, August 11 – 13, 2010, "CFD Simulation Enhances A Data Center's Expansion Process.", Fourth National Conference of IBPSA, New York, USA

27 C. D. Patel, C. E. Bash and C. Belady, "Computational Fluid Dynamics Modeling of High Compute Density Data Centers to Assure System Inlet Air Specifications", ASME International Electronic Packaging Technical Conference and Exhibition (IPACK) USA, 2001

28 M. D. Lloyd, 2010, "Unique Airflow Visualization Techniques for the Design and Validation of Above-Plenum Data Center CFD Models", Master's Thesis Report, Department of Architecture, Massachusetts Institute of Technology, USA

29 ANSYS FLUENT-Solver Theory Guide, ANSYS Inc. Release 13.0, South Pointe, 275 Technology Drive, Canonsburg, PA 15317 November 2011

30 Gambit Tutorial Guide, Gambit Fluent Inc. Release 2.4.6, 2007

31 Tecplot 360 User Guide, Tecplot Inc. Release 2010

32 B. E. Launder, D. B. Spalding, "The Numerical Computation of Turbulent Flows", Computer Methods in Applied Mechanics and Engineering vol. 3, p. 269-289, 1974

33 S. V. Patankar and D. B. Spalding, “A Calculation Procedure for Heat Mass and Momentum Transfer in Three Dimensional Parabolic Flows”, International Journal of Heat & Mass Transfer, vol. 15, p. 1787, 1972.

34 P. V. Nielsen, “Specification of a two-dimensional test case”, Research item No. 1.45, ISSN 0902-7513 R9040, Department of Building technology and Structural Engineering, Aalborg University, Denmark

35 J. D. Posner, C. R. Buchanan, D. Dunn-Rankin, “Measurement and Prediction of Indoor Air Flow in a Model Room.”, ELSEVIER Journal of Energy and Buildings 35, 515-526, 2003